THE ONSET OF GRAVITATIONAL COLLAPSE IN MOLECULAR CLOUDS

Paul Campbell Clark

A Thesis Submitted for the Degree of PhD
at the
University of St Andrews

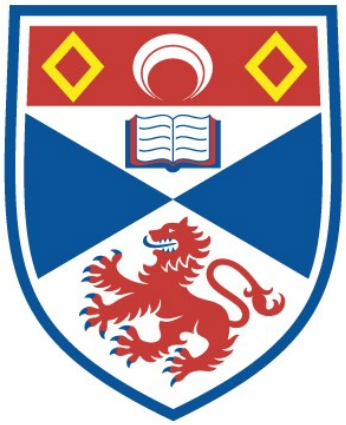

2005

THE UNIVERSITY OF ST. ANDREWS

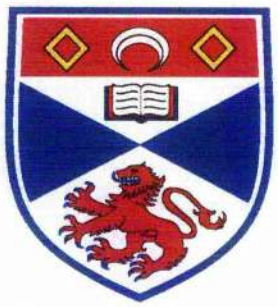

University
of
St Andrews

The Onset of Gravitational Collapse in Molecular Clouds

Paul Campbell Clark

Submitted for the degree of Ph.D.

May 10, 2005

DECLARATION

I, Paul Campbell Clark, hereby certify that this thesis, which is approximately 50000 words in length, has been written by me, that it is the record of work carried out by me and that it has not been submitted in any previous application for a higher degree.

May 10, 2005

I was admitted as a research student in October 2001 and as a candidate for the degree of Ph.D. in October 2001; the higher study for which this is a record was carried out at the University of St. Andrews between 2001 and 2005.

May 10, 2005

In submitting this thesis to the University of St. Andrews I understand that I am giving permission for it to be made available for use in accordance with the regulations of the University Library for the time being in force, subject to any copyright vested in the work not being affected thereby. I also understand that the title and abstract will be published, and that a copy of the work may be made and supplied to any *bona fide* library or research worker.

May 10, 2005

I hereby certify that the candidate has fulfilled the conditions of the Resolution and Regulations appropriate for the degree of Ph.D. in the University of St. Andrews and that the candidate is qualified to submit this thesis in application for that degree.

May 10, 2005

THE UNIVERSITY OF ST. ANDREWS

The Onset of Gravitational Collapse in Molecular Clouds

Submitted for the degree of Ph.D.

May 10, 2005

Paul Campbell Clark

ABSTRACT

We conduct an investigation into the role that turbulence plays in the formation of stars. In small clouds, with masses of ~ 30 $M_{\odot}$ and where the turbulence is only injected at the start, we find that the turbulence does not trigger star formation. Instead, the dissipation of the kinetic energy allows the mean Jeans mass of the cloud to control the formation of stars. The equipartition of the kinetic and thermal energies in the final stages before star formation, allows the pre-protostellar clumps to fragment. Binary and multiple systems are thus a natural product of star formation in a turbulent environment. We find that globally unbound clouds can be the sites of star formation. Furthermore the star formation efficiency is naturally less than 100%, thus in part providing an explanation for the low efficiency in star forming regions. Globally unbound GMCs not only form stars, and naturally disperse, within a few crossing times, but also provide a mechanism for the formation of OB associations.

ACKNOWLEDGMENTS

There are quite a few people who deserve my thanks in the completion of this thesis. First I suppose that my parents, Jim and Fiona, deserve special consideration, since without their patience and hard work I would probably have never made it this far! My maths teacher in school, Marilyn Richards also deserves a mention here, for endlessly prodding me to do some work (the woman has the patience of a saint). From my undergraduate degree, I'd like to thank Andrew Cameron for helping me realise that I am indeed far too lazy to be an observer.

With regards to the actual work presented for this PhD, I'd like to give a big thanks to Ian Bonnell for his tireless enthusiasm, inspiration, attempting to teach me to ski, and, perhaps most importantly, for resisting the urge to sing. I'd also like to thank Ant Whitworth and Ralph Klessen for refereeing two of the papers that have been published as part of the work in this thesis. Also, thanks to Hans Zinnecker and Matthew Bate for agreeing to be co-authors on one of these papers. Their comments and encouragement have been warmly received.

I would like to acknowledge UKAFF (UK Astrophysical Fluids Facility), for granting the computer time to perform the simulations presented in chapter 8. I would also like to acknowledge a UKAFF Fellowship.

All the work may have been a bit dull though if it were not for the various office mates that I've had the pleasure of knowing in my time in St Andrews. Two that spring instantly to mind are Ken and Steve, who managed to show us all how to have a good time, despite their ever increasing age and parental status. The donkey comment still makes me grin. I'd also like to give a big thanks to Mike, Claire and Chris for putting up with my endless questions and ranting at the world. Steve and Claire get an extra mention here for being fabulous travelling companions.

Lastly I'd like to thank my girlfriend Joanna, for suffering my endless moaning and random bouts of poverty/homelessness. I really couldn't have got this finished without you.

Cheers Guys,

"Pooh," said Rabbit kindly, "you haven't any brain"
"I know," said Pooh humbly.

CONTENTS

LIST OF FIGURES

LIST OF TABLES

CHAPTER 1

Introduction

1.1 Overview

In the last 20 years or so, the field of star formation has greatly benefited from the advent of new technology, such as advances in instrumentation, larger telescopes, and the arrival of space based observatories. Radio and millimetre, and infra-red wavelength astronomy now permit astronomers to probe the massive clouds of molecular gas where stars form. These regions, due to the high gas and dust densities are opaque at optical wavelengths. With these new instruments, we are gradually building up a picture of how stars form, and the typical conditions that surround their birth. We now have a wealth of information that covers three main stages that appear to be important in the star formation process: the formation of dense cores; the fragmentation of these cores into small groups, such as binary and multiple systems; and the formation of clusters (say roughly $\geq$ 10 stars). It has become clear from these observations that star formation occurs in groups, and thus the clustered environment is likely to play an important role in a young star's life.

It is however unfair to say that star formation has only recently received observational motivation. Two features of the adult stellar population that have been known for some time, namely the high field star binary fraction (Heintz, 1969; Abt, 1983; Duquennoy & Mayor, 1991) and the distribution of stellar masses (Salpeter, 1955), have provided star formation with perhaps its most taxing benchmark for potential theories. It appears that roughly 50% of all stellar systems are actually (at least) binary systems, thus some two thirds of all stars exist as part of a binary, or higher order, system. It also appears that the mass distribution of stars is well defined. In any given sample, there will always be a certain fraction which are $1M_{\odot}$ stars, a certain fraction which are $10M_{\odot}$ stars, and so on. Although derived from field star observations, this distribution of stellar masses (the initial mass function, or IMF) is also observed to exist in very young protostellar clusters, while there is evidence to suggest (which we will discuss in section 1.3) that the binary fraction is even higher in protostellar systems than it is in the field star population.

Unfortunately, the most complete star formation theory that has been presented to date (Shu et al., 1987), completely fails to explain, or even address, the origin of stellar masses and the observed binary fraction. The singular isothermal sphere (SIS) around which this theory is based, first presented by Shu (1977), prevents the formation of multiple systems, since the r^{-2} density profile of the collapsing gas makes fragmentation

very difficult. Explaining the existence of short period binaries, i.e. those with periods of less than a few days, also appears to be a problem. A $1M_{\odot}$ star starts life as a region of gas with a radius of 0.04pc, assuming a typical gas temperature of 10K (see the 'Jeans mass' and 'Jeans radius' in chapter 4.2). If the SIS model can only form one stellar object from a region of this size, then binaries must be formed via some sort of capture mechanism. Pure N body simulations show that this mechanism delivers too small a binary fraction and the properties of the binary systems are not consistent with those observed by Duquennoy & Mayor (1991).

The SIS model of Shu and co-workers actually appears to be flawed in a number of ways (for a discussion of these problems see Whitworth et al. (1996)), and thus we must now abandon at least some aspects of the theory. More recently, there has been a move away from trying to explain star formation in terms of a set of equations, and to instead try and describe star formation in terms of statistical processes that are governed by a few underlying physical mechanisms. Numerical simulations have provided a means of testing these ideas, and some promising results are already emerging. In particular, the binary and IMF problems are being quite naturally explained in terms of the accretion and interaction processes that occur in small clusters.

The work in this thesis will concentrate on the numerical simulation approach to star formation. The regions where stars form are known to include supersonic turbulent motions. The first part of this thesis will be to examine the role this 'turbulence' plays in the star formation process. We will then go on to use numerical simulations to study the star formation in clouds which are globally unbound.

In the discussion that follows, we describe the properties of the clouds that play host to star formation (section 1.2), and the properties of the young clusters that are known to form within these clouds (section 1.3). We then go on in section 1.4 to discuss the major findings that numerical simulations have brought to the star formation theory. In the final section (1.5) we give a plan of the thesis, describing how we plan to build upon the numerical work to date.

1.2 Giant molecular clouds

Giant molecular clouds (GMCs), vast regions of molecular hydrogen, are the sites of almost all star formation in the Galaxy (e.g. Blitz & Williams 1999). From a point of view of constructing a star formation theory, the GMC can thus be thought to represent the initial conditions from which star and cluster formation can proceed. As a result, they have received considerable attention from extensive observational surveys at many wavelengths in an attempt to probe the physical conditions that characterise these clouds. Here, we give an overview of GMCs, including their typical properties, structure, formation and lifetimes.

1.2.1 General properties and internal structure

There has always been a problem when it comes to the definition of a GMC, mainly because star formation is known to occur in molecular clouds that come in a vast array of shapes and sizes (see Blitz 1991). In terms of mass, the values can range from a few $10^4 M_\odot$ for the smaller GMCs, to as high as $10^6 M_\odot$ (Cernicharo, 1991).

The temperature of the gas in a GMC, especially in regions far away from patches of star formation is generally very low, with typical values of 10-15K. The gas is also thought to behave isothermally, since this temperature is maintained over at least 5 orders of magnitude in density within the cloud. The reason for the low temperature is that the inner regions of the cloud are shielded from the interstellar UV field, which acts to dissociate molecules, leaving cosmic rays and local star formation as the only heating sources. Until the star formation starts, the molecular species of H_2 and CO are able to prevent the cosmic rays from the heating the clouds above $\sim$ 20K, keeping the GMCs cool (see Genzel 1991 for a discussion of the heating and cooling processes in GMCs).

Observations of the line-widths from surveys of the molecular tracers, such as ^{12}CO and ^{13}CO, reveal that GMCs have considerable non-thermal internal motions (Larson, 1981; Dame et al., 1986; Myers & Goodman, 1988; Blitz & Williams, 1999), which at most scales are highly supersonic. In what has become a landmark paper, Larson (1981) compared the line-widths of the clouds to their size-scale and came up with the relation,

$$\Delta v \propto L^{\alpha} \tag{1.1}$$

where Δv is the velocity dispersion of the cloud, L its length, and α a power which is found to be 0.38. The similarity of this relation to that of Kolmogorov (1941) for incompressible turbulence, which has a power of $\alpha = 0.33$, has lead to the suggestion that the internal motions of molecular clouds are 'turbulent'. While the motions are clearly not from systematic rotation or in-fall (Blitz, 1991), it is still unclear as to whether they represent true turbulence. More recent studies of the velocity dispersion inside a single cloud have yielded an α of 0.5 (e.g. Heyer & Brunt 2004).

The origin of these motions is still unknown but have been attributed to Alfvén waves, feedback from young stars, thermal instabilities to name but few. The Alfvén wave origin has received some support. Crutcher (1999) reports that the magnetic and kinetic energies are roughly equal, suggesting that the turbulent motions are the result of Alfvén waves. However, one also expects bulk motions to produce a magnetic field with an energy roughly equal to that of the turbulence. Thus is is not clear from these observations alone whether the magnetic field results in turbulence or the turbulence results in the magnetic field. This highlights a frequent problem in star formation, in that it is not always possible to identify what is the cause and what is the effect.

As well as having random internal hierarchical motions, the density inside a GMC is also extremely non-uniform, with most of the mass being contained in dense regions, generally referred to as 'clumps', with number densities of $n_{H_2} \sim 10^2 - 10^3$ cm^{-3}. Within these clumps can be found star forming 'cores', with densities $n_{H_2} \geq 10^4 - 10^5$ cm^{-3}. The term 'core' is generally used to refer to a region of dense gas in which a small group of

stars is being formed, or a region where collapse looks inevitable (the magnitude of the gravitational energy is much larger than the sum of the supporting energies).

The mass spectrum of the clumps within GMCs also appears to be similar to the mass spectrum of molecular clouds as a whole. The cloud mass spectrum for the outer and inner galaxy are remarkably similar, both having a rough relationship of $\mathrm{d}N/\mathrm{d}m \propto m^{-1.7}$ (Sanders et al., 1985; Heyer & Terebey, 1998). Williams et al. (1994) compare the Rosette star forming GMC to the non-star forming cloud of G216-2.5 (Maddalena & Thaddeus, 1985). The clump mass spectrum for the two clouds are both very similar, and also comparable to the mass spectrum for GMCs and molecular clouds in general. What distinguishes the clumps in the non-star forming GMC is that they are generally larger (i.e. for the same mass, less dense) and have greater line-widths such that they are all unbound. Since the unbound clumps in G216-2.5 have the same mass spectrum as the more bound clumps in the Rosette cloud, it appears unlikely that gravity plays a dominant role in determining the large-scale internal structure of GMCs. Neither does the presence of star formation appear to be important in controlling the GMC morphology, since the Rosette cloud has extensive star formation while G216-2.5 has none.

The picture of clumps and cores has existed since the early molecular cloud surveys (Blitz & Thaddeus, 1980; Myers & Benson, 1983; Blitz & Stark, 1986) and remains the preferred description of the inhomogeneous structure of GMCs. There has been another description however, which draws on the idea of structure within structure that is suggested by the clump-core description. The alternate view is to regard molecular clouds as scale-free, or fractal (Bazell & Desert, 1988; Scalo, 1990; Falgarone et al., 1991). From this view point, the clumps and cores description is merely a product of the observational procedure, such as the survey resolution, the need to trace different densities with different species and the human tendency to categorise objects by shape, such as filaments and shells.

The hierarchical nature of fractal clouds has been argued to be the result of shock density enhancement from the turbulent motions that are known to be inside the GMCs (Larson, 1992; Henriksen, 1986, 1991; Elmegreen, 1993, 1997, 1999, 2000b). The scale free nature of the turbulence is thus the cause of scale free density structure in the clouds. Elmegreen (2000b) suggests that this leads to not only a hierarchical distribution of stars in clusters (e.g. NGC 1333 Lada et al. 1996) but provides a possible explanation for the the shape of the IMF, since the locations of star forming cores are viewed as the bottom of the structure hierarchy (see also Padoan & Nordlund 2002). Certainly, this is a much more complex description of GMCs than the simple clump and core description.

For a cloud to be truly fractal it has to have the same degree of self-similarity, as measured by its fractal dimension, over all scales. In more recent years there has been evidence that there may be a break in the self-similar nature of clouds, both in their density and velocity structure. Goodman et al. (1998) show that there is generally a break in the Larson relation (equation 1.1) at small scales, of roughly 0.1pc. By plotting the mean surface density of companions against angular separation for young stars in Taurus, Larson (1995) finds that there is a break in the clustering at 0.04pc, which corresponds to the distinction between the binary regime and that of the general clustering. The study of Blitz & Williams (1997) supports the ideas of Larson by showing that the gas too has a departure from self similarity as one approaches smaller scales. It would therefore appear that at the scale of star formation, where the final stages of cloud fragmentation occur,

the scale free nature of the gas is destroyed by the existence of a characteristic scale on which structure is ordered. Larson (1995) and Blitz & Williams (1997) suggest that this is simply the Jeans mass of the cloud controlling the fragmentation. Thus the cores in which star formation occurs might well represent the end of the self-similar regime.

Over the past 10 or so years, there has been an effort to examine the properties of star forming cores in an attempt to try and build up a picture of how and why star formation occurs. One study that has received considerable attention is the observations of Motte et al. (1998), who present the results of a submillimetre continuum mapping of the cores in ρ Ophiuchus. They find that the mass spectrum of these cores is consistent with the IMF, since they are well fitted by $\mathrm{d}N/\mathrm{d}m \propto m^{-2.5}$, for m $> 0.5\mathrm{M}_{\odot}$. Testi & Sargent (1998) find a similar result in their comparable study of the Serpens molecular cloud.

These studies imply that there exists a one-to-one mapping between the mass of a core and the mass of a star, even if the star formation efficiency of the core is not 100%. These observations support the idea that fragmentation of the clumps into a core population can produce an IMF. The fact that the slope of the mass spectrum at the high mass end is steeper than that found for clumps, as was discussed above, is again suggestive of a break in self-similarity on small scales in GMCs. However it is not certain that gravity, via the process of fragmentation, is the cause of the core mass spectrum. While the continuum emission from the dust is thought to provide accurate estimates for the mass, it contains no information as to the dynamical state of the cores. Many of the objects that are observed by Motte et al. (1998) and Testi & Sargent (1998) could well be transient features produced from turbulent flows.

1.2.2 Formation mechanisms

The formation of GMCs is an important area of research, since the manner in which GMCs form relates to the very first stage of star formation. The theories for the appearance of GMCs from the ISM fall into three groups:

1. Collisional agglomeration of smaller 'cloudlets' (Oort, 1954; Field & Saslaw, 1965; Kwan, 1979; Scoville & Hersh, 1979; Cowie, 1980; Kwan & Valdes, 1983).
2. Gravitational and thermal instabilities (Parker, 1966; Mouschovias et al., 1974; Shu, 1974; Elmegreen, 1982b,a)
3. Shock accumulation theories. (Opik, 1953; Herbst & Assousa, 1977; Kimura & Tosa, 1993; Franco et al., 1988).

It is still unclear which of these theories might represent the dominant process. Partly this is due to difficulties in defining a clear separation between the models. Although pure thermal instabilities models exist, with local thermal cooling providing a means by which condensation can occur, the main 'thermal' instability models actually refer to macroscopic motions. The cooling in such a model is the result of kinetic dissipation from collisions between 'cloudlets'. The fact that both the thermal instability and collisional agglomeration models rely on interactions between smaller clouds to produce the GMCs,

is a source of confusion when trying to identify the dominant formation mechanism. This dissipation of kinetic energy also helps large scale gravitational instabilities to set in, which in turn results in further coagulation once the collapse starts. The shock accumulation model also has problems in that it too results in conditions that increase the chance of cloud-cloud collisions.

The existence of low surface density gas in the inter-arm regions, suggest that gravity alone may not be the controlling factor in GMC formation (Heyer et al., 1998). These inter-arm clouds or, 'chaff' as they are referred to by Blitz & Williams (1999), appear to have similar properties to the high latitude clouds (HLCs) which have been discovered to lie well above the Galactic plane (Blitz et al., 1984). These clouds are known to be unbound by their internal motions. Gravity clearly cannot have played a role in their formation. Interestingly, there is evidence to suggest that they are part of the same population as the strongly self-gravitating GMCs (Heyer & Terebey, 1998), since they have essentially the same mass spectrum. The existence of these clouds would suggest that there is one mechanism responsible for the formation of all clouds, and it is unlikely to be dominated by self-gravity, at least locally on the scale of the cloud.

1.2.3 Lifetimes and dynamical states

Until the last decade or so GMCs were generally believed to be long-lived structures, with some estimates of ages reaching as high as 10^8 Myr (Solomon, Sanders, & Scoville, 1979; Scoville, Solomon, & Sanders, 1979; Scoville & Hersh, 1979). It was generally believed that the chemistry of turning atomic species into molecules would require millions of years before an object like a GMC would be detectable via its CO abundance (Jura, 1975). One also had the problem that the CO mass in the galaxy, coupled with estimates of the star formation rate, suggested that GMCs had to live for tens of millions of years if the star formation efficiency was to remain at the observed level of a few percent (Zuckerman & Evans, 1974; Zuckerman & Palmer, 1974).

One piece of observational evidence that is generally used to support the long lifetime model for GMCs it the fact that molecular clouds are seen in the inter-arm regions of the Galaxy. The implication here is that the clouds must last for a very long time if they are to only be formed in the spiral arms yet manage to survive well after the arm passage. Elmegreen (1991) objects to this argument in two ways. Firstly, he points out that the inter-arm regions do have sites of star formation, although both the clouds and the sites are much smaller than one finds in the spiral arms. These could just be bursts of secondary star formation that follow from the original burst that occurred in the spiral arms, via triggering by winds or supernovae events. The second point that he makes is that the time between successive spiral arm passages is not really that long. The arm to arm transit time in the inner Galaxy is only 100Myrs and he notes that the inter-arm time is shorter yet. Also he notes that the arm to arm transit time at our location in the Galaxy is $\sim$ 200 Myrs and very few inter-arm clouds are seen at our Galactic radius.

A short lifetime model would thus appear to be more consistent with the way in which clouds are located in the Galaxy. Recent observations of embedded clusters tend to suggest that the whole process of star formation, including GMC formation and dispersal,

occurs on roughly the crossing time for the region (Elmegreen, 2000a). Not only do most molecular clouds in the solar neighbourhood contain signs of star formation in the form of clusters, but the age determination of these clusters suggests they are very young, typically less than 10Myr (Hartmann, 2000). This suggests that star formation occurs quickly in GMCs after their formation. The fact that clusters with ages greater than ~ 5 Myr are seldom associated with molecular gas, suggests that clouds in which they form are dispersed quickly (Leisawitz, Bash, & Thaddeus, 1989).

In the original cloud lifetime proposition, it was assumed that all of the CO observed in the galaxy was associated with molecular hydrogen involved in star formation. We now realise that the vast majority of the gas that comprises a GMC is never involved in the star formation process. In fact the star formation efficiency in GMCs is only a few percent. The reason behind this lies with the fact that little of the cloud is actually dense and bound enough to turn into stars in the cloud's lifetime (Padoan, 1995; Hartmann, 1998; Zinnecker, 2002). Also, if GMCs are short-lived features then there is little time for the more tenuous parts of the cloud to get involved in the star formation via accretion.

The old GMC model also required the cloud to be supported and in virial equilibrium, since that would permit them to remain as coherent structures for as long as was necessary. This support pressure had to be in the form of non-thermal kinetic energy, such as turbulence (Larson, 1981), since the thermal energy component of these clouds is typically very small. To counteract the gravity on the large scales however requires motions which are supersonic, and it is known that these quickly damp in shocks (Mac Low et al. 1998; Stone, Ostriker, & Gammie 1998), even in the presence of magnetic fields. Thus the bound GMC model requires some method of continually driving the turbulence on the large scale. These driving mechanisms are not necessary in the short cloud lifetime model, and there also is no need to assume that the clouds are in virial equilibrium. GMCs can therefore exist in a variety of dynamical states.

Heyer, Carpenter, & Snell (2001) have examined the stability of molecular clouds in the outer galaxy and come to the conclusion that most clouds are indeed globally unbound by their internal motions. They also point out the difficulty in producing mass estimates (which a great number of papers on the subject of GMCs pass over) and note that even mass estimates determined via CO measurements (both ^{12}CO and ^{13}CO) assumes at some stage the cloud is bound. Although they do find the clouds approach dynamical stability at large masses ($> 10^5 M_\odot$), there is still considerable scatter in the data, suggesting that there is no typical dynamic state for GMCs.

Pringle, Allen, & Lubow (2001) have argued that it might also be possible to build GMCs by accumulating very low density hydrogen gas, already in a molecular state. Their study came in response to the ideas presented by Elmegreen (2000a), in an attempt to provide a new mechanism for GMC formation that can occur quickly. They point out that it is quite possible that a large fraction of the interstellar medium may be in molecular form, but either simply too low a density to be detectable by current methods or too far away from illuminating sources. The GMCs are then formed from large scale shocks, from spiral arm passage or feedback from high mass stars, such as winds and supernovae. This cloud formation can occur within a few million years. Pringle et al. (2001) also point out that GMCs are probably not in virial equilibrium, and note that their wind-swept appearance suggests that they are anything but.

1.3 Clustered star formation

When star formation occurs in GMCs, it would appear from observations that it generally occurs in the form of clusters, i.e. groups of about 10 or more stars (Lada & Lada, 2003). These groups are referred to as 'embedded', since they are still enshrouded by the gaseous reservoir out of which they condensed. A survey of L1630 in Orion concluded that between 60 to 100% of all the star formation in the cloud is occurring in just 3 rich clusters (Lada et al., 1991). Similarly, Carpenter (2000), who examined the young stellar content of 4 nearby molecular clouds, found that 50 - 100 % of the star formation was confined to embedded clusters.

If most star formation occurs in GMCs and most star formation in GMCs occurs in embedded clusters, can we say practically all star formation occurs in groups rather than in isolation? In the review of embedded clusters by Lada & Lada (2003), they combine the results of many observational surveys in an attempt to examine the properties of young stellar clusters. For the known stars within 500pc of the sun, they get an estimate of the local star formation rate to be 3×10^{-9} $M_{\odot}$ yr^{-1} pc^{-2}. This is comparable to the value of $3 - 7 \times 10^{-9}$ $M_{\odot}$ yr^{-1} pc^{-2} derived by Miller & Scalo (1979) for the field stars in the solar neighbourhood. This result suggests that embedded clusters account for practically all the star formation in the Galaxy.

This embedded phase of star formation is not thought to last for long. Although age determinations of young clusters is notoriously difficult (Tout, Livio, & Bonnell, 1999; Siess, 2001), due to the choice of pre-main-sequence tracks (PMS), age spreads are much better constrained by the use of single set of PMS tracks (Haisch et al., 2001). Embedded clusters would seem to have age spreads of less than a few Myr (e.g. the Trapezium Hillenbrand et al. 2001a), and ages of up to roughly 5 Myr. Clusters with ages older than 5Myr are rarely associated with molecular gas, suggesting that there is a dispersal time of ≤ 5 Myr which sets a time frame for the embedded phase of star formation (Lada & Lada, 2003). Typical star formation efficiencies in clusters are thought to be 10 - 30% (Carpenter et al., 1996; Phelps & Lada, 1997). All this evidence suggests that cluster formation occurs quickly and the accretion and emergence process is also fairly rapid.

The clustered environment is therefore likely to play an important role in the evolution of the young stars. Two important features of the field star population in particular are likely to be influenced by the grouping of young stellar objects: the mass distribution, or IMF, and the frequency of binary stars. Theories where stars form in isolation and have masses determined by purely local conditions may not be relevant as a general theory of star formation.

The best determination of the IMF for a young embedded cluster is that of the Trapezium cluster in Orion, containing roughly 700 stars (Hillenbrand & Carpenter, 2000; Muench et al., 2002), which is situated in front of a molecular cloud, which helps to distinguish cluster members from the background stars. The similarities between the IMF of the Trapezium and that of the stars in the field are remarkable, suggesting that the IMF of a cluster is consistent with that of the field (Muench et al., 2002). It has also been shown that there is a good agreement between the IMFs for the Trapezium, IC 348, and Ophiuchi (Luhman et al., 2000). It would therefore seem that nearly all star formation is

governed by a process that results in the distribution of masses that are described by the IMF.

There is also evidence to suggest that the binary fraction in embedded clusters matches that found for the field stars (e.g. Simon et al. 1999, Duchêne et al. 1999 and Simon et al. 1995 for the Trapezium, IC 348 and Rho Ophiuchi respectively). The low mass star forming region of the Taurus-Auriga association is unusual in that nearly all the stars are in binaries, a factor of 2 higher than the binary fraction in the Galactic field (Ghez, Neugebauer, & Matthews, 1993). There has been the suggestion that the binary fraction found in Taurus-Auriga represents the primordial result of gravitational collapse and fragmentation, such that all protostars initially appear in a binary system. The binary fraction can then be reduced via interactions with other such systems (Kroupa, 1995a,b), as one would expect in an embedded cluster. Time scales for this process in a cluster the size of the Trapezium are thought to be as little as 1 Myr or less (Kroupa et al., 1999, 2001).

The fact that both the mass spectrum of stellar objects and the binary fraction in embedded clusters are practically identical to their counterparts in the field star population, suggests that the clustering environment may play an important role in the evolution of young stellar objects. As we will discuss below, the clustering environment may actually be responsible for the form of the IMF (Bonnell et al., 2001a,b).

1.4 Numerical modelling of star formation

The fact that binaries and clusters make up so much of the stellar, and even protostellar, population suggests that the isolated star formation model is too simplistic. A full analytical model for star formation is probably out of reach. Numerical studies however can get round the difficulties of peculiar geometries, complex interactions, and non linear evolution that is associated with the formation of multiple protostars. Here we review the major advances made in numerical studies of star formation that are most relevant to the work presented in this thesis.

Most of the early numerical work focused on the fragmentation of small clouds which were close to stability (Larson, 1978). This was an attempt to find conditions under which fragmentation occurs, and results in binary formation (e.g. Boss & Bodenheimer 1979; Boss 1986, 1993). The geometries of the clouds in these studies were chosen to be close to those expected/observed for pre-protostellar cores, in that they are roughly in equilibrium and contain some form of rotation. These studies can be characterised by the parameters $\alpha = E_{thermal}/|E_{grav}|$, the ratio of thermal to gravitational energy and $\beta = E_{rot}/|E_{grav}|$, the ratio of rotational to gravitational energy. The general results are that in order to form a binary system, the cloud (or core) must have an $\alpha < 0.4$. The dependence on β is less clear. Analytic results suggest that $\alpha\beta < 0.12$, suggesting that $\beta < 0.3$. However the high resolution simulations of Tsuribe & Inutsuka (1999), suggest that the value of β is less important, with the only real constraint that the cloud be bound (i.e. $\alpha + \beta < 1$).

Since the dense structure of molecular clouds is also know to contain filaments, they have also been extensively studied as a source of binary and multiple system formation

(Bonnell et al., 1991; Monaghan, 1994; Inutsuka & Miyama, 1992). The results of these studies is that cylinders can fragment only into as many Jeans masses as they initially contain. This appears to be true for pressure bounded slabs as well (Doroshkevich, 1980; Lubow & Pringle, 1993; Clarke, 1999). A simple criterion is thus beginning to emerge: a cloud will only fragment into as many objects as it has Jeans masses initially. Furthermore, is appears that this criterion holds for a wide variety of geometries.

The internal motions and clumpy structure of GMCs has inspired the idea that star formation in molecular clouds may be triggered by collisions between clumps (e.g. Kwan 1979). Simulations of collisions between identical clumps reveal that this process can lead to the formation of binary and multiple systems, especially when the clumps are slightly offset from one another during the collision (Chapman et al., 1992; Bhattal et al., 1998). The results of these simulations suggest that it should be possible to form a wide range of binary separations and component masses via random collisions by clumps of varying size/mass etc. Gittins et al. (2003) took this process a stage further, evolving an ensemble of such clumps with random motions, the aim being to investigate the idea of building an IMF via the collisions. It was found that the majority of collisions occurred at too high a Mach number, which did not generally result in a merging of the clumps. Although it would therefore appear that this process would not be useful in building an IMF, it must be noted here that the clumps are all the same size in the simulations of Gittins et al. (2003), and thus have similar cross-sections. It is still unclear how the interaction between an ensemble of clumps of different sizes might effect these results.

In the simulations mentioned so far, the evolution is generally terminated soon after the formation of the 'protostars', however such objects are defined in the study. The properties of binaries however can evolve fairly rapidly, due to accretion from the surrounding gas such as circumbinary or circumstellar discs (Bonnell & Bastien, 1992). This process has been studied in detail by Bate & Bonnell (1997) and Bate (2000), who studied the effects on the mass ratio and separation of accretion onto an initially circular binary. The results generally concluded that accretion of low specific angular momentum gas both enhances the difference in the mass of the stars and decreases their separation. The opposite was found to be true for high momentum gas, in that the mass ratio is driven toward unity and the separation of the protostars is increased. This highlights that numerical simulations must be allowed to evolve the star formation for at least several crossing times if one is to establish the form of the binary/cluster properties.

In recent years, with advances in computing power, there has been a move away from the study of forming individual and binary stars toward simulations that follow the evolution of clusters of stars (e.g. Boss 1996 Klessen, Burkert, & Bate 1998 Bonnell et al. 1997, Bhattal et al. 1998) These have come to include some form of turbulent motions, in an attempt to mimic the conditions in star forming regions. The work of Klessen (2001) studied the effects of driven turbulence on the star forming ability of a region of gas. Since turbulence decays on the local crossing time (e.g. Mac Low et al. 1998) , Klessen (2001) constantly replenished the turbulence in his simulations, injecting the energy at specific wavelengths. He found that when the energy is injected at large wavelengths, the star formation occurs in clusters throughout the computational volume, while driving the turbulence at small scales results in a more isolated, spatially sporadic, mode of star formation. The large scale driving also results in a range of protostellar masses that is more consistent with the field IMF than is found in the simulations with small scale driving.

The highest resolution simulations conducted so far, and also those which are left to follow the evolution of the star formation the longest (at the local crossing time), are those of Bate et al. (2003a); Bate & Bonnell (2005). These simulations started from uniform spheres in which the gravitational energy was initially balanced by turbulence. Unlike the study of Klessen (2001) however the turbulence was free to decay on the crossing time, rather than being driven. The simulations form a small cluster with the protostars fragmenting out from filaments and discs. The studies showed that binary formation, including the formation of short period systems, can occur rapidly, $\leq 2t_{ff}$, resulting from a combination of the accretion process discussed by Bate & Bonnell (1997) and the removal of angular momentum via interactions. Encounters between protostars were frequent in these simulations. Most notably this gave rise to the ejection of small objects from their gaseous reservoir, thus starving them of further accretion. Practically all the sub-stellar objects formed in these simulations were ejected in this manner, suggesting that ejection may be the main method of creating brown dwarfs. The IMF in the studies was found to have a shape consistent with that for the field stars. Bate & Bonnell (2005) also concluded that the median, or characteristic, stellar mass is related to the mean Jeans mass in the cloud. The number of substellar objects is also higher when the Jeans mass is lower, but note that neither of the simulations form more stars than the initial number of Jeans masses they contain.

Although the main motivation behind many of the simulations conducted is to investigate the origin of stellar masses, this is not always as simple as one might expect. Despite the results from Bate & Bonnell (2005) that the Jeans mass effects the mass of the stars that form, is it not straight forward to prove this. The lack of ideal geometry that arises from the turbulent motions prevents one constructing simple analytical expressions for the energy of the structure in which the stars form. Essentially the complexity of the dynamics in the simulation masks the physical mechanism behind the star formation.

Recent papers have also tried to put the form of the IMF in the context of turbulent compression, suggesting that the random flows can generate the core mass spectrum which then directly maps onto the stellar IMF (Larson, 1992; Henriksen, 1986, 1991; Elmegreen, 1993, 1997, 1999, 2000b; Padoan, Nordlund, & Jones, 1997). The Jeans mass, the mass required for gravity to overcome internal thermal support, is dependent on the temperature and density, such that $m_J \propto \rho^{1/2}T^{3/2}$, for a spherical cloud of constant density. Since the gas in molecular regions is essentially isothermal, the local Jeans mass is almost completely controlled by the density. The velocity dispersion at a given length scale can thus be taken to be responsible for a range of density enhancements and in turn a series of associated Jeans masses (see section 4.2 for more details). This spectrum of Jeans masses is argued to be similar to that of the IMF (e.g. Padoan & Nordlund 2002). The IMF is then simply an extension of the same self-similar structure that is observed to characterise GMCs.

The main observational motivation for the link between turbulence and the IMF comes from the study of Motte et al. (1998) who showed that the mass spectrum of 'pre-protostellar' cores is consistent with that for stars in the same mass range. This is also similar to the density structure created by turbulence (Padoan et al., 2001). In this picture the IMF is primordial, with the final stellar mass having a close relationship with the mass of the condensation in which the star forms. However, as is noted above, the dynamical state of cores in Motte et al. (1998) is unknown. It could well be that many of these objects are simply transient density features produced by the turbulence

(Vázquez-Semadeni, Passot, & Pouquet, 1995; Ballesteros-Paredes, Vázquez-Semadeni, & Scalo, 1999b) since it is now well known that the mass spectrum of transient cores formed via turbulence can closely resemble the IMF (Padoan et al., 2001). However a recent paper by Greaves et al. (2003), which shows that there are a population of bound planetary mass clumps in ρ Oph B, suggests that further work should be done in this area.

A starkly conflicting theory, 'competitive accretion' has also been forwarded as a possible origin for the IMF (Zinnecker, 1982), in which stellar 'seeds' compete for a common gaseous reservoir. Bonnell et al. (2001a) constructed a model for the IMF based on competitive accretion which was motivated by the results of numerical studies (Bonnell et al., 1997, 2001b). In this theory, the IMF is not primordial, but has to dynamically evolve to its final state. Also, the mass of any one star depends on the influence of its neighbours. The model can produce an IMF consistent with observations, for objects with masses ≥ 0.5 $M_{\odot}$. An added feature of the model is that it naturally results in a mass segregated cluster within a few crossing times.

A problem with the simulations which include turbulence is that it is not really clear whether turbulence or competitive accretion is controlling the final mass of the stars. Obviously accretion plays some role, but the importance here is whether the gas reservoir for the stellar 'seed' is the core in which it forms, or some larger region which may contain many such cores. If many objects form in a single core (e.g. Goodwin, Whitworth, & Ward-Thompson 2004), then some local competition between the protostars may be important before the objects start to accrete from a larger region.

1.5 Outline of this thesis

As was discussed above, the exact cause and details surrounding the onset of star formation has not been identified from the simulations of Klessen (2001), Bate et al. (2003a) and Bate & Bonnell (2005). These simulations were concerned with the end states of clusters and evolving detailed interactions between young protostars. In particular, it is not clear how the structure produced by the turbulence is linked to the protostar formation.

The main aim of this thesis is to examine the origins of the star formation in small clouds, such as those studied by Bate et al. (2003a), Bate & Bonnell (2005) and Delgado-Donate et al. (2004). Consistent with these studies, we will use a Smoothed Particle Hydrodynamics (SPH) code to model the evolution of the clouds in a series of simulations. The turbulent velocity fields will also be inserted as initial conditions, just as they are in the studies above. We will then use a clump finding algorithm to identify the structure created by the turbulence, and to examine this structure's energy.

A review of the SPH technique used here can be found in chapter 2, and a description of the random velocity field generation is given in chapter 3.1. Chapter 3.2 gives a description of the clump finding algorithm that we use to examine the density structure. We also give a brief overview of some of the physical concepts, such as the Jeans mass and shock density enhancements, that will be used in much of the discussion in this thesis. This can be found in chapter 4.

We start our examination of the star formation in turbulent clouds in chapter 5 by looking at the effect of the strength of the turbulence on how the star formation proceeds. The clouds used in this study are fairly small, with masses and sizes of ~ 30 $M_{\odot}$ and 0.13 pc, respectively. We include in this discussion: an examination of the clump mass spectra; a brief look at the masses of bound clumps; and the accretion histories of the protostars (point masses) that form in the simulations. We also show that the accretion process can reveal important information as to how the star formation occurs. The next chapter (6) builds on the findings of chapter 5. Here we look more closely at the energy of the clumps as the simulations progress toward protostar formation. We use the Lagrangian nature of SPH to examine the energy state of the gas that is eventually involved in the star formation in a variety of ways. This allows us to construct a picture of how the star formation proceeds in such a turbulent environment. The motivation for this chapter is to examine the transition from unbound to bound clumps, and how this relates to the star formation. In particular, we are interested in the mass required for clumps to be bound. We also address the role that the turbulence plays in creating this bound structure.

In the last two chapters of this thesis, we explore the possibility of stars forming from unbound molecular clouds (e.g. Heyer, Carpenter, & Snell 2001). This work has been motivated by the work of Vázquez-Semadeni, Passot, & Pouquet (1995); Ballesteros-Paredes, Vázquez-Semadeni, & Scalo (1999b); Ballesteros-Paredes (2004), Vázquez-Semadeni et al. (2005), who have suggested that molecular clouds of all sizes, including GMCs, may just be transient density features in a larger scale turbulent flow. Molecular clouds may therefore exist in a variety of dynamical states.

In chapter 7, we study the nature of star formation in a small unbound cloud of ~ 30 $M_{\odot}$. Clouds of this size are comparable to the star forming cores that have been observed in Chamaeleon (Mizuno et al., 1999) and it would also appear that some of these objects are unbound by their internal motions. We concentrate our discussion on two important parameters of the clouds: the energy evolution of the cloud, and the resulting star formation efficiency. We argue that clouds (or cores) of this type may possibly be the root of the low star formation efficiency that has been observed for GMCs. The last section of the thesis, chapter 8, takes the work in the previous chapter to the size and mass scales of a typical GMC. We model a cloud of mass 1×10^5 $M_{\odot}$ and size 20pc where the internal kinetic energy in the turbulent field is twice that of the GMCs self-gravity. To get a rough idea of the star formation efficiency in this cloud, we make some assumptions about the form of the star formation in small bound regions. We also suggest that such GMCs can be the origin of OB associations, since the star forming regions in the unbound cloud, are naturally expanding away from one another.

Although magnetic fields are known to be present in star forming regions, and there is the suggestion that they are comparable in terms of energy to the turbulent motions, we do not include their effects in this PhD. It is evident from the discussion above that we do not yet properly understand the role that turbulence plays in the star formation of the mentioned simulations. Adding magnetic fields to this problem will only add to the confusion.

CHAPTER 2

Overview of Smoothed Particle Hydrodynamics

For this PhD, we use the method of Smoothed Particle Hydrodynamics, or SPH, to model the fluid in the star formation simulations. In SPH the fluid is modelled as a population of particles which are free to move with respect to one another. The particles represent the local properties of the fluid at their location, obtaining physical parameters by sampling the properties of the particles in their immediate region. This is the origin of the 'Smoothed' in SPH, since the fluid properties are evaluated by smoothing the properties of neighbouring particles.

This method was discovered independently by Lucy (1977) and Gingold & Monaghan (1977). Although SPH has come a long way since the basic prescription outlined by these first studies, it still remains a fairly rough method of integrating the fluid equations. In particular, the method is not good for problems where the details of a shock front are needed, or when one wishes to follow complex instabilities. In these problems, the grid based techniques of finite-difference schemes and PPM (Piece-wise Parabolic Method) give measurably better results.

However there are situations when SPH becomes the only method that can achieve useful results. One of its major strengths is the fact that SPH is inherently Lagrangian in nature. This by-passes the need for grids and all the associated problems, such as mesh tangling, distortion and the spurious transportation of angular momentum. Another feature of SPH is that an increase in density involves particles getting closer together, naturally providing increased resolution (provided variable smoothing lengths are involved, as is discussed below). SPH is therefore naturally suited to problems such as star formation modelling, due to the range of densities and lack of geometry associated with the gas as it evolves to form stars.

We give an overview of the SPH method in this chapter, with emphasis on the implementation of Benz (Benz et al., 1986; Benz & Hills, 1987; Benz et al., 1990) used for the simulations in this thesis. More general discussions of the SPH method can be found in Benz (1990), Monaghan (1992) and Morris (1994).

2.1 The basic formalism

Consider a physical parameter A, which varies in space such that $A = A(\mathbf{r}')$. The value of $A(\mathbf{r}')$ at a point $\mathbf{r}' = \mathbf{r}$ can thus be given by,

$$A(\mathbf{r}) = \int A(\mathbf{r}')\delta(\mathbf{r} - \mathbf{r}')\mathrm{d}\mathbf{r}' \tag{2.1}$$

If we replace the delta function with a one which is more spread out in space, an interpolating kernel, $W(\mathbf{r}', \mathbf{h})$, we have,

$$A_i(\mathbf{r}) = \int A(\mathbf{r}')W(\mathbf{r} - \mathbf{r}', h)\mathrm{d}\mathbf{r}' \tag{2.2}$$

where h is measure of the linear extent of W. $A_i(\mathbf{r})$ now denotes the interpolated value of A at the point $\mathbf{r}$. It is thus a 'smoothed' version of $A(\mathbf{r})$. For the above to be true, the kernel must satisfy,

$$\int W(\mathbf{r} - \mathbf{r}', h)\mathrm{d}\mathbf{r}' = 1 \tag{2.3}$$

and

$$\lim_{h \to 0} W(\mathbf{r} - \mathbf{r}', h) = \delta(\mathbf{r} - \mathbf{r}') \tag{2.4}$$

In SPH, the fluid is represented as a discrete population of particles. The properties of the fluid are evaluated by integrating the contributions of the neighbouring particles, each weighted by the interpolating function W. Since we are dealing with a series of discrete points rather than a full spectrum, we replace the integral in the above analysis with a summation over the particles, at positions $\mathbf{r}_b$:

$$A_i(\mathbf{r}) = \sum_b A_b \frac{m_b}{\rho_b} W(\mathbf{r} - \mathbf{r}_b, h) \tag{2.5}$$

where m_b and ρ_b are the mass and density, respectively, of particle b . We see from 2.5 that the kernel has physical units of inverse volume.

2.2 Gradients

One method of evaluating the gradient of a field can be given simply by,

$$\nabla A_i(\mathbf{r}) = \sum_b A_b \frac{m_b}{\rho_b} \nabla W(\mathbf{r} - \mathbf{r}_b, h) \tag{2.6}$$

but one tends to use,

$$\nabla A_i(\mathbf{r}) = \frac{1}{\rho}[\nabla(\rho A) - A\nabla\rho] \tag{2.7}$$

$$= \frac{1}{\rho_a}\sum_b m_b(A_b - A_a)\nabla W(\mathbf{r} - \mathbf{r}_b, h) \tag{2.8}$$

where the gradient in A is used explicitly since this is more accurate. This method is less susceptible to particle disorder.

From here on we will use

$$W_{ab} = W(\mathbf{r}_a - \mathbf{r}_b, h) \tag{2.9}$$

and let $\nabla_a W_{ab}$ denote the gradient of W_{ab} taken with respect to $\mathbf{r}_a$. We will use a similar notation for other quantities, such as $\mathbf{v}_{ab} = \mathbf{v}_a - \mathbf{v}_b$. We will also drop the i subscript, and assume that our interpolated values are equivalent to the actual value at position $\mathbf{r}_a$.

2.3 Fluid Properties

Using 2.5, the density at a point $\mathbf{r}$ can be given by,

$$\rho(\mathbf{r}) = \sum_b m_b W(\mathbf{r} - \mathbf{r}_b, h) \tag{2.10}$$

Each SPH particle has its mass smoothed out in space, and to find the density at the point $\mathbf{r}$, one simply adds the contributions from the surrounding particles. Provided the number and masses of the particles remains constant in the simulation, the continuity equation is explicitly satisfied. Obviously edge effects will be present, and a particle near a free boundary will always have its density underestimated by the use of 2.10. For situations where free boundaries are important or the particle mass needs to change, it is possible to introduce a $\mathrm{d}\rho(\mathbf{r})/\mathrm{d}t$ term (see Morris 1994 for a discussion) but for our purposes this will not be necessary.

The pressure of the fluid is defined via an equation of state. The equation of state used in this these is the simple case of an isothermal fluid,

$$p = c^2\rho \tag{2.11}$$

where c is the sound speed.

In our simulations the total energy is not conserved since $p\mathrm{d}V$ energy is assumed to be perfectly radiated away rather than converted into heat. As a result the particle energy, and thus sound speed, is always constant. The energy equation is thus redundant for the work in this thesis but we include it below for completeness.

2.4 The momentum equation

The particles are moved by,

$$\frac{\mathrm{d}\mathbf{r}_a}{\mathrm{d}t} = \mathbf{v}_a \tag{2.12}$$

and

$$\frac{\mathrm{d}\mathbf{v}_a}{\mathrm{d}t} = -\frac{1}{\rho_a}(\nabla p)_a \tag{2.13}$$

The obvious method of evaluating the pressure gradient is to use 2.7 to obtain,

$$(\nabla p)_a = \frac{1}{\rho_a}\sum_b m_b(p_b - p_a)\nabla_a W_{ab}. \tag{2.14}$$

However this does not conserve linear and angular momentum exactly. Instead, the preferred method (and that used here) is to use,

$$\frac{\nabla p}{\rho} = \nabla\left(\frac{p}{\rho}\right) + \frac{p}{\rho^2}\nabla\rho \tag{2.15}$$

which when used in 2.13 gives,

$$\frac{\mathrm{d}\mathbf{v_a}}{\mathrm{d}t} = -\sum_b m_b\left(\frac{p_a}{\rho_a^2} + \frac{p_b}{\rho_b^2}\right)\nabla_a W_{ab} \tag{2.16}$$

Since this equation is symmetric when swapping the dummy indices, the momentum is explicitly conserved. There are two other features of the code, namely the use of multiple particle time-steps and tree node gravity, that cause the momentum equation to lose its symmetry. In practice however, these do not tend to be a major problem.

2.5 The energy equation

The equation for the evolution of the energy per unit mass in an inviscid, ideal, fluid is given by the first law of thermodynamics,

$$\frac{\mathrm{d}u}{\mathrm{d}t} = -\frac{p}{\rho}\nabla\cdot\mathbf{v} \tag{2.17}$$

which can be translated into the SPH form by using 2.7 to get,

$$\frac{\mathrm{d}u_a}{\mathrm{d}t} = \frac{p_a}{\rho_a^2} \sum_b m_b \mathbf{v}_{ab} \cdot \nabla_a W_{ab} \tag{2.18}$$

Benz (1990) and Morris (1994) show that the above form conserves energy explicitly by showing that the total energy of the ensemble is given by a function which is symmetric in a and b.

2.6 Capturing shocks with artificial viscosity

All the equations derived thus far were for an inviscid fluid. As a result, they are not capable of evolving the fluid accurately when shocks are present, since there is no method of converting the kinetic energy that would be dissipated in shocks into heat. The mechanism that takes care of kinetic energy dissipation in a real fluid is viscosity, and we therefore need to add something similar to our fluid equations if shocks are to be treated in the simulations. In astrophysical fluids, this viscosity is very small such that the fluids are essentially inviscid and only really becomes important in shocks. We thus need a form of viscosity for our fluid that is zero except in the presence of shocks.

This is done in SPH with 'artificial viscosity', which is 'artificial' in the sense that it is invoked only when it is needed. The most commonly used form of artificial viscosity, and the one implemented in this code, is the viscous pressure,

$$\Pi_{ab} = \begin{cases} \frac{-\alpha \bar{c}_{ab} \mu_{ab} + \beta \mu_{ab}^2}{\bar{\rho}_{ab}} & \mathbf{v}_{ab} \cdot \mathbf{r}_{ab} \leq 0 \\ 0 & \mathbf{v}_{ab} \cdot \mathbf{r}_{ab} \geq 0 \end{cases} \tag{2.19}$$

where

$$\mu_{ab} = \frac{h \mathbf{v}_{ab} \cdot \mathbf{r}_{ab}}{\mathbf{r}_{ab}^2 + 0.01 h^2} \tag{2.20}$$

and $\bar{\rho}_{ab} = \frac{1}{2}(\rho_a + \rho_b)$ and $\bar{c}_{ab} = \frac{1}{2}(c_a + c_b)$. The factor $0.01h^2$ is included to prevent μ_{ab} from diverging when $\mathbf{r}_{ab}$ is very small.

The viscosity tensor Π_{ab} in the code is actually the combination of two viscous pressures, which have the form,

$$P_\alpha = \Pi_\alpha \rho^2 = -\alpha \rho l c \nabla \cdot \mathbf{v} \tag{2.21}$$

and

$$P_\beta = \Pi_\beta \rho^2 = -\beta \rho l^2 (\nabla \cdot \mathbf{v})^2 \tag{2.22}$$

where α and β are free parameters which control the strengths of the viscous pressure. The parameter l is the length scale over which the shock is spread. In SPH this is given

the value of the smoothing length h, such that shocks will always be $\sim h$ in size. The first α pressure provides bulk and shear viscosity. The second, involving the β parameter, is required to provide sufficient damping in shocks and is a standard second-order, von Neumann-Richtmyer-type, viscosity. The β viscosity is required for preventing particle inter-penetration in the shocked region. Bate (1995) showed that $\alpha = 1$ and $\beta = 2$ gives good all round performance, since it provides a compromise between particle inter-penetration and shock size and we therefore use these values for the work in this thesis. The fact that the viscosity is only non zero for colliding flows (i.e. $\mathbf{v}_{ab} \cdot \mathbf{r}_{ab} \leq 0$ ensures that it only appears in shocks and is zero for the rest of the fluid.

Since the viscosity converts kinetic energy into heat, we need to modify both the momentum and the energy equations accordingly. The momentum equation (2.16) becomes,

$$\frac{\mathrm{d}\mathbf{v_a}}{\mathrm{d}t} = -\sum_b m_b \left(\frac{p_a}{\rho_a^2} + \frac{p_b}{\rho_b^2} + \Pi_{ab} \right) \nabla_a W_{ab} \tag{2.23}$$

and the energy equation (2.18) becomes,

$$\frac{\mathrm{d}u_a}{\mathrm{d}t} = \frac{p_a}{\rho_a^2} \sum_b m_b \mathbf{v}_{ab} \cdot \nabla_a W_{ab} + \frac{1}{2} \sum_b m_b \Pi_{ab} \mathbf{v}_{ab} \cdot \nabla_a W_{ab} \tag{2.24}$$

For the case when the polytropic equation of state is used, the entropy is evolved instead of the internal energy. The internal energy is then given explicitly by,

$$u = \frac{K}{\gamma - 1} \rho^{\gamma - 1} \tag{2.25}$$

The expression for the time evolution of the entropy is then,

$$\frac{\mathrm{d}K_a}{\mathrm{d}t} = \frac{\gamma - 1}{2\rho_a^{\gamma - 1}} \sum_b m_b \Pi_{ab} \mathbf{v}_{ab} \cdot \nabla_a W_{ab} \tag{2.26}$$

2.7 The form of the interpolating kernel

Provided that the expressions 2.3 and 2.4 are satisfied, the SPH kernel can take many different forms. The original kernel (Gingold & Monaghan) in three-dimensions had the form of a spherical Gaussian,

$$w(r,h) = \frac{1}{\pi^{3/2} h^3} exp(-v^2) \tag{2.27}$$

where $r = |\mathbf{r} - \mathbf{r}'|$ and $v = r/h$. Unfortunately, all the particles in the simulation contribute to the fluid properties at $\mathbf{r}$ and this results in a poor use of computational resources.

In this code, we use a spline kernel developed by Monaghan & Lattanzio (1985). The kernel has 'compact support', meaning that it becomes zero at a finite radius, and so the evaluation of the fluid properties at $\mathbf{r}$ only requires summation over a sub-set of the simulation particles. The kernel has the form,

$$W(r,h) = \frac{\sigma}{h^d} \begin{cases} 1 - \frac{3}{2}v^2 + \frac{3}{4}v^3 & \text{if } 0 \leq \mathrm{v} < 1, \\ \frac{1}{4}(2-v)^3 & \text{if } 1 \leq \mathrm{v} < 2, \\ 0 & \text{otherwise} \end{cases} \tag{2.28}$$

where d is the number of spatial dimensions and σ is the normalisation constant, with values of $2/3$, $10/(7\pi)$ and $1/\pi$ in one, two and three dimensions respectively. All the simulations in this thesis have three spatial dimensions.

A consequence of the compact support is that the summations in the SPH equations above are only performed over a sub-set of the particle population: those within $2h$ for the spline kernel above. These particles (the b's in the notation used here) are termed the 'neighbours' of particle a. We shall come to see how the neighbour lists are worked out in 2.10.

2.8 Variable smoothing lengths

In the SPH technique, the smoothing length h is the scale by which the fluid properties can be resolved. Allowing each particle to vary its smoothing length in time permits the code to automatically adjust its resolution. For example, SPH provides a density increase by increasing the number of particles inside a fixed volume. By allowing the particles to reduce their smoothing lengths as they enter regions of increasing density, the code is then able to maintain resolution inside the dense regions. Similarly, in regions of low density, the code can increase the smoothing lengths to prevent particles from becoming isolated and having no neighbours. Since regions of low density have few particles, it makes sense that the resolution length in these regions is larger than in regions of high density, as there are fewer points (the particles) providing a description of the fluid. With variable smoothing lengths, SPH becomes mass limited in resolution, whereas grid based codes are spatially limited in resolution.

To introduce the variable smoothing length into the SPH formalism, we simply replace the h with $h = h(\mathbf{r}_a, \mathbf{r}_b)$. This takes the form of a new averaged $h_{ab} = 0.5(h_a + h_b)$, where the subscript denotes the intrinsic h of each particle. The fact that h_{ab} is symmetric for each pair of particles, ensures that momentum and energy are explicitly conserved.

Since the smoothing length is now dependent on both position and time, new terms should appear in the SPH equations, since,

$$\nabla_a W_{ab} = -\frac{1}{u}\frac{\partial W}{\partial u}\mathbf{u} + \frac{\partial W}{\partial h}\nabla_a h \tag{2.29}$$

where $\mathbf{u} = \mathbf{r}_a - \mathbf{r}_b$. The new terms involving the gradient of the smoothing length should ideally be included in the SPH equations, and similar terms should appear when consider-

ing time derivatives. These terms however are difficult to estimate and are generally not included in SPH codes. It has been shown that provided h varies on a scale similar to that of the other variables, the errors are of $O(h^2)$ (Evrard, 1998).

We now need some method by which to decide upon and evolve the smoothing lengths. The most common method is to adjust the smoothing length such that the number of particles is roughly constant. In 3-dimensions, the number of desired neighbour is generally 50 particles. This provides a compromise between sufficient accuracy in evaluating the fluid parameters and computational efficiency. For our spline kernel (2.28) this means that within $2h$, we desire each particle to have 50 neighbours.

The obvious way to determine the smoothing length is use the density,

$$h = h_o \left(\frac{\rho_o}{\rho} \right)^{1/3} \tag{2.30}$$

where ρ_o and h_o are the initial particle density and smoothing length respectively. This however requires knowledge of the density, which is a problem since we need the smoothing length to find the local density. Using the density from the previous time-step is fine for situations where the density is not varying quickly, but not a good approximation in shocks.

In this code we instead adopt the alternative method given by Benz (1990). First, we take the derivative of 2.30,

$$\frac{\mathrm{d}h}{\mathrm{d}t} = -\frac{1}{3}\frac{h}{\rho}\frac{\mathrm{d}\rho}{\mathrm{d}t} \tag{2.31}$$

and make use of the continuity equation to replace the time derivative of the density,

$$\frac{\mathrm{d}h_a}{\mathrm{d}t} = -\frac{1}{3} h \nabla \cdot \mathbf{v}_a \tag{2.32}$$

This equation is then added to the other time derivatives to be updated at each time-step. This equation is used to keep the smoothing length such that the number of neighbours is in the range of 30 to 70. Generally, 2.32 evolves the smoothing length very well. If however the method does begin to fail, and the number of neighbours starts to stray to close to the upper or lower limits, then we replace 2.32 with,

$$\frac{\mathrm{d}h_a}{\mathrm{d}t} = \frac{\exp(\mathrm{x})(\mathrm{h}\nabla \cdot \mathbf{v}_\mathrm{a})/3 \pm \exp(-\mathrm{x})2\mathrm{h_a}}{\exp(\mathrm{x}) + \exp(-\mathrm{x})} \tag{2.33}$$

where $+$ is chosen if the smoothing length is to increase and $-$ is chosen if the smoothing length is to decrease. The exponent is

$$x = \begin{cases} (N_{upper} - N_n)/(0.3 n_{range}) & \text{if } (\mathrm{N_{upper}} - \mathrm{N_n}) < \mathrm{n_{range}}, \\ (N_n - N_{lower})/(0.3 n_{range}) & \text{if } (\mathrm{N_n} - \mathrm{N_{lower}}) < \mathrm{n_{range}}, \\ \infty & \text{otherwise} \end{cases} \tag{2.34}$$

where N_{upper} and N_{lower} are the upper and lower bounds on the number of neighbours that we wish a particle to have (70 and 30 respectively, from above), and n_{range} is 12 in 3-dimensions.

We discuss how the neighbours for each particle are found in section 2.10.

2.9 Gravitational forces

To study star formation, our fluid code must include a method of evaluating self-gravity. In this code, it is the method described by Benz (1990) that is used. This method uses that fact that the kernel can be interpreted as a particle's density distribution, which in this case is spherical. We start with Poisson's equation,

$$\nabla^2\phi = \frac{1}{r^2}\frac{\mathrm{d}}{\mathrm{d}r}\left(r^2\frac{\mathrm{d}\phi}{\mathrm{d}r}\right) = 4\pi G\rho \tag{2.35}$$

The usual solution of this equation for a pair of particles has the form,

$$-(\nabla\phi_a)_b = -G\frac{M(r_{ab})}{r_{ab}^2}\frac{\mathbf{r}_{ab}}{r_{ab}} \tag{2.36}$$

Normally, for a pair of point masses the term with the mass in the numerator is simply the mass of particle b. In the SPH formalism however the mass of a particle is smoothed out, with the density distribution controlled by the kernel. This means that the mass term is a function of position, such that,

$$M(r_{ab}) = 4\pi\int_0^{r_{ab}} u^2\rho(u)\mathrm{d}u = 4\pi\int_0^{r_{ab}} u^2 W(u, h_{ab})\mathrm{d}u \tag{2.37}$$

To evaluate the total gravitational force on a particle a, we therefore have,

$$-\nabla\phi_a = -G\sum_{b=1}^{N}\frac{M(r_{ab})}{r_{ab}^2}\frac{\mathbf{r}_{ab}}{r_{ab}} \tag{2.38}$$

where N in the summation denotes the sum over all other particles in the simulation. Note that this term is different to all the other SPH terms, where summations are performed only over the neighbouring particles. We thus have a problem that the gravitational term requires a process that computationally scales as $N^2/2$, where N is the number of particles that represent the computational volume.

The code gets around the N^2 problem by using an hierarchical tree to evaluate the gravitational forces. A binary tree is used here, which was written by Press (e.g. see Benz et al. 1990). The idea behind a binary tree is very simple. It takes all the particles and sorts them into pairs of mutual nearest neighbours (i.e. it pairs each particle with its closest companion). It then creates a 'node' at the position of the centre of mass of

the two particles. Once this is done for all the particles, the process is repeated for the nodes themselves, again creating new larger nodes from pairs of the smaller nodes. This is repeated until eventually the simulation contains only one node, which contains the combined information of all the particles in the simulation. Note that the binary tree is inverted, such that it is constructed from the particle level up to the whole simulation. An octal tree in contrast, starts by breaking the whole simulation into eight equal zones, then keeps splitting each zone into eight new zones until each particle has a zone to itself.

The nodes in the binary tree have mass $M_{node} = M_a + M_b$ and are given a smoothing length, $h_{node} = \mathrm{MAX}(\mathrm{h_a}, \mathrm{h_b})$, where a and b denote the constituent nodes or particles that make up the new node. The nodes are also given a radius which is set by ensuring that all constituent nodes are contained within this radius, measured from the centre of mass of the node. This is defined in our code by,

$$R_n = \mathrm{MAX}\left(\frac{M_a}{M_{node}} R_{ab} + R_b, \frac{M_b}{M_{node}} R_{ab} + R_a\right) \tag{2.39}$$

The node structure can now be used to assist the gravitational forces calculation. Nodes that are sufficiently far away from the particle under evaluation, can be incorporated into the calculation as a full object, rather than broken up into its constituent particles. Since the node is not a point mass but rather an extended object, the contribution of the node to the particle's gravitational force must be calculated using the node's quadrupole moment. This moment is calculated while the node is being created.

The code decides whether or not a node should be expanded by the relation,

$$\frac{R_{node}}{r_{a\ node}} < \theta \tag{2.40}$$

where a is the particle, $r_{a\ node}$ is the distance between the particle a and the node in question and θ is some opening angle. In the limit that $\theta \to 0$, all the nodes are opened. and the tree reverts to the usual $N^2/2$ operation. As θ is increased, then nodes increasingly closer to the particle are left unopened and contribute to the force calculation via the quadrupole moment approximation. A value of $\theta = 0.5$ is used for the work in this thesis, and has been found to give negligible errors (e.g. Bate 1995). Obviously the criterion of 2.40 may not necessarily apply to the whole node, in that while a node may need to be opened, its constituent node may satisfy 2.40 and can thus remain closed. In this manner, the code only opens the required nodes.

The use of the smoothing length to determine the mass distribution of the particles is desirable for the SPH self-gravity, since it provides a natural softening of the potential which prevents divergence of the force for small particle separations. However, since our smoothing length is also variable in time and space, we have the problem that 2.36 no longer conserves energy, and changes the zero point of the gravitational energy of the system. Benz (1990) showed that this can be given by,

$$\mathrm{d}H = -G \sum_{a<b} m_a m_b \frac{\partial \phi}{\partial h_{ab}} \mathrm{d}h_{ab} \tag{2.41}$$

where ϕ is the smoothed potential found from 2.35. This difference in the gravitational energy is included in the code we use.

2.10 Finding neighbour lists

The use of a tree to sort the particle distribution for the gravity calculation can also be used to evaluate the neighbour lists. The neighbour lists can therefore be evaluated while the code is working out the gravitational forces. This introduces a new condition for the opening of a node (along with 2.40), since constituent particles may be neighbours of particle a if,

$$R_{node} + h_a + h_{node} < r_{a\ node} \tag{2.42}$$

The particles in the expanded node are then checked to see if they satisfy $r_{ab} \leq 2h_{ab} = h_a + h_b$.

2.11 Time integration and individual particle time-steps

The code uses a second order Runge-Kutta-Fehlberg method (Fehlberg, 1968) which was first suggested for SPH integration by Benz (1984). The Felhberg modification to the original scheme was the inclusion of a tolerance parameter which can be used to let the integrator control the time-step. The code examines the difference in several fluid properties in order to assess the time-step that governs the evolution of the fluid. The properties used for the error determination are the particle's velocities, acceleration, internal energy and smoothing lengths. The global time-step is then given by,

$$\delta t_{RKF} = \sqrt{\frac{512 \delta t_{old} \lambda}{|Q_{new} - Q_{old}|}} \tag{2.43}$$

where Q is each of the physical quantities mentioned, λ is the tolerance parameter and t_{RKF} and t_{old}, are the new and old time-steps respectively. This is evaluated for all particles in the simulation and the minimum value is used to evolve the entire particle population.

For simulations where all the particles are involved in similar magnitudes of interaction, this method allows the gas to be evolved efficiently. In a typical star formation simulation this is unfortunately not the case. The process of gravitational collapse ensures that some particles are not only much denser than others but are experiencing much stronger forces. The minority of particles directly involved in the star formation thus control the time-step for which all particles are advanced. Considerable computational resources are thus wasted, on evolving most particles with time-steps that are much smaller than necessary.

The code we use gets around this problem by integrating each particle with its own time-step (Bate, 1995). In this manner, no particles are integrated with more accuracy than is needed, resulting in a considerable saving in calculation time. Rather than letting every particle have whatever time-step it likes, the code has a fixed set of possible time-steps, into which the particles are binned. This ensures that there are as many particles as possible being evolved at once. The spectrum of possible time-steps is given in this code by integer multiples of 2, in the manner $\delta t = \delta t_{sync}/2^n$, where t_{sync} is the synchronisation time, or the largest time-step possible, and n is the integer power defining the required time-step. This use of integers in defining the time-step overcomes the problem of rounding errors. For standard FORTRAN integers, the code then has a total time-step range of 2^{20}.

In order to ensure the correct integration of the system, two more time-step constraints are necessary. The first is the Courant Condition,

$$\delta t_{cc} = \frac{0.3h}{c_s + h|\nabla \cdot \mathbf{v}| + 1.2(\alpha c_s + \beta h|\nabla \cdot \mathbf{v}|)} \tag{2.44}$$

where α and β are the two artificial viscosity parameters. The last term in the denominator is only included if $\nabla \cdot \mathbf{v} < 0$. The term $\nabla \cdot \mathbf{v}$ can be evaluated from 2.7. The Courant condition ensures that numerical transportation of information is faster than the physical rate, i.e. the sound speed.

The individual particle time-step system does not always react quickly enough to rapidly changing fluid properties, such as those involved in shocks. Monaghan suggests a new force constraint to the time-step where,

$$\delta t_{force} = 0.3\sqrt{\frac{h}{|\mathbf{f}|}} \tag{2.45}$$

and $\mathbf{f}$ is the net acceleration on the particle. When this is added to the time-step evaluation, the individual and common particle time-step methods converge.

2.12 The inclusion of 'Sink' particles

When gravitational collapse occurs, SPH particles move toward the focus of the collapse. Obviously this results in high densities and thus small separations between neighbouring particles. The forces in such a densely packed environment are much larger than in the rest of the cloud and eventually the time-steps for the particles at the centre of the dense region become so small that the code spends all its time evolving the very dense region. The rest of the cloud is not evolved at all and the simulation grinds to a halt.

In order to simulate star formation we must therefore find a way round this problem. As it happens, the details of the very dense inner regions, such as the structure of the protostar, are not generally of interest to current star formation work, which instead focuses more on how and where the collapse occurs, and what gives rise to collapse in the first place, i.e. the initial conditions for star formation. The equation of state governing the

dynamics in the protostar/disc system are also unknown. Also one is generally interested in how much mass, or momentum, ends up in a particular star. These are very rough details of the collapsing object and do not require a detailed evolution of their internal workings. We can thus neglect the evolution of a protostar beyond a certain density, and treat it as essentially a spherical region that can accrete gas and interact with other such spheres via gravity.

This code includes the modification by Bate et al. (1995) which does just that: dense, bound, regions of gas are replaced by point masses, or 'sink particles'. The sinks interact only via gravity but are able to accrete gas particles within their accretion radius, r_{acc}. These sinks allow the code to model the dynamical evolution of accreting protostars, without integration times becoming prohibitively small.

Sink particles are not really added to the code in the sense that a new particle is introduced, but instead a normal SPH particle is turned into a sink particle once certain criteria have been met. The particle undergoes as series of tests once it has reached a threshold density. Once this density is reached, two preliminary tests are conducted. The first is to see whether the smoothing length of the particle is less than half the accretion radius of the sink particle that it will become. This ensures that when the sink particle forms it can instantly accrete at least ~ 50 neighbouring particles. The second test is to make sure that the potential sink particle and its neighbours are on the same integration time-step.

Once these two conditions are met, the dynamical state of the possible sink particle and its neighbours are assessed to ensure that the particles are indeed undergoing gravitational collapse and are not about to re-expand from their dense state. This takes the form of a further four tests. Firstly,

$$\alpha \leq \frac{1}{2} \tag{2.46}$$

where α is the ratio of the thermal energy to the magnitude of the gravitational energy of the particles. Secondly,

$$\alpha + \beta \leq 1 \tag{2.47}$$

where β is the ratio of rotational energy to the magnitude of the gravitational energy. The third condition is that the total energy of the particles must be negative, and finally the forth test is that the divergence of the accelerations must be less than zero. The final check ensures that the group of particles is not in the process of being tidally disrupted or bouncing. If all these tests are passed, the particle becomes a sink and the mass, momentum (both linear and angular) of the neighbours is added to the sink particle.

The accretion onto the sink particles is controlled by the accretion radius, r_{acc} mentioned above. This is chosen before the start of the simulation and depends on the resolution required. Any gas (SPH) particle that passes through the volume about a sink particle defined by this radius is checked to see whether is should be accreted by the sink. First, the gas particle must be bound to the sink. Second, the specific angular momentum

of the gas particle must be less than than that required to form a circular orbit at r_{acc} about the sink particle. These tests ensure that particles on highly eccentric, parabolic or hyperbolic orbits, that would normally leave the accretion volume are not accreted by mistake. Finally, the gas particle must be more tightly bound to the candidate sink particle than any other for which it meets the above criteria. Care must also be taken to ensure that the accretion occurs when both the sink particle and the gas particle are on the same time-step. When the particle is finally accreted, its mass and linear momentum are added to the sink particle, and the sink particle's position is shifted to the centre of mass of the two particles. Finally the 'spin' of the sink is updated to take into account of the angular momentum of the orbiting gas particle. This 'spin' is never used in any of the calculations and is only kept for studying momentum transport and ensuring the code is keeping track of angular momentum sufficiently well.

An important feature of the sink particles, and one which makes them fairly easy to implement into an SPH code, is that they only interact with other particles, that is both gas and other sink particles, via the force of gravity. Also, gas particles on one side of a sink do not interact with the gas particles on the other side. The sharp boundary caused by the removal of gas particles inside the accretion radius can have an adverse effect on the accretion rates when one is studying discs etc. Since this is not really a relevant problem for this thesis we will not mention this any further but simply point the reader to Bate et al. (1995) for a discussion of the necessary boundary corrections. The sink-sink interactions in this thesis are smoothed with a standard gravitational smoothing term,

$$f = -\frac{Gm_a m_b}{(r_{ab}+\epsilon)^2}\frac{\mathbf{r}_{ab}}{|r_{ab}|} \tag{2.48}$$

where ϵ is set to some small value and defines the minimum separation for a binary system. In this thesis, ϵ is generally set to equal the accretion radius (r_{acc}) of the sinks.

2.13 Resolution requirements

Using the kernel 2.28 to provide the gravitational softening in 2.36, Bate & Burkert (1997) found that SPH can accurately handle fragmentation if the local Jeans mass is always resolved by roughly $2N_{neigh}$ particles, where N_{neigh} is the number of neighbouring particles inside a smoothing length. If this condition is not met, there is a concern that numerically artificial fragmentation may arise from the collapse of spurious substructure. While this was shown to be a problem for highly idealised geometries, such as those studied in Bate & Burkert (1997), failure to resolve the Jeans mass properly is generally regarded as merely preventing possible fragmentation (Whitworth, 1998). This has been confirmed by Klessen and Bonnell (2004, both private communications) who confirm that higher resolution generally results in more aggressive fragmentation. This is simply a result of the increased ability to resolve substructure and perhaps even angular momentum transport.

It is generally desirable for fragmentation calculations to have a resolution down to the 'opacity limit' (Low & Lynden-Bell, 1976; Rees, 1976), the minimum mass for fragmentation. This requires resolving self-gravitating objects down to a mass of $\sim 10^{-3}\mathrm{M}_{\odot}$.

The simulations presented in this thesis do not however achieve this resolution, since we feel that high resolution is not particularly important for the work that we wish to do here. In this thesis we are interested in the effect that the turbulent field has on producing the seeds for fragmentation.

Our investigation of the effects of turbulence on the star formation does however introduce a certain constraint on the resolution. Our simulations all contain some form of turbulent motions (see chapter 3.1 for a discussion), which are present in a gas that has an isothermal equation of state. The shocks that occur from the supersonic motions are therefore responsible for density enhancements that follow the standard isothermal jump conditions, such that $\rho = \rho_o \mathcal{M}^2$, where ρ_o is the pre-shock density and $\mathcal{M}$ is the Mach number of the turbulence. We therefore must ensure that we resolve the Jeans mass in the density enhancements induced by the turbulence. This Jeans mass will be referred to in this thesis as $m_{J,turb}$. With the exception of that modelling a GMC, all our simulations are able to resolve this Jeans mass, typically by at least an order of magnitude.

To ensure that we do not attempt to resolve beyond our resolution limit, we introduce sink particles at the point where the mass resolution for the simulation is reached. The mass resolution is used as a Jeans mass, and from that a density and Jeans radius is evaluated. These are used for the sink particle creation density threshold and sink accretion radius respectively. Details of these parameters are given in the thesis where necessary.

CHAPTER 3

Generating turbulence and examining the density structure

3.1 The inclusion of turbulent velocity fields

As was discussed in the opening chapter of the thesis, the molecular clouds in which stars form are know to contain a significant amount of energy in the form of random, or turbulent, motions. One of the main focuses of this PhD is to identify the role that these motions play in the star formation, so we require some method by which to include them in our simulations.

Observations of line widths are usually expressed in the form,

$$\sigma \propto \lambda^{\xi} \tag{3.1}$$

where σ denotes the velocity dispersion and λ the size scale to which the velocity dispersion relates. The value of ξ is not that well constrained, and can vary from region to region. Larson found a value of $\xi = 0.37$ for a range of scales $1 < \lambda < 1000$pc, while looking at smaller scales, Myers (1983) found $\xi = 0.5$ for $0.04 < \lambda < 10$pc. Goodman et al. (1998) demonstrated that the value of ξ can even change when one uses a different tracer species to measure the line-widths, and that for a single cloud, a single value of ξ may not hold over all scales.

In this PhD we will generally assume a value of $\xi = 0.5$ for the velocity dispersion, since we are generally dealing with smaller structures than those included in the original Larson relation study. When dealing with turbulence, it has become normal practice to express the velocity-scaling relation in the language of spectra analysis, in which the velocity field corresponds to a Gaussian random field with a power spectrum given by,

$$P(k) \equiv \langle |\mathbf{v}_k|^2 \rangle \propto k^{\alpha} \tag{3.2}$$

Unfortunately there is no linear relationship between ξ and α. However the work of Myers & Gammie (1999) show that an α of -4 in the power spectrum corresponds to a ξ of 0.5. This value of α is consistent with the observations and so is adopted for the turbulence in our simulations. We also use a larger α of -6 in one simulation, to provide

a comparison of the nature of the turbulent field. According to Myers & Gammie (1999) this simulation has an effective ξ of 0.95.

To obtain a random realisation of a turbulent velocity field that conforms to expression 3.2, we use a code developed by Bromm that is based on a method to provide Gaussian random density structures. The details below follow from the studies of Dubinski et al. (1995) and Myers & Gammie (1999) as well as details from the actual code.

The first stage is to assume a divergence-free incompressible gas, such that $\nabla \cdot \mathbf{v} = 0$. It follows from this that the velocity can now be expressed in terms of a velocity potential vector, $\mathbf{A}$:

$$\nabla \times \mathbf{A} = \mathbf{v} \tag{3.3}$$

The components of $\mathbf{A}$ can also be described in terms of a Gaussian random field. By comparing the expressions 3.2 and 3.3, one can show that the power spectrum of the vector potential $\mathbf{A}$ is,

$$P_A(k) \equiv \langle |\mathbf{A}_k|^2 \rangle \propto k^{\alpha-2} \tag{3.4}$$

The code samples the components of the Fourier transform of the vector potential at equally spaced points on a lattice of size N^3, where N is a power of 2. In Fourier space, $\mathbf{A}_k$ is described in terms of its amplitude $\mathbf{a}_k$ and phase ϕ_k and has the form $\mathbf{A}_k = \mathbf{a}_k e^{i\phi_k}$, where $k = \sqrt{k_x^2 + k_y^2 + k_z^2}$. Amplitudes are randomly sampled from a Rayleigh distribution:

$$D(\mathbf{a}_k) = \frac{\mathbf{a}_k}{s^2} e^{\frac{\mathbf{a}_k^2}{2s^2}} \tag{3.5}$$

where s is the dispersion given by the power spectrum $P_A(k)$. The phases are drawn from a uniform distribution between $-\pi$ and π. This is equivalent to sampling from a cylindrical bivariate Gaussian. The Fourier transform of the velocity can then be obtained from the curl of $\mathbf{A}_k$ in the Fourier domain,

$$\mathbf{v}_k = i\mathbf{k} \times \mathbf{A}_k \tag{3.6}$$

The real component to the velocity field is then obtained by taking the inverse Fourier transform of $\mathbf{v}_k$,

$$v_x(x,y,z) = \sum_k [k_y \times a_{k_z} sin(\mathbf{k} \cdot \mathbf{r} + \phi_{k_z}) - k_z \times a_{k_y} sin(\mathbf{k} \cdot \mathbf{r} + \phi_{k_y})] \tag{3.7}$$

This is done at each of the node points to obtain grids of velocities for the x, y and z components of the velocity field. These are then super-imposed onto the SPH particle distribution and the velocities for the particles are linearly interpolated between the grid points. Different realisations are obtained by altering the values of the seeds that are used

to control the random sampling of the amplitude and phase distributions for the vector potential.

In this PhD we tend to use velocity fields from a 16^3 lattice. If one injects energy at a scale smaller than the smoothing length, the SPH formalism results in the energy being quickly smoothed and dissipated. To ensure that this unphysical feature of SPH does not effect the natural dissipation of kinetic energy in colliding flows, we require that there be $\sim$ 50 SPH particles in every grid cell of the turbulent field distribution. For the computation power available to us during the course of this PhD it was only practical to keep the number of particles in the simulation under 1 million. As a result, the largest grid that was practical to use was 16^3, since a 32^3 grid requires $\sim$ 1.6 million particles, while the 16^3 grid only requires $\sim$ 200,000 particles, for the shocks to be accurately captured.

Also note that the initial conditions of the simulations in this PhD are not cubes but spheres. Thus we only use the central cores of the velocity cubes when we set up the runs. As a result, the velocities in the spheres are not in practise strictly divergence free, and some net expansion/contraction of the particles is generally present, due to their appointed velocities. Lastly, we include no mechanism for driving this turbulence. The kinetic energy is left to freely decay in the shocks that it produces. For particular motions at a particular length-scale, this occurs on the associated crossing time, $t_{cr} = 2\lambda/\sigma$ (Mac Low et al., 1998; Stone et al., 1998).

3.2 A clump finding algorithm

Supersonic motions produce density enhancements in the gas, and a general assumption by much of the star formation community is that these structures are the origin of the clumps and cores in molecular clouds. Since one of the primary goals of this PhD is to examine what role turbulence plays in star formation, it is vital that we can analyse these density features, or clumps, in the gas. This requires being able to automatically pick out structure from the simulations.

The method used here is similar to that of Klessen & Burkert (2000) for finding clumps in SPH data, which in turn was based on the method used by Williams et al. (1994) who developed a routine for finding clumps in observational x-y-v data cubes. One of the major advantages of this method is that it doesn't assume a density profile for the structures, unlike previous routines which tried to fit Gaussian profiles to the density structure as a method of defining and identifying clumps.

The clump finding algorithm used here works in the following way:

1. Neighbour lists are found for each particle using the binary tree described in section 2.10.
2. Particles are sorted into descending density
3. The first particle in list (i.e. the densest particle in the simulation) is selected, and assigned to 'clump 1', *along with all its neighbours*. All these particles are flagged as having been assigned to a clump, in this case 'clump 1'

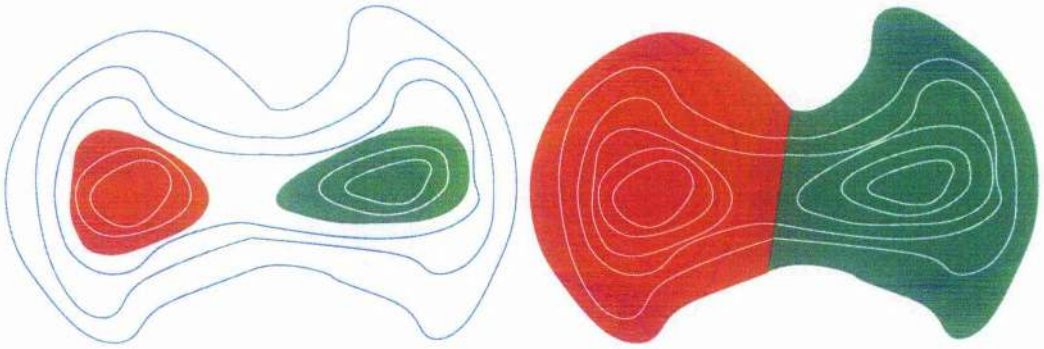

Figure 3.1: Shown here are two different methods by which a clumps can be defined from a density distribution. The contour plots on the left show the method commonly used in observational studies, by which a clump is defined to be only that material which is more dense than its surroundings. The method of defining the clumps shown on the right is that of Klessen & Burkert 2000 and is also the method used here. This method introduces an interface between the clumps, allowing them to be associated with more of the low density gas.

4. The code then works down the list of particles in decreasing density until it comes to the next most dense particle that has yet to be assigned to a clump. The code now has to select one of 2 options:

   (a) If the particle's neighbours do not belong to any clump, then it is deemed to be the peak particle of a new clump and labelled as belonging to a new clump (e.g. 'clump 2').

   (b) If the particle has neighbours which already belong to other clumps, then the particle is assigned to whichever clump the largest fraction of its neighbours belong. Note that only this particle is assigned to the clump. Neighbours of this particle that are not yet assigned to a clump are left to be assigned by the same process, rather than being forced at this point.

5. This process (i.e. step 4) is repeated until all the particles in the simulation have been assigned to a clump.

6. Clumps which have less than 100 particles are then deleted from the clump population. These are comprised entirely of low density noise in the under-resolved regions of the simulation, and are not real features.

One advantage of this technique is that it makes use of the SPH smoothing length in finding the clumps. In regions of high density, the smoothing lengths are small and thus so too is the local resolution. In regions of low density, the smoothing lengths are large and thus the resolution is poor. By using the smoothing lengths (or, equivalently, the neighbour lists) to determine clump memberships of the particles, the algorithm ensures that no clumps are identified that cannot be resolved by SPH.

The method used here does differ slightly from that of Klessen & Burkert (2000) in that the densities of their particles are first binned into equally spaced logarithmic density steps. This allows them to automatically provide core populations above a certain density

threshold, and quickly produce density contour plots. Both of these are not required by our investigation.

There is however one difference in the definition of the clumps in Klessen & Burkert (2000), and those used here, compared to that commonly used in observational studies. Consider the density distribution shown by the contour plots in figure 3.1. We see that a region of high density has split into 2 smaller sub-regions. This is the kind of situation that may be expected to arise in the fragmentation of a star forming core. We show two ways in which the region can be divided up into 'clumps'.

The left image shows the method frequently used by observers. Clumps are defined only down to the lowest contour that is uniquely associated with the peak material. In terms of the contour plot shown in the middle panel of figure 3.1, we see that the green and red 'clumps' have been defined down to the third most dense contour line. If they go any lower down the contours, they would have to share the material. The clumps in this definition are therefore only the features that rise above the local normal.

The right image shows the method of clump definition used by Klessen & Burkert (2000), which we also adopt for this thesis. Rather than the clumps being defined as just the peaks on an underlying density distribution, an interface between the two objects is introduced and the objects are allowed to be associated with the mass down to the lowest contour. This division of the common material and its association to the density peaks occurs naturally from the process outlined in step 4 above.

There are certain situations when both these techniques for defining clumps are useful. For observations of GMCs, the observer's method allows one to usefully examine the density features on a particular length scale, since it detaches the features from the hierarchical structure with which they may be associated. The method is also useful for studying hierarchical fragmentation, for the same reason. However, for trying to examine the cause of star formation, and the scale at which things become bound, this method is no longer useful. If, for example, a bound region fragments during collapse, this method will only concentrate on the new features. The original clump, the bound region that caused the collapse in the first place, will not be defined any more.

By adopting the approach used by Klessen & Burkert (2000) which is shown in the right hand image in figure 3.1, we ensure that the densest points are, at least to some degree, associated with the mass that was responsible for their formation. Considering the aim of this thesis is to examine the onset of gravitational collapse, this is an important point.

CHAPTER 4

Fragmentation concepts

4.1 Overview

In this section we briefly discuss the necessary conditions for gravitational collapse, and how this relates to the density of the gas. We then examine how turbulence can affect the ability of the gas to fragment into a stellar population. We do this by assuming the idealised case that all turbulent motions results in a head on collision between two similar flows.

4.2 Basic fragmentation concepts

The minimum requirement for a body of gas to undergo fragmentation and collapse is that the gravitational energy is greater than the internal thermal energy. This is known as the Jeans condition (Jeans, 1902) and for a sphere of uniform density and constant temperature there is a characteristic mass and radius given by,

$$m_J = \left(\frac{4\pi\rho}{3}\right)^{-1/2}\left(\frac{5}{2}\frac{kT}{G\mu}\right)^{3/2} \tag{4.1}$$

and

$$r_J = \left(\frac{4\pi\rho}{3}\right)^{-1/2}\left(\frac{5}{2}\frac{kT}{G\mu}\right)^{1/2} \tag{4.2}$$

which can be simply obtained by setting $|\mathrm{E_{grav}}| = \mathrm{E_{therm}}$, where

$$|E_{grav}| = \frac{3}{5}\frac{Gm^2}{r} \tag{4.3}$$

and

$$E_{therm} = \frac{3}{2}\frac{kT}{\mu}m \tag{4.4}$$

and using the relation, $m = (4/3)\pi r^3\rho$, for a uniform density sphere. Once a body of gas has a mass and radius greater than or equal to those given in 4.1 and 4.2, the body will collapse on the free-fall time,

$$t_{ff} = \left(\frac{3\pi}{32G\rho}\right)^{1/2} \tag{4.5}$$

For a cloud containing more than one Jeans mass, it can be shown that the number of Jeans masses present is given by

$$N_J = \frac{M_{cloud}}{m_J} \equiv \left(\frac{|E_{grav}|}{E_{therm}}\right)^{3/2} = J^{3/2} \tag{4.6}$$

where the ratio of gravitational to thermal energy, J, is commonly referred to as the Jeans number. This is an important number in fragmentation theory since $N_J = J^{3/2}$, the number of Jeans masses, is the number of individual objects that can collapse independently from one another .

From equation 4.1 we see that the Jeans mass is controlled by the density and temperature of the gas. Taking the usual assumption that the molecular gas in star forming regions behaves isothermally, the Jeans mass is then only responsive to local fluctuations in the density. A known source of density enhancement arises from supersonic turbulent flows. In an isothermal gas, colliding supersonic flows can produce shocks with an associated increase in the density of

$$\frac{\rho_{turb}}{\bar{\rho}} = \mathcal{M}^2 \tag{4.7}$$

where $\bar{\rho}$ is the mean pre-shock density and $\mathcal{M}$ is the Mach number of the flows, given by v_{flow}/c_s, with c_s denoting the isothermal sound speed.

The idea behind 'turbulent fragmentation', as we will refer to it from now on, is that supersonic shocks produce an increase in the local density which results in a decrease in the local Jeans mass. Or more quantitatively,

$$m_{J,turb} = \bar{m}_J\mathcal{M}^{-1} \tag{4.8}$$

where $\bar{m}_J$ is the Jeans mass in the pre-shocked cloud gas of density $\bar{\rho}$. The local Jeans mass is then controlled by the strength of the turbulence in the cloud.

We note here however that the definition of Jeans mass given in equation 4.1 is only really applicable to spherical geometry and not to the dense sheets produced by shocks. This is generally overlooked in turbulent fragmentation theory. If one takes a Jeans mass and squashes it in one direction, the resulting object still has a similar potential energy

to what it had initially (e.g. see Clarke 1999), thus the shocks must exist on scales larger than the initial Jeans mass, $\bar{m}_J$. A number of authors have studied the fragmentation of layers produced by flows, in which the spherical assumptions for the Jeans mass are relaxed and more realistic fragmentation masses are calculated (Elmegreen & Elmegreen 1978; Doroshkevich 1980; Vishniac 1983; Bertschinger 1986; Nishi 1992; Yoshida & Habe 1992; Lubow & Pringle 1993; Whitworth et al. 1994; Clarke 1999). However as Whitworth et al. (1994) point out, there are considerable differences in the boundary conditions used by these studies, such that it is not clear when one author's dispersion relation should be used over another. Only Elmegreen (1993) has gone on to use the results of the layer fragmentation to describe the formation of hierarchical structure in a turbulent environment.

Since turbulence is regarded as being a hierarchical phenomenon, most generally described in observational studies as following a Larson type relation $\sigma \propto L^{\xi}$ (Larson, 1981), one can envision from equation 4.8 that a range of Mach numbers acting on different scales produce local variations in the Jeans mass. It is these local variations that are postulated to be responsible for the shape of the IMF (e.g. Padoan & Nordlund 2002), such that there is a one-to-one mapping between bound clumps formed by turbulence and protostars. One of the goals of this thesis is to examine whether this mechanism for forming a range of stellar masses is indeed viable.

4.3 Colliding Flows

Whitworth et al. (1994) studied the fragmentation of a gaseous layer which has been created, and still confined by, head-on colliding flows. For an isothermal gas, it was found that the mass and size of the fastest growing gravitational instability in the layer are given by,

$$M_{frag} \sim \frac{c_s^3}{(G^3 \rho_o \mathcal{M})^{1/2}} \tag{4.9}$$

$$L_{frag} \sim \frac{c_s}{(G \rho_o \mathcal{M})^{1/2}} \tag{4.10}$$

where ρ_o is the density of the gas in the flows, c_s is the sound speed of the gas and $\mathcal{M}$ is the Mach number of the gas in the flows given by $\mathcal{M} = v_{flow}/c_s$, where v_{flow} is the flow velocity. Note that all constants of order unity are neglected from these relations. The time taken for these objects to fragment out of the layer is given by,

$$t_{frag} \sim (G \rho_o \mathcal{M})^{-1/2} \tag{4.11}$$

This time is simply the time taken by the flows to collect the required M_{frag} in the layer. Whitworth et al (1994) show that the fragmentation of the layer occurs while the confinement is dominated by the external pressure provided by the flows that create the layer.

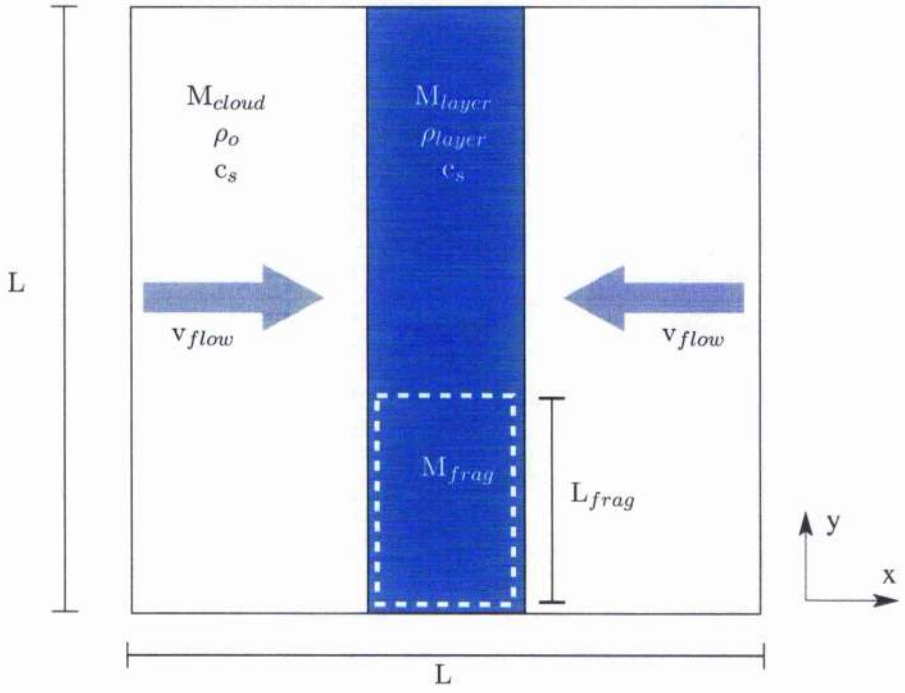

Figure 4.1: Shown here is the layout of the colliding flows

The length of flow required to instigate this collapse can therefore be determined from,

$$l_{flow} \sim v_{flow} t_{frag} \sim \mathcal{M}^{1/2} c_s t_{ff} \tag{4.12}$$

where t_{ff} is roughly equal to $(G\rho_o)^{-1/2}$. Note that $c_s t_{ff}$ is roughly the Jeans length in the unshocked gas.

4.3.1 Number of Jeans masses in the layer

The minimal requirement for gravitational collapse is that the gas must contain one thermal Jeans mass. This assumes the only supporting mechanism is the thermal energy of the gas and thus neglects other sources of support such as rotation, random motions or magnetic fields. Thus the minimal requirement for fragmentation to occur, is that there must be two or more thermal Jeans masses present in the gas. The number of Jeans masses is related to the thermal and gravitational energies by

$$N_J = \frac{M}{m_J} = \left(\frac{|E_{grav}|}{E_{therm}} \right)^{3/2} = J^{3/2} \tag{4.13}$$

where M is the total mass present and J is the Jeans number, the ratio of the magnitude of the gravitational energy to thermal energy. The Jeans number gives us a convenient

method of measuring the ability of a body of gas to fragment.

For our purpose, we will imagine a cube of gas, with constant density ρ_o and side length L, and that this cube has a velocity distribution along the x-axis such that there is a shock running down the middle in the manner shown in figure 4.1. We thus have a cube with colliding flows which can generate a shocked layer in which the relations from Whitworth et al (1994) will apply.

The mass contained in the layer at a time t will thus be given by,

$$M_l(t) = L^2 \rho_o v_{flow} t \tag{4.14}$$

At the point of fragmentation, that is $t = t_{frag}$ which is given by equation 4.11, the mass in the layer will then be given by,

$$M_{l,frag} \sim \frac{L^2 \rho_o^{1/2} c_o \mathcal{M}^{1/2}}{G^{1/2}} \tag{4.15}$$

The number of Jeans masses in the layer (again, at the point of fragmentation) will be given by,

$$N_{J,l} \sim J_l^{3/2} \sim \frac{M_{l,frag}}{M_{frag}} \sim \frac{L^2 \rho_o G \mathcal{M}}{c_s^2} \tag{4.16}$$

Prior to this, the number of Jeans masses in the original unshocked cloud is given by

$$N_{J,o} = \frac{M_{cloud}}{m_{J,o}} \sim \rho_o L^3 \left(\frac{c_s^3}{G^{3/2} \rho_0^{1/2}} \right)^{-1} = \left(\frac{G^{1/2} \rho_0^{1/2} L}{c_s} \right)^3 \tag{4.17}$$

Thus we can determine the ratio of the number of Jeans masses in the layer to that in the preshocked gas,

$$\frac{N_{J,l}}{N_{J,o}} \sim \frac{L^2 \rho_o G \mathcal{M}}{c_s^2} \frac{c_s^3}{G^{3/2} \rho_o^{3/2} L^3} = \frac{c_s \mathcal{M}}{G^{1/2} \rho_o^{1/2} L} \tag{4.18}$$

Since the free-fall time of the cloud is roughly $t_{ff} \sim (G\rho_o)^{-1/2}$ and $c_s \mathcal{M} = v_{flow}$, the velocity of the colliding flows, then we can express the above ratio as,

$$\frac{N_{J,l}}{N_{J,o}} \sim t_{ff} \frac{v_{flow}}{L} \sim \frac{t_{ff}}{t_{cr}} \tag{4.19}$$

This simple result shows that the ratio of the number of Jeans masses in the layer to that in the original cloud is given by the ratio of the cloud's free fall time to the crossing time for the flows in the cloud.

For a uniform density spherical cloud, the free fall time in the cloud is given by $t_{ff} = (3\pi/32G\rho)^{1/2} = (\pi^2 R^3/8MG)^{1/2}$ and the crossing time is $t_{cr} = 2R/v = (2R^3/\alpha GM)^{1/2}$, where α is the ratio of kinetic to gravitational energy (or our ϵ^{-1}). Thus if we ignore the constants of order unity, $t_{ff}/t_{cr} \sim \alpha^{1/2}$.

If we thus apply our idealised case of colliding flows to the turbulence in clouds, we see that if the clouds are close to dynamical stability, even to within an order of magnitude, the turbulent motions are incapable of significantly increasing the number of Jeans masses in the shocked regions *at the point of fragmentation.* Since turbulence is actually much less idealised than the above description of colliding flows, it is unlikely that we will see any increase in the number of Jeans masses in our simulations.

An interesting consequence of this is that if one does not have a flow comprising a Jeans mass to begin with, then the layer will not have a Jeans mass either. This result can be seen in the study of Gittins, Clarke & Bate 2003 which investigated clump-clump collisions using SPH to model the evolution of a population of Bonner-Ebert spheres (the 'clumps') moving with supersonic random motions. They find that collisions between spheres only result in collapse if the spheres each contain half a Jeans mass to begin with, regardless of the Mach number of the collision.

An easier way of thinking about the lack of increase in the Jeans number is just the idea mentioned above that by squashing a Jeans mass, the potential energy of the new mass distribution is practically the same as it was when it was perfectly spherical. Unless one has cooling, it is therefore not possible to get more Jeans masses out than one originally puts in.

4.3.2 Hierarchical fragmentation

Whitworth et al. (1994) point out that the first instabilities to form in shocked layers are not self-gravitating, like the one discussed above. Instead, the first instabilities lead to the generation of motions inside the layer. In the derivation of the layer fragmentation, these are assumed to be small enough to ignore. If it were possible to quantify the magnitude of these motions, then they could be included into the layer fragmentation discussion as an effective contribution to the sound speed, providing of course that they are sufficiently isotropic.

The question may arise as to whether these motions inside the layer may be able to instigate further collapse, thus resulting in hierarchical fragmentation of the gas. Is the hierarchical structure observed for some clusters (e.g. NGC1333 Lada et al. 1996), simply a result of hierarchical layer-type fragmentation?

From the discussion above regarding the number of Jeans masses in the layer, it would appear that this type of triggered hierarchical fragmentation is impossible. One needs a Jeans mass before the shock to produce a Jeans mass after the shock. Thus the motions inside a region with size L_{frag} and mass M_{frag}, could only produce one new object. While this could potentially continue down the size scales, the region of size L_{frag} will never be able to harbour any more than one object. Rather than producing a hierarchically structured cluster, one would get individual stars that were separated by a

distance $\sim L_{frag}$. Depending of the original size over which the largest scale flows occur, this could potentially result in *isolated* rather than clustered star formation.

CHAPTER 5

Dynamical cloud support

5.1 Introduction

The aim of this thesis is to examine the onset of star formation in environments where the energy in bulk motions, or 'turbulence', is at least as dominant as the gravitational energy. We start our investigation in this chapter, by looking at the star formation process in clouds that contain different levels of dynamical support. This support will be provided in the form of a random Gaussian velocity field, as is described in chapter 3.1, and the amount of support will be varied.

The motivation for the work presented in this chapter is two-fold. Firstly, we wish to provide a comparison to previous work. The simulations of Bate et al. (2003b) and Delgado-Donate et al. (2004) have modelled the fragmentation and protostellar accretion in small clouds ($m \leq 50 M_{\odot}$) supported by turbulence, where the region has initially been in dynamical balance. If these regions are formed from large scale turbulent flows in a giant molecular cloud they could have a range of dynamical states, depending on the efficiency of the large scale shock in removing the internal kinetic support. Indeed, clumps with masses from $\sim$ few $M_{\odot}$ to $\sim$ 100 $M_{\odot}$, in Chameleon have been observed to exhibit a wide range of dynamical states (Mizuno et al., 1999).

Our second reason for this study, and perhaps the most important given the current theoretical work in star formation, relates to the role of the supporting turbulence. There has been considerable interest in the last 10 years or so in the subject of 'turbulent fragmentation' (Larson, 1992; Henriksen, 1986, 1991; Elmegreen, 1993, 1997, 1999, 2000b; Padoan, Nordlund, & Jones, 1997; Padoan & Nordlund, 2002). The main concept in this theory is that the shocks produced by the observed turbulent flows are responsible for density enhancements in the gas, which become the sites of star formation. It has been suggested that the density enhancements are able to locally alter the Jeans mass, the minimum mass required for gravity to overcome thermal support, in such a manner that the Jeans mass distribution resembles the IMF. Each Jeans mass represents a star forming core, such that the mass function of the cores is the same as the mass function of the stars. This implies that there is a one-to-one mapping between cores and stars. The turbulence is hence proposed to be directly responsible for triggering star formation and controlling the form of the IMF (see chapter 4 for details).

Sim	ϵ	Δv	$\mathcal{M}$	M_{cloud}	R_o	ρ	$m_{J,i}$
		km s^{-1}		$M_\odot$	pc	g cm^{-3}	$M_\odot$
1 & 2	10	0.36	1.8	32.6	0.132	2.23×10^{-19}	1.0
3	1	1.13	5.5	32.6	0.132	2.23×10^{-19}	1.0
4	1	1.13	5.5	6.3	0.026	5.55×10^{-18}	0.2
5 & 6	0.5	1.60	7.8	32.6	0.132	2.23×10^{-19}	1.0

Table 5.1: This table contains the details of the initial conditions for each of the simulations. All simulations are given a unique Gaussian random velocity field which is scaled such that the ratio of gravitational to kinetic energy is some value ϵ, which is shown in column 2 of the table. This results in a velocity dispersion for the turbulence, Δv, which is used to calculate a turbulent Mach number $\mathcal{M} = \Delta v \ / \ c_s$, where c_s is the sound speed. The density in column 7 is simply the mean density of the spherical cloud, defined from a uniform sphere of mass M_{cloud} and radius R_o. From this density, and the temperature of the cloud (all of which have a temperature of 10K), the mean initial Jeans mass of the cloud, $m_{J,i}$, can be found from equation 4.1.

In this chapter, altering the dynamical state of a simulation results in changing the magnitude of the supporting energy provided by the turbulence. The regions therefore have different mean Mach numbers and thus the role of turbulence in creating structure can be explored. In the turbulent fragmentation theory, the mass of protostars is controlled by the Mach number, thus we can provide an environment which tests this theory.

Goodwin, Whitworth, & Ward-Thompson (2004) have recently performed calculations investigating how low levels of turbulence affect the fragmentation of small clumps. They performed a series of simulations in which the supporting turbulent energy of clumps with masses $5.4M_\odot$ was varied. They found that the clumps with stronger turbulence were generally able to fragment more easily. However, we note that in all the clumps in the study, the gravitational energy was much larger than the kinetic energy in the turbulence. The resulting Mach number of these clouds was, as a result, very much less than 1, such that the turbulence was comprised of sub-sonic flows. The fragmentation in these simulations is probably just a result of local pockets of angular momentum providing support against collapse, rather than the 'turbulent fragmentation' process detailed by Padoan & Nordlund (2002). The main mechanism for the formation of the multiple systems in their study is thus disc fragmentation.

We describe the details of our simulation setup in 5.2 and the general evolution of the clouds in section 5.3. In section 5.4 we discuss the evolution of the clumps that form within these clouds, and examine their energy states as the clouds progress toward star formation. Section 5.5 examines the role that accretion plays in each of the dynamical cloud models. General discussion and conclusions are given in sections 5.6 and 5.7.

5.2 The Simulations

Details of the simulations are given in table 5.1. All the simulations presented here start from a uniform density sphere at 10K, with the gas modelled isothermally. With the

exception of simulation 4, they have a mass of $32.6M_{\odot}$ and an initial Jeans mass of $1M_{\odot}$ (initial density $\rho_o = 2.23 \times 10^{-19}$ g cm^{-3}). Simulation 4 has a mass of $6.3M_{\odot}$ and an initial Jeans mass of $0.2M_{\odot}$. These conditions are such that all the simulations have a Jeans number (equation 4.6) of 10, and thus have $\sim$ 32 Jeans masses initially. We use 4×10^5 particles to model the clouds in these simulations, which for all the simulations except simulation 4, give a mass resolution (i.e. $\sim$ 100 SPH particles) of $0.0082M_{\odot}$ (Bate & Burkert, 1997; Whitworth, 1998). For simulation 4, the corresponding mass resolution is 0.0016, which is close to the value thought to be the limit of fragmentation (Low & Lynden-Bell, 1976; Rees, 1976).

The clouds are given a turbulent velocity field to provide support against collapse, although the amount of support given is varied in this chapter. The support is parameterised by $\epsilon = E_{grav}/ E_{kin}$ with values of 10, 1 and 0.5 being used here. We have defined ϵ in this manner such that it can be thought of as a kinetic version of the Jeans number. The initial velocities are taken from a Gaussian random field with power spectrum $P(k) \propto k^{-4}$, which corresponds to a Larson type relation of $\sigma \propto \lambda^{1/2}$ (see chapter 3.1 for details). Each of the simulations presented in this chapter have a different random velocity field. We stress here that the turbulent field in this study is left to freely decay. We do not include any driving mechanisms.

To ensure that we do not attempt to resolve beyond our resolution limit, we introduce sink particles at the point where the limiting mass resolution is reached. In simulations 1, 2, 3, 5 & 6, the sinks are created at 3.312×10^{-15}g cm^{-3} with an accretion radius of 1.1×10^{15}cm, while in the higher density run, simulation 4, the density and accretion radius are 8.700×10^{-14}g cm^{-3} and 2.1×10^{14}cm respectively. We also smooth the gravitational forces between sink particle pairs to the same size as their accretion radius (see equation 2.48). This prevents binaries with separations smaller than the accretion radius from forming and slowing the evolution of the code, since these objects are not of primary interest to this study.

5.3 General evolution of the clouds

In this section we concentrate on differences in the star formation for clouds of different ϵ. We start by giving an overview of the evolution of each of the ϵ parameter cloud pairs. We then go on to compare the features in the different simulations, such as the number of stars formed and the basic cluster properties.

5.3.1 The $\epsilon = 10$ clouds

Column density images for simulations 1 & 2, with $\epsilon = 10$, are shown in figure 5.1. The cloud's evolution is shown at t = $0.5t_{ff}$, at the onset of star formation (t_{SF}) and the point where the stellar population has accreted 10 percent of the cloud mass, which is also the point at which the simulations are terminated (t_{end}).

At t = $0.5t_{ff}$, both simulations 1 & 2 show a centrally condensed cloud, with some mild filamentary structure. The central concentration is simply a result of the cloud's

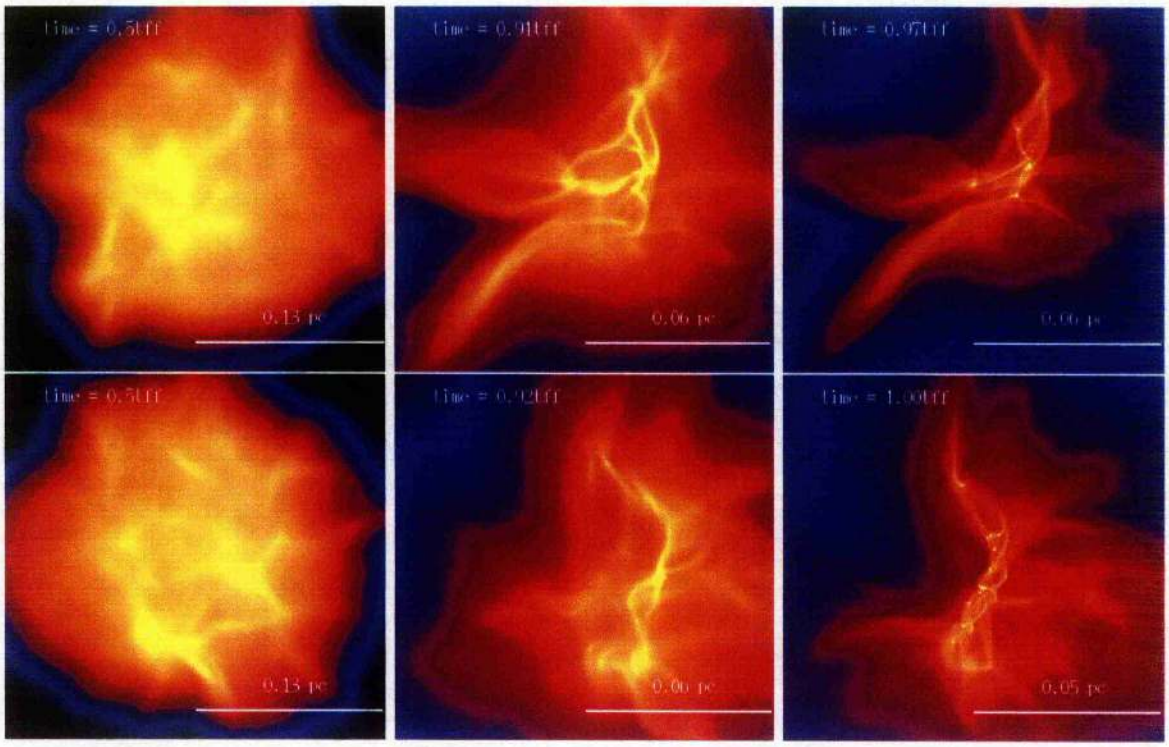

Figure 5.1:
Shown here are the logarithmic column density images for simulations 1 (top row) and 2 (bottom row) with $\epsilon = 10$. The images are taken at three points during the evolution of the simulations: half a free-fall time, the onset of star formation and the point at which the protostars have accreted 10 % of the cloud's gas (which is also the termination point). For these clouds, a free-fall time, t_{ff}, is 1.4×10^5 years. The left hand, middle and right hand panels have show a maximum column density of 1, 40 and 500 g cm^{-3} respectively. All the images have a minimum column density of 0.001 g cm^{-3}.

global collapse. At the onset of star formation, t_{SF} (middle panels), the gas is still centrally condensed but we see now that the extremely dense regions are confined to very distinctive filaments. It is in these filaments that the star formation occurs, just before the free fall time in both clouds. At $t = t_{end}$ we see the the star formation has occurred in one elongated cluster, which is at the centre of the cloud. The filamentary structure is still present and in fact has actually become more distinct. The stellar population has managed to accrete 10 percent of the gas by roughly $t = t_{ff}$.

5.3.2 The $\epsilon = 1$ clouds

The column density images from simulations 3 & 4 can be found in figure 5.2. Both the simulations show distinct filamentary structure at $t = 0.5t_{ff}$, and it would appear that the clouds have become irregularly shaped by their supersonic internal motions. This point in the evolution is actually the half crossing time for the turbulence in these clouds, and is generally when turbulently formed structure is at its highest. The onset of star formation occurs at roughly the free-fall time, and at this point in the evolution we see

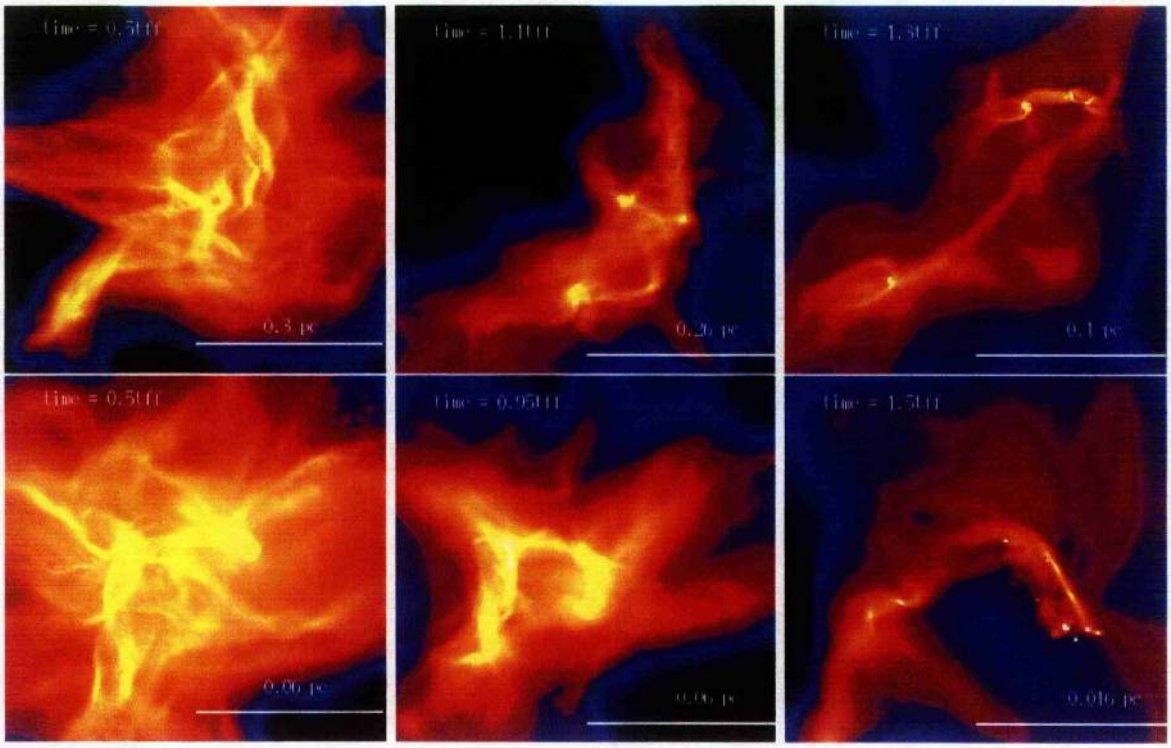

Figure 5.2:
Shown here are the logarithmic column density images for simulations 3 and 4 with $\epsilon = 1$. For clouds 3 and 4, a free-fall time, t_{ff}, is 1.4×10^5 years and 2.8×10^4 respectively. For simulation 3 (top row), the left hand, middle and right hand panels show a maximum column density of 1, 40 and 500 g cm^{-3}. In the bottom row depicting the evolution of simulation 4, the left hand image has a maximum column density of 15 g cm^{-3} and the the middle and right hand images have the same maximum column density as is shown in the panels above, for simulation 3. All the images have a minimum column density of 0.001 g cm^{-3}.

that the gas has lost some of its chaotic appearance, with the density features now much more rounded, rather than the sharp filaments that dominated at $t = 0.5t_{ff}$. Looking at the column density images at the end of the simulations, $t = t_{end}$, we see that star formation has occurred in two distinct groups. These star forming regions have some filamentary structure once more, presumably caused by the gravitational collapse that forms the individual stars.

5.3.3 The $\epsilon = 0.5$ clouds

The column density images from simulations 5 & 6 can be found in figure 5.3. At $t = 0.5t_{ff}$ we see that the cloud structure is dominated by the supersonic turbulent motions. Star formation in these simulations doesn't occur until relatively late: $1.7t_{ff}$ for simulation 5 and $2.4t_{ff}$ for simulation 6. At the point of star formation, the density distribution of the gas is very smooth and no filamentary structure is present. There is thus now little indication that the gas has passed through a turbulently dominated phase. The

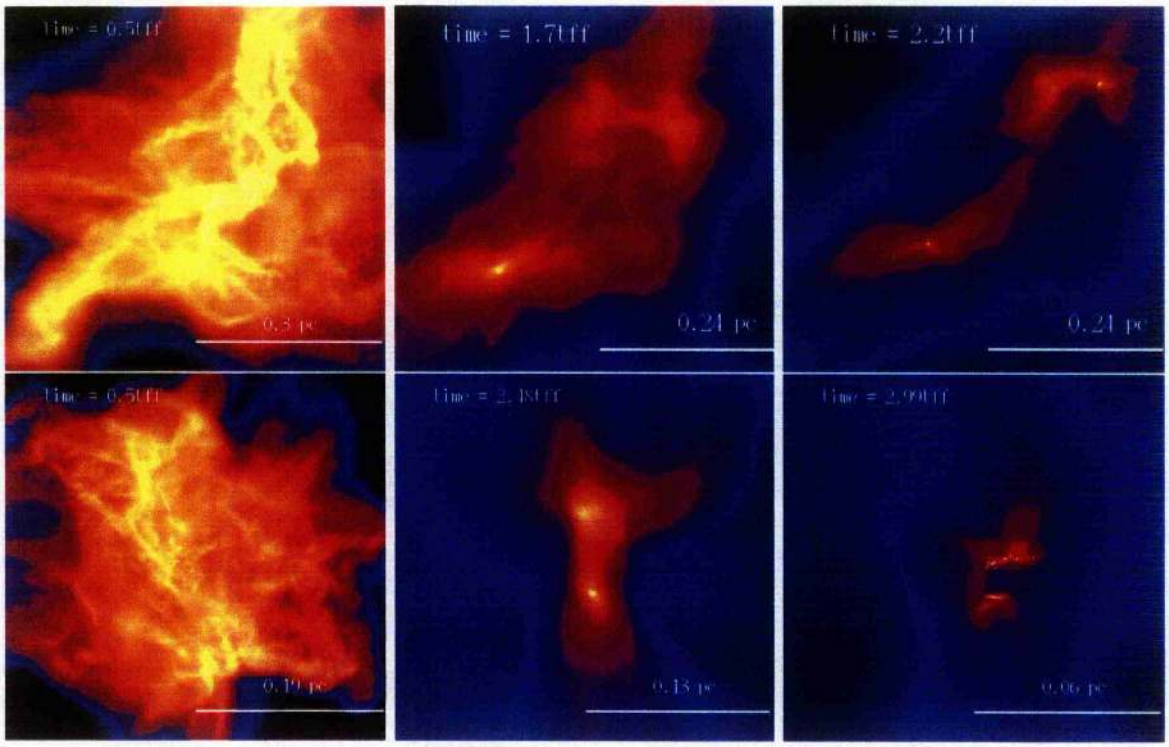

Figure 5.3:
Shown here are the logarithmic column density images for simulations 5 (top row) and 6 (bottom row) with $\epsilon = 0.5$. For these clouds, a free-fall time, t_{ff}, is 1.4×10^5 years. The left hand, middle and right hand panels show a maximum column density of 1, 40 and 500 g cm^{-3}. All the images have a minimum column density of 0.001 g cm^{-3}.

star formation occurs in two distinct groups, with the stellar population not accreting 10 percent of the gas until $2.2t_{ff}$ for simulation 5 and $3t_{ff}$ for simulation 6.

5.3.4 Comparisons and cluster properties

Some basic details of the stellar populations can be found in table 5.2. The first point we note here, is that increasing the level of turbulent support in the cloud does not decrease the time taken for star formation to set in. In fact the stronger the turbulent motions, the later the star formation occurs. The $\epsilon = 10$ clouds form stars at roughly a free-fall time (t_{ff}), whereas the $\epsilon = 0.5$ clouds take over $2t_{ff}$ before stars (sink particles) start to form. Also, higher levels of turbulence result in the formation of fewer stars. Again, comparing the $\epsilon = 10$ & 0.5 clouds, we see that the average number of stars formed is 22.5 and 8 respectively.

The clouds with lower support have more concentrated regions of star formation. It is possible that two effects, the number of stars and the concentrations of star forming locations, are linked. Figure 5.4 shows how the mean Jeans mass in the cloud evolves as the gas proceeds toward star formation. This mean Jeans mass is defined from a volume averaged density, $\bar{\rho}_{cloud}$, which is defined by the half mass volume. The value of $\bar{\rho}_{cloud}$

used to calculate $\bar{m}_J$ is also shown on the right hand axis of figure 5.4.

We see from the figure that the average density of the inner have of the cloud is only really constant for the $\epsilon = 1$ simulations. For the clouds with $\epsilon = 10$ & 0.5 however, we see that there is considerable evolution of the average density. This in turn causes the mean Jeans mass, $\bar{m}_J$ to evolve accordingly. If the parameter $\bar{m}_J$ is connected to the star formation, then one would expect the clouds with higher mean Jeans masses to form fewer stars, and to form them further apart, than the clouds with smaller mean Jeans masses. This is exactly what we see in the simulations, suggesting that the mean Jeans mass is linked to the star formation process.

Although the general appearance and formation of the clusters is dependent on the dynamical state of the cloud, the energy properties of the final cluster do not appear to be that sensitive to the cloud environment. The ratio of gravitational to kinetic energy, ϵ_{clust}, does not appear to be related to the initial value of ϵ for the cloud. The velocity dispersion of the cluster is also not a function of ϵ, and as a result, neither is the gravitational radius. Also the fact that the star formation sometimes occurs in distinctly separate locations, especially in the $\epsilon = 1$ simulations, may render the gravitational radius less effective at describing the cluster.

The mean stellar mass is however a clear function of the ϵ parameter of the cloud. The clouds with less support have a lower mean stellar mass than those with the higher support. This is shown in figure 5.5. This is actually in stark contrast to the theory of turbulent fragmentation, which predicts that high Mach number flows are responsible for small objects. It is consistent though with the idea that the star formation is regulated by the mean Jeans mass.

The last point we wish to note in this section is the remarkably similar behaviour of simulations 3 and 4. Although these two simulations involve very different sizes and densities of clouds, they appear to have very similar evolutions. These clouds do however have exactly the same dynamical and thermal balance with respect to gravity (i.e. they both have $\epsilon = 1$ and $J_o = 10$). While the mean stellar mass in simulation 4 is smaller than simulation 3, when we compensate for the difference in mass scales by dividing the mean stellar mass by the initial Jeans mass in both simulations, we see that the two values are comparable (as is shown in table 5.2). Even the velocity dispersions for the resulting clusters are similar.

5.4 Evolution of structure and cloud fragmentation

5.4.1 clump mass distribution

In this section we examine the clumps that are produced by the turbulence. To determine these clumps we use the clump finding algorithm described in section 3.2. Figure 5.6 contains the clump distributions sampled at $0.5t_{ff}$ and t_{SF}. At the point of star formation, t_{SF}, we also plot the clump population that is thermally bound, i.e. has a thermal Jeans mass or more, and the clumps that are completely bound with gravity overcoming kinetic and thermal support.

Sim	t_{SF} (t_{ff})	t_{end} (t_{ff})	N_*	ϵ_{clust}	Δv_{clust} (km s^{-1})	R_{grav} (R_o)	$R_{M/2}$ (R_o)	$\bar{M}_*/m_{J,i}$
1	0.91	0.97	22	2.58	1.87	0.014	0.030	0.14
2	0.92	1.00	23	3.33	1.79	0.012	0.015	0.16
3	1.12	1.33	12	2.08	1.00	0.063	0.258	0.26
4	0.96	1.51	12	3.44	0.97	0.192	0.292	0.20
5	1.73	2.19	5	2.38	0.41	0.303	0.379	0.54
6	2.48	2.99	11	1.99	1.31	0.038	0.030	0.30

Table 5.2: Contained in the table are details of the protostellar clusters, as sampled at the end of the simulation when 10% of the mass of the cloud is in the form of protostars. The number of stars at the end of the simulation is N_*. The kinetic energy of the cluster is calculated from velocities measured with respect to the group velocity of the protostellar system. This is used to work out the ϵ and Δv_{clust} for the cluster. The value of Δv is then used to determine a gravitational radius, $R_{clust} = (2GM_{clust})/\Delta v^2_{clust}$, were we point out that $M_{clust} = 0.1M_{cloud}$ (see table 5.1) since that is our condition for terminating the simulation. $R_{M/2}$ is the 'half mass radius' of the cluster and $\bar{M}_*/m_{J,i}$ is the average stellar mass, normalised into units of the initial Jeans mass of the cloud, $m_{J,i}$ (again see table 5.1).

The clump mass spectra look quite different for each of the ϵ cloud sets, although there is a general trend that connects the spectra since they all contain a peak in the distribution toward the lower masses. There is also a slope at the high mass end, which in some of the distributions appears to be roughly similar to the Salpeter (1955) slope. Note that the sharp cut-off in the low mass population is simply the result of our resolution. We also see that at $0.5t_{ff}$, the clump mass distributions get progressively narrower as we move to higher levels of turbulence. This is probably as feature of our clump finding algorithm. Higher levels of turbulence produce more resolvable features, and the clump finding algorithm always selects the dense, smallest, features first.

The clump mass spectrum is not constant in time. The $\epsilon = 1$ and 0.5 simulations lose some of their small scale structure, and gain some larger structure, as the cloud evolves. This implies that there is a coagulation process at work (which we will discuss in more depth in chapter 6). There are three potential reasons for why the slope of the distributions get shallower. First, we do not drive our turbulence, so after the field has lost its energy by structuring the gas, there is no more energy to keep this structure confined. The clumps simply re-expand, and the sound speed acts to smooth everything back to a more uniform state. The second process is coagulation, where the random motions of the clumps result in collisions which produces larger objects. The third process may simply be that the collapse of self gravitating regions are just pushing the clumps together.

Motte et al. (1998) have suggested that the clump mass spectrum may be similar in form to the stellar IMF, leading to the idea that the mass spectrum of stars and clumps have the same origin (Padoan et al., 1997; Padoan & Nordlund, 2002). In figure 5.6 we see that while some of the simulations have clump mass spectra that look similar in shape to the IMF, this is only true for the unshaded distribution, representing all the clumps in the simulation. The vast majority of these clumps are unbound and thus transient. They are hence not representative of the protostellar population that appears

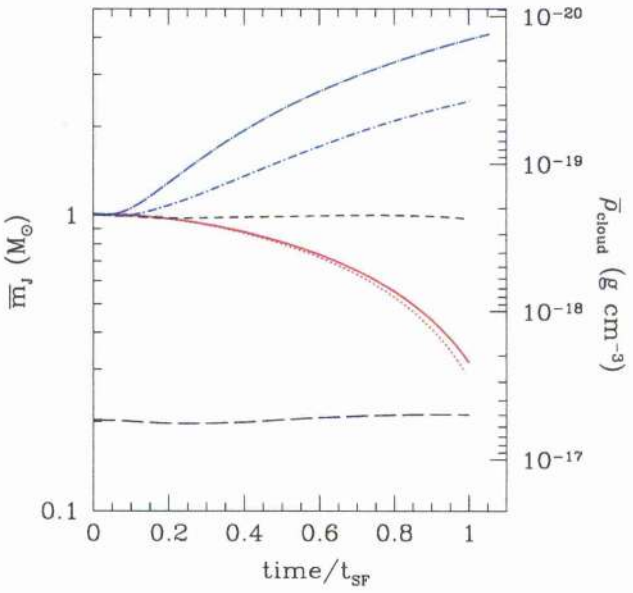

Figure 5.4:
Shows the evolution of the mean effective Jeans mass in each of the simulations and the associated mean density from which it is calculated. The mean density is defined from the spherical volume that contains half the mass of the cloud, as viewed from the cloud's centre of mass. This is then used in the standard equation for a spherical Jeans mass to obtain the mean Jeans mass. Simulations 1 and 2 (with $\epsilon = 10$) denoted by the solid and dotted lines respectively. Simulations 3 and 4 ($\epsilon = 1$) have the short and long dashed lines respectively. Lastly, simulation 5 is shown by the dot-short dash line and simulation 6 is given by the dot-long dashed line, and both have $\epsilon = 0.5$.

in the simulation. The shaded distributions in the clump spectra show the populations of thermally bound (hashed) and totally bound (black) clumps. We now go on to discuss these shaded distributions.

The most distinct population of thermally bound clumps is found in the $\epsilon = 10$ simulations. The distribution of these clumps is quite similar for both simulations. Since this distribution is absent from the other ϵ cases, it suggests that the origin of this clump population is connected to the dynamical state of these clouds. The distribution of the thermally bound clumps is broadly similar in shape to the Miller-Scalo IMF. It also appears to be centred around $0.2M_\odot$ in both simulations. We see from figure 5.4, that this is roughly the mean Jeans mass in the region of star formation at $t = t_{SF}$. It is therefore likely that the properties of the clumps in the $\epsilon = 10$ clouds are controlled by the global properties of the region. The decrease in the Jeans mass caused by the spherical contraction of the cloud under its self gravity, allows the formation of a population of cores that become thermally bound at a mass lower than the original Jeans mass of the cloud.

While the thermally bound clumps are a stage closer to forming stars than their completely unbound companions, a lot will depend on whether they can rid themselves of their excess internal kinetic energy. The thermally bound population does not automatically represent the initial stellar population. We do see however that the clumps which are

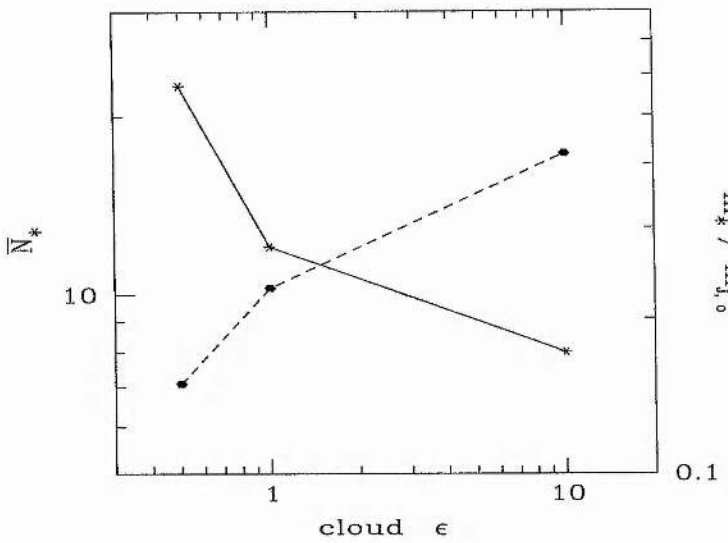

Figure 5.5: This plot shows how cluster properties vary with ϵ. The hexagonal points (connected by the dashed line) show how the mean number of stars varies with the cloud's support (ϵ). The mean is calculated from the two simulations with the same ϵ value. The solid line connecting the starred points shows how the mean mass from the simulations varies with ϵ. The star masses are given in terms of the initial Jeans mass in the cloud.

totally bound (i.e. those in which the thermal and the kinetic energies are overcome by gravity) lie at the centre of the thermally bound clump distribution. These bound clumps are thus also similar in mass to the mean Jeans mass, suggesting that the thermally bound clumps are more likely to get involved with star formation. Note that only one or two fully bound cores exist at the point of star formation.

The $\epsilon = 1$ and 0.5 clouds show a different picture. The thermal and fully bound population at the point of star formation is much smaller and also tends to be confined to the larger clumps in the clouds. These simulations do not show a specific distribution for thermally bound clumps like that presented for simulations 1 and 2. In simulation 3 however we note that there appears to be a few thermally bound clumps with masses $1M_\odot$. Since at the point of star formation in the cloud, the mean Jeans mass is roughly $1M_\odot$, it thus appears that there has been a decrease in the local Jeans mass. This decrease is consistent with that expected from the turbulent compression, outlined in chapter 4, so there is some evidence to suggest that the turbulence may be responsible for controlling the mass at which clumps with $|E_{grav}| \geq E_{therm}$ can form, although local gravitational collapse can also produce the same effect, as we discussed for the $\epsilon = 10$ simulations above. Note however that the clumps with $|E_{grav}| \geq E_{therm}$ are still *unbound*. We see a similar result in simulation 6.

The clumps which are bound however, appear to be the largest of those present in the distribution. They are also consistent with the mass of the mean Jeans mass in the region (as we can see in figure 5.4), and not that produced by the turbulence. Simulation 4 is a bit of an anomaly in that the star forming clump is not totally 'bound', although it is thermally bound. Obviously to form a star there must be some bound material, and

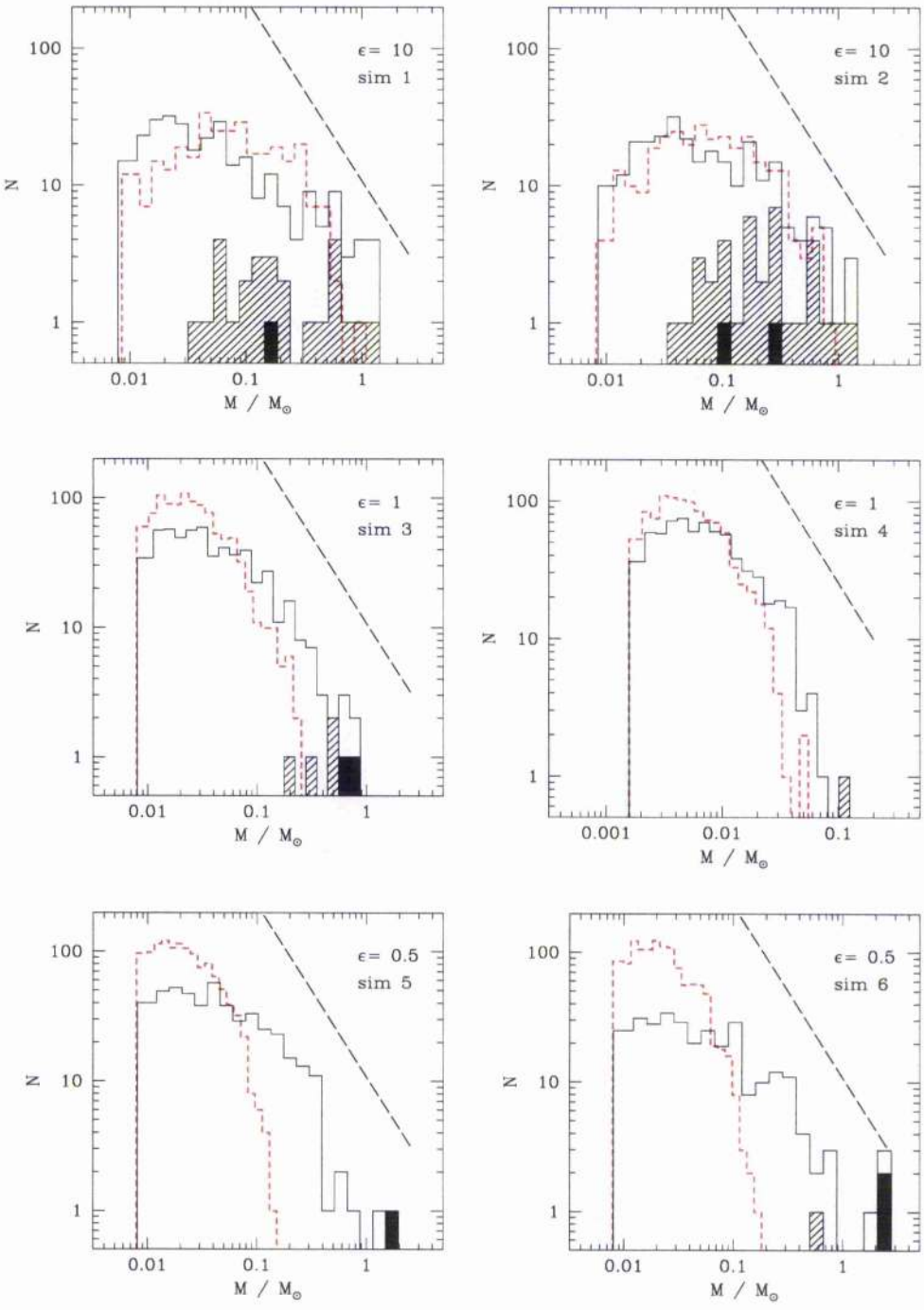

Figure 5.6:
Shown here is the clump mass distributions as recovered by our clump finding algorithm. The red dotted line distribution denotes the clump population at $0.5t_{ff}$. The three black distributions show clump spectra just before the formation of the first protostar. The black line (unfilled) shows the whole clump population, the hashed region denotes the clumps that are thermally bound (i.e. possess 1 or more thermal Jeans masses) and the solid black distribution is the clumps that are completely gravitationally bound (i.e. taking kinetic *and* thermal energy into account). The long-dashed line shows the slope of the Salpeter IMF (i.e. -2.35).

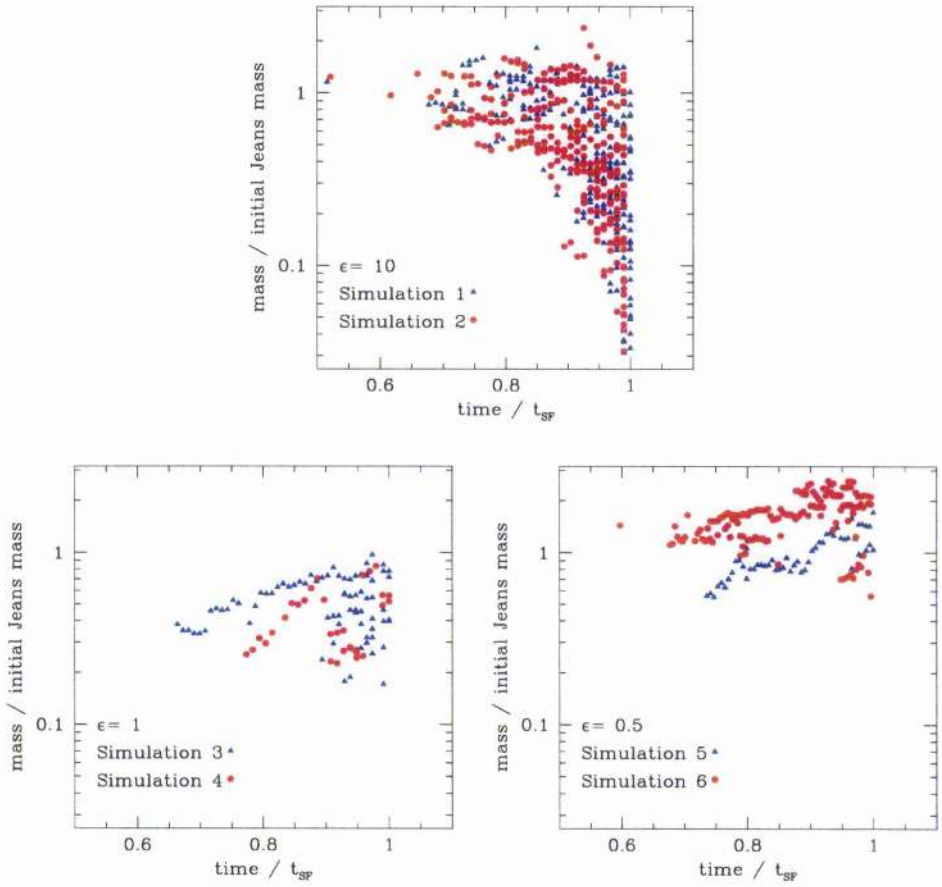

Figure 5.7:
Plotted here are the masses of clumps, at each instant, that have $|E_{grav}| \geq E_{therm}$. Thus the points represent the mass of a clump that at any instant has a Jeans mass or more. The time is plotted in units of the 'star formation time', t_{SF}. This allows us to compare the evolution of the clumps for simulations where the onset of star formation occurs at quite different times.

this material needs to be in a bound state for a while in order to have time to collapse, thus somewhere in this clump a fully bound region must exist. The fact that this clump still forms a star therefore shows that what is defined as a 'clump' may not have much to do with the star formation process.

5.4.2 Evolution of bound structure

In the above discussion of the clump population we noted that the clumps which are bound at the point of star formation always have a mass similar to the mean Jeans mass in the cloud. In this section we take a look at how the Jeans mass of the clumps develops with time. Figure 5.7 plots the mass of those clumps that are thermally bound ($|E_{grav}| \geq E_{therm}$, and thus by definition contain a thermal Jeans mass or more) before the point of star formation.

The $\epsilon = 10$ simulation again produces the most striking results. The masses of the clumps that contain a Jeans mass decreases with time, up the point of star formation. The number of clumps with a Jeans mass increases with time and the spread of masses of these clumps increases as the simulations progress toward star formation. The clumps plotted in this figure at the point of star formation are the same as those denoted by the hashed distribution in figure 5.6. The spread of clump masses follows the evolution of the mean Jeans mass. This shows that the global gravitational collapse of the cloud is reflected in the structure that forms. The conditions for star formation are therefore linked to the conditions in the collapsing cloud.

In contrast to the results of the $\epsilon = 10$ simulations, the simulations with ϵ =1 and 0.5 show a different evolution in figure 5.7. In these simulations, the mass at which clumps achieve $|E_{grav}| \geq E_{therm}$ starts lower than the mean Jeans mass in the cloud, then increases as the cloud evolves toward star formation. At the point where the condition $|E_{grav}| \geq E_{therm}$ is first satisfied, the associated clump mass is roughly what would be expected from turbulent fragmentation, i.e. the clumps have a mass of $\sim m_{J,turb}$, which for simulations 3 & 4 is $\sim 0.2\bar{m}_J$and for simulations 5 & 6 is $\sim 0.13\bar{m}_J$(see equation 4.8). Gradually the clumps that are thermally bound (i.e. containing a Jeans mass or more) become more massive for a period, before a wider spread of masses develops (probably due to fragmentation). The largest of these clumps are also the ones which are shown as the black region in figure 5.6. Thus for the simulations with $\epsilon = 1$ or less, there seems to be a period of growth before the clumps can be the sites of star formation. We note here again that the mass of the clumps at the onset of star formation is roughly equal to the mean Jeans mass in the cloud.

5.5 Protostellar Accretion

The main aim of this study is to assess the manner by which stars form and how turbulence and the level of dynamical support can affect the origin of the stellar masses, the possible origin of the IMF. In particular, we wish to distinguish between two conflicting theories which have been proposed for how stars gain mass. In the picture outlined by Motte et al. (1998), there is an implied one-to-one mapping between the clumps and stars. Each clump is assumed to form one star and the mass of the star is directly related to the mass of the clump. This model supports the idea the turbulence is responsible for the star formation by creating the population of clumps in which the protostars evolve (Padoan & Nordlund, 2002). In the contrasting view, stars form in groups from a large region of gas, with the fragmentation controlled by the mean Jeans mass. The young protostars then compete for the gas reservoir (Bonnell et al., 2001a,b).

As we shall show, these two conflicting theories for the IMF involve quite different modes of accretion. We can thus use the accretion rate to determine whether stars are forming from individual clumps, such as is suggested by Motte et al. (1998), or if the stars are fragmenting out of a larger structure. Thus we can reveal whether accretion is a local feature, dictated by the star forming clump, or is a global phenomenon that is controlled by the larger region in which the stars are are embedded. In the latter case, we should point out that the final mass of a star depends on the behaviour of its siblings.

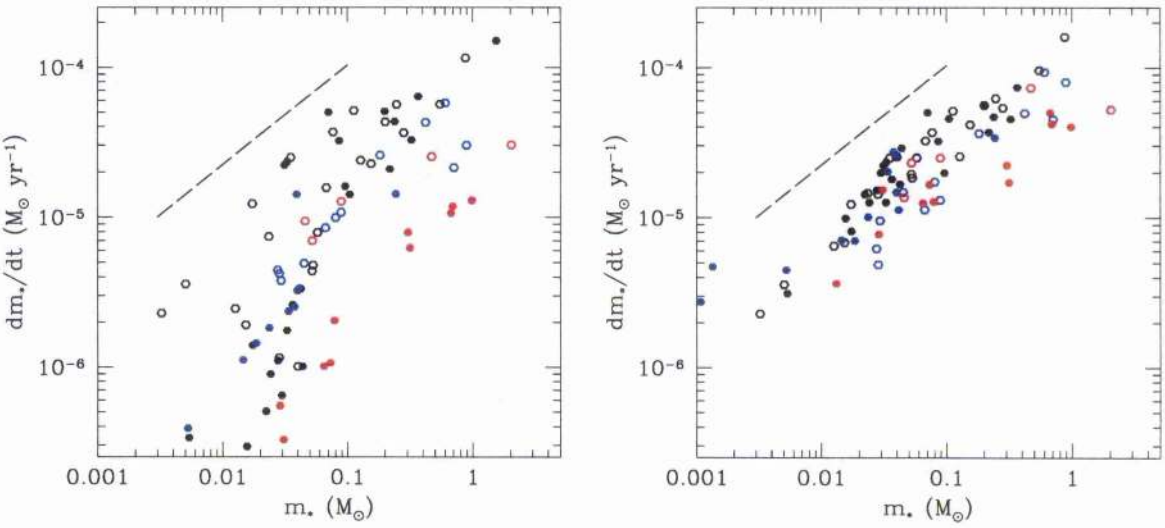

Figure 5.8: The left hand plot shows the mean accretion rate of each protostar, plotted against its final mass. The right hand panel plots the maximum accretion rate for each protostar against its mass. The black points are for the protostars in the clouds with $\epsilon = 10$, the blue points for $\epsilon = 1$ and the red points for $\epsilon = 0.5$. The open circles are the first simulation and the closed circles the second simulation in that energy state, e.g. black-open circle is simulation 1 and red closed circle is simulation 6. The long-dashed line shows a slope of 2/3, as one would expect from the competitive accretion model.

We start with the simple case, where the single protostar forms in a gravitationally unstable clump, with this clump being responsible for the evolution of the protostar since it provides the sole reservoir for the subsequent accretion. Since the clump collapses, it has by definition a Jeans mass. For a uniform density and temperature sphere this is,

$$m_J = \left(\frac{4\pi\rho}{3}\right)^{-1/2}\left(\frac{5}{2}\frac{kT}{G\mu}\right)^{3/2} \tag{5.1}$$

which is the same as the clump mass M_{clump} if we assume that the only form of support is the internal thermal energy of the gas. For an isothermal gas we can remove the temperature dependency and simply say that

$$m_J \propto \rho^{-1/2} \tag{5.2}$$

The accretion rate in such a clump will simply be the mass of the clump divided by the free-fall time of the cloud, where the free fall time is given by

$$t_{ff} = \left(\frac{3\pi}{32G\rho}\right)^{1/2} \tag{5.3}$$

or simply $t_{ff} \propto \rho^{-1/2}$. So the accretion rate for a star forming from a collapsing clump in isolation is simply,

$$\dot{m}_* \propto \frac{m_{clump}}{t_{ff}} \propto \frac{m_J}{t_{ff}} \propto \frac{\rho^{-1/2}}{\rho^{-1/2}}$$
$$\dot{m}_* = const. \tag{5.4}$$

Thus for a protostar forming and evolving in individual star forming clumps, the accretion rate is always the same, regardless of the size of the forming protostar or its pre-protostellar clump, provided the sound speed of the gas is constant. This is essentially the result that Shu (1977) arrives at in his model of the singular isothermal sphere.

We now take the opposing view, whereby protostellar seeds are competing for the accretion of gas in a common reservoir. The derivation given here is just a small part of the original work by Bonnell et al. (2001b). The accretion rate of a star moving through at velocity v_{rel} with respect to a background gas is given by,

$$\dot{m}_* = \pi \rho v_{rel} R_{acc}^2 \tag{5.5}$$

where ρ is the density of the gas and R_{acc} is the accretion radius of the star. Normally one would assume assume Bondi-Hoyle type accretion and thus use the corresponding radius as the accretion radius. The Bondi-Hoyle radius is given by

$$R_{B-H} = \frac{2Gm_*}{v_{rel}^2 + c_s^2} \tag{5.6}$$

where c_s is the sound speed of the gas. However for clusters at a similar stage in their evolution as those we present here, the protostars do not dominate the potential since they have very little of the mass. It is the gaseous reservoir that provides the dominant potential and thus controls the velocities of the protostars. The result of such a potential is that the protostars do not move significantly with respect to the background gas. In such an environment, the Bondi-Hoyle radius does not provide a good measure of the accretion radius. A better estimate for R_{acc} is given by the tidal lobe radius.

$$R_{tidal} \approx \frac{1}{2} \left(\frac{m_*}{M_{enc}} \right)^{1/3} R \tag{5.7}$$

where R is the distance of the star from the cloud centre. The tidal lobe radius defines a volume inside which the gas is more bound to the star than to the rest of the cluster. Using R_{tidal} for R_{acc} in the accretion rate, we get

$$\dot{m}_* \propto \rho v_{rel} R^2 \left(\frac{m_*}{M_{enc}} \right)^{2/3} \tag{5.8}$$

In a collapsing isothermal region, the gas density had a radial dependence of $\rho \propto R^{-2}$ and the velocity of the protostar is independent of its mass and position in the cluster. The mass enclosed is simply $M_{enc} \propto R$. The accretion rate is then,

$$\dot{m}_* \propto \left(\frac{m_*}{R}\right)^{2/3} \tag{5.9}$$

In this type of cluster, the mass accretion rate is therefore related to the mass of the object and its position in the cluster. High mass stars accrete faster than low mass stars, and are thus naturally to be found in the cluster centre, where R is small. Note that if the density profile of the gas is uniform, rather than centrally condensed, then the R dependency goes away, leaving

$$\dot{m}_* \propto m_*^{2/3} \tag{5.10}$$

although we see that the mass dependency is unchanged. We therefore have a very simple method of testing whether the protostellar mass is determined by the initial fragmentation process or whether it is a result of competitive accretion in a much larger region: are the protostellar accretion rates a function of the protostellar mass?

Figure 5.8 plots the accretion histories for all the protostars formed in our simulations. The left hand plot shows the mean accretion rate for each protostar and the right hand plot shows the maximum accretion rate. Despite the obvious differences in the evolution and fragmentation in the clouds that is brought on by the ϵ value, it is clear from the figure that all the stars formed in the set of simulations follow explicit trends with regards to accretion.

There is a strong dependence on mass for both the maximum and mean accretion rates. Explicitly, these accretion rates are well fitted by $\dot{m}_* \propto m_*^{2/3}$, indicating that the protostars are competing for the gas in the manner outlined above. Note that our choice of plotting the accretion rates as a function of the final mass will always have some scatter, since 5.9 (or 5.10) is really dependent on the instantaneous mass, rather than a final mass. It is clear however that the accretion rate for each protostar is not consistent with the isolated clump accretion model, in which $\dot{m}$ is constant. Rather, competitive accretion dominates regardless of the ϵ of the cloud.

That competitive accretion is the dominant mechanism controlling the protostellar masses in our simulations is not that surprising. As was pointed out in Bonnell et al. (1997), this should occur for any region with multiple Jeans masses. Basically, the fragmentation and collapse of each individual Jeans mass occurs on the same timescale as the collapse of the region as a whole. This timescale is simply the free-fall time, t_{ff}, associated with the region's density. Thus the collapsing fragments are interacting with each other. The only way this can be avoided is if the local free-fall time of a small region is much shorter than that of the larger region in which it is embedded. This is essentially the idea behind the turbulent fragmentation scenario, but as we have seen from our simulations, the turbulence appears unable to instigate the collapse, since the structures (or clumps) it creates are unbound.

Is there any difference between the accretion process in the simulations? The times given in table 5.2 yield useful information about the accretion rates of the clouds as a whole. The average time between the onset of star formation and the point where 10 % of the cloud mass has been accreted is $0.07t_{ff}$, $0.38t_{ff}$ and $0.49t_{ff}$ for cloud ϵ of 10, 1 and 0.5

respectively. This corresponds to mean accretion rate in the $\epsilon = 10$ clouds of $\sim 3 \times 10^{-4}$ $M_\odot$ yr^{-1}, while in the $\epsilon = 0.5$ clouds the mean accretion rate is $\sim 5 \times 10^{-5}$ $M_\odot$ yr^{-1}. The dynamical balance of the clouds hence significantly alters the accretion rate. The $\epsilon = 10$ simulations has a higher accretion rate than the $\epsilon = 1$ simulations which in turn has a higher accretion rate than the $\epsilon = 0.5$ simulations. The clouds that are initially more bound therefore have a higher dynamical accretion rate, and as a result the star formation is more aggressive. This is simply controlled by the mean density in the clouds.

5.6 Discussion

5.6.1 The formation of low mass objects

The fact that the clouds with little kinetic support (simulations 1 and 2) form the most stars, potentially has relevance to the study of Delgado-Donate, Clarke, & Bate (2004). This study showed that the form of the turbulent power spectrum can influence the resulting sub-stellar population. They found that for clouds with $E_{kin} = E_{therm}$, a low value of the turbulent power spectrum indice α (as in $P(k) \propto k^{\alpha}$) results in the formation of more objects and a larger fraction of sub-stellar objects. The low value for α was -3 and their high value was -5, chosen to be sufficiently different and also to straddle the $\alpha = -4$ used by (Bate et al., 2003a). The differences in the resulting protostellar populations were attributed to the formation of much smaller structure in the $\alpha = -3$ case. Our results here may provide an alternative explanation.

Turbulence is known to decay on the local crossing time for whatever scale the motions are present (Mac Low et al. 1998; Stone, Ostriker, & Gammie 1998). For large scale flows, the time for the dissipation of turbulence is longer than those at small scales. The amount of kinetic energy at a given scale depends on the power law modelling the turbulence, such that $\alpha = -3$ has more power on smaller scales than $\alpha = -5$. Thus the $\alpha = -3$ simulations in Delgado-Donate et al. (2004) would have been able to lose energy, which is preferentially on small scales, faster than the $\alpha = -5$ simulations. The loss of the kinetic energy on small scales will result in an essentially uniform loss of support against gravity throughout the cloud. The $\alpha = -3$ simulations will thus eventually reach a situation similar to our $\epsilon = 10$ clouds.

We have shown in our study that a collapse of this nature is favourable to multiple fragmentation, due to a decrease in the global Jeans mass. We also see that due to the dominance of competitive accretion in this mode of star formation, that multiple fragmentation also results in a wider spectrum of object masses. Thus not only will the cloud yield a larger population of stellar 'seeds' but there will be a better chance of forming sub-stellar objects. This can explain both the increased number of protostars and the higher fraction of brown dwarfs.

5.6.2 Identifying the physical processes at work

One of the problems with this type of study, and a source of endless confusion for the last decade, is that it is extremely difficult to separate out the role of turbulence and the role of gravity in forming the stellar population. Although the study here attempts to look at the effect of altering the Mach numbers, the resulting global dynamical state of the cloud appears to be the main factor which governs the cloud's evolution. This masks any local processes of the turbulence that may be of interest.

It is difficult to change the initial conditions to compensate for this. The parameter ϵ is related to the properties of the gas by $\epsilon \propto (M/R^2)/(Mv^2) \propto (Rv)^{-2}$. Doing the same for the Jeans number, we get $J \propto (Rc_s)^{-2}$. This gives the ratio of kinetic cloud support to Jeans number of $\epsilon/J \propto \mathcal{M}^{-2}$. So for a fixed number of Jeans masses, the study of different Mach numbers automatically alters the dynamical state of the cloud. The only way to get around this problem is to also change the number of Jeans masses each time. This however introduces the problem that the nature of the star formation will be different, since the number of Jeans masses always seems to control the number of final protostars.

5.7 Conclusions

In this study, we have found that turbulence does not appear to play the role in the star formation process that has been widely attributed to it in recent studies (e.g. Henriksen 1991; Larson 1992; Elmegreen 1993; Padoan & Nordlund 2002). Rather than triggering gravitational collapse, increasing the level of turbulence delays the onset of star formation. This would tend to suggest that turbulence is more of a hindrance than a help to the star formation process. In all the areas that this chapter explores, we find evidence that it is the mean Jeans mass in the cloud that controls the star formation.

The clump distributions at the point of star formation are broadly similar in shape to the IMF. However the vast majority of the clumps in these simulations are unbound. In all the simulations, the clumps which are bound at the onset of star formation, i.e. the clumps in which the first star formation occurs, have a mass which is close to the mean Jeans mass in the cloud.

The initial dynamical state of the cloud does appear to have an effect on the stellar population that forms. The clouds with lower levels of turbulence also produce more stars than those with higher levels of turbulence. The general properties of the clusters are loosely connected to the initial dynamical state of the parent cloud. The clouds with low levels of turbulent support generally form smaller clusters, with more objects, than those with stronger turbulence. The result is that the star formation occurs more quickly, and more with more protostars, in the clouds with lower support.

In all the simulations the dominant mechanism controlling the mass of the protostars is 'competitive accretion' (Bonnell et al., 2001a,b). As a result, it appears unlikely that the shocks produced by the turbulence are able to directly control the masses of the stars or regulate their formation in any way other than simply dissipating kinetic energy.

CHAPTER 6

The formation and fragmentation of protostellar cores

6.1 Introduction

In the previous chapter we showed that the presence of turbulence in small molecular clouds does not significantly change the manner by which stars gain their final mass. In this chapter, we examine the star formation process in more detail, by analysing the energy properties of the clump structure as the simulations evolve towards star formation. In particular we will be interested in the mass at which clumps become bound, and the properties of the clumps as they approach becoming bound.

6.2 Simulation setup and initial conditions

Details of the simulations are given in table 6.1. All the simulations presented here start from a uniform density sphere at 10K, with the gas modelled isothermally. With the exception of simulation 3, they have a mass of $32.6M_{\odot}$ and an initial Jeans mass of $1M_{\odot}$ (initial density $\rho_o = 2.23 \times 10^{-19}$g cm^{-3}). The radius of the clouds at the beginning is 4.07×10^{17}cm. Simulation 3 has a mass of $6.3M_{\odot}$ and an initial Jeans mass of $0.2M_{\odot}$. The initial radius of this cloud is 8.14×10^{16}cm and the density initially is therefore 5.55×10^{-18}g cm^{-3}. These conditions are such that all the simulations have a Jeans number (equation 4.6) of 10.

The clouds are given a turbulent velocity field to provide support against collapse, although the amount of support given is varied in this paper. The support is parameterised by $\epsilon = |E_{grav}|/E_{kin}$ with values of 1 and 0.5 being used here. We have defined ϵ in this manner such that it can be thought of as a kinetic version of the Jeans number. We stress here that the turbulent velocity field in this study is left to freely decay.

All the simulations are given unique random velocity fields. The turbulence is modelled by a Gaussian random field with a power spectrum $P(k) \propto k^{\alpha}$, where k is the wavenumber of the velocity perturbations. This can be more easily understood in terms of a line width-size relation such as that found by Larson (1981) of the type $\sigma \propto L^{\beta}$, where σ is the velocity dispersion at a length scale L. Larson found a value of $\beta = 0.37$ for a range of scales $1 < L < 1000$pc. Looking at smaller scales, Myers (1983) found

$\beta = 0.5$ for $0.04 < L < 10$pc. Unfortunately there is no linear relationship between β and α. However the work of Myers & Gammie (1999) show that an α of -4 in the power spectrum corresponds to a β of 0.5. This value of α is consistent with the observations and so is adopted for the turbulence in our simulations. We also use a larger α of -6 in one simulation, to show how the star formation process differs when the turbulence has energy on larger scales. According to Myers & Gammie (1999) this simulation has an effective β of 0.95.

In this study, we are interested in whether the turbulent velocity field can trigger star formation by locally reducing the Jeans mass, and thus decreasing the mass required for a region to become bound. We mentioned in a previous section, that 1 dimensional, isothermal, compression does not result in a significant increase in the magnitude of the gravitational potential energy. As a result, the gas must have roughly a Jeans mass *before* compression, for it to have a Jeans mass *after*. Thus we must ensure that we have enough energy on scales larger than the initial Jeans length in our simulation if the turbulence is to have any chance of triggering star formation. In our simulations, the largest scale motions (or in the power spectrum notation, the longest wavelength modes or smallest wave-numbers) are the size (diameter) of the cloud. Where the initial mean Jeans is $1M_{\odot}$ in our simulations, the radius of the cloud is 0.13pc, while the Jeans radius is 0.04pc. Similarly for simulation 3 with an initial mean Jeans mass of $0.2M_{\odot}$, the cloud radius is 2.6×10^{-2}pc and Jeans radius is 8×10^{-3}pc. Since the velocity-size relation that we use here is $\sigma \propto L^{1/2}$, the kinetic energy scales as $E_{kin} \propto M(L)\sigma^2 \propto L^4$, for our initially constant density clouds. Thus most of the kinetic energy is on the largest scale of the cloud: the clouds diameter. Since the cloud's diameter is always roughly 3 times the initial mean Jeans diameter, the turbulence is present on a scale larger than the initial mean length.

Two particle resolutions are presented. The lower resolution simulations have 204,800 SPH particles, while the higher resolution runs have 400,000 SPH particles. To ensure that we do not attempt to resolve beyond our resolution limit, we introduce sink particles at the point where the mass resolution is reached. Thus in simulation 1, the sinks form at a density of 8.382×10^{-16}g cm^{-3} with an accretion radius of 2.1×10^{15}cm. In simulations 2, 4 & 5, the sinks are created at 3.312×10^{-15}g cm^{-3} with an accretion radius of 1.1×10^{15}cm, while in the higher density run, simulation 3, the figures are 8.700×10^{-14}g cm^{-3} and 2.1×10^{14}cm. We also smooth the gravitational forces between sink particle pairs to the same size as their accretion radius. This prevents binaries with separations of less than the accretion radius from being formed, and thus prevents the code from slowing down while trying to evolve their orbits.

6.3 Evolution of the clouds

We start our analysis by looking at the properties of the clouds with $\epsilon = 1$ and a turbulent power index of $\alpha = -4$, which are found in simulations 1, 2 & 3. These simulations have physical conditions that are believed to be close to the observed conditions in star forming regions. They also have the same initial dynamical state and type of turbulence as the clouds in a number of previous studies (for example Bate et al. 2003b and Delgado-Donate

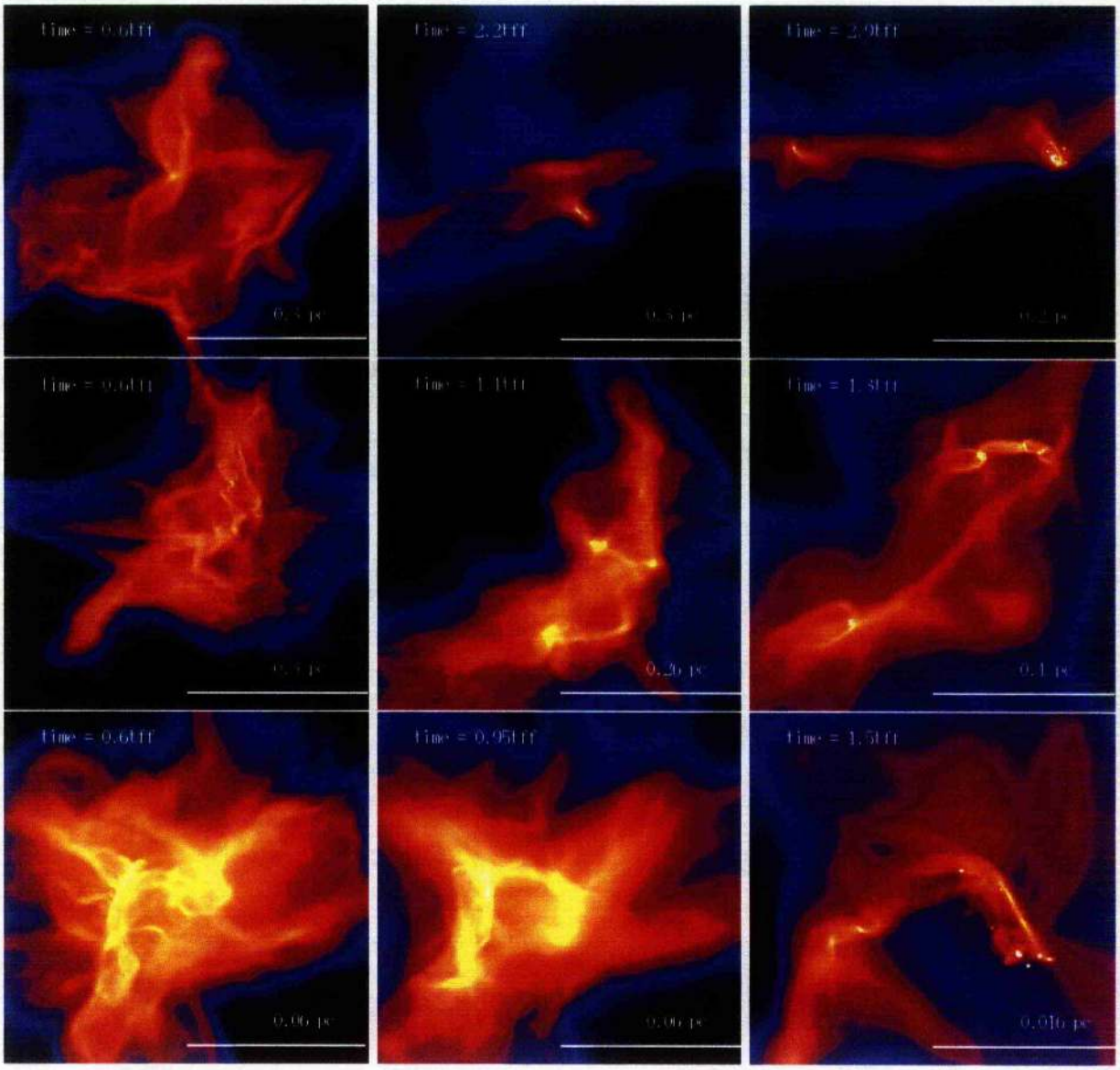

Figure 6.1: The panels show column density images from simulations 1, 2 and 3, which are positioned in the first, second and third rows respectively. The first column shows the state of the gas after $\sim 0.6\ t_{ff}$. The second column panels show the gas just before the onset of star formation (i.e. just before the first sink particle forms) and the last column shows the clouds after 10% of the gas has been accreted/turned into stars.

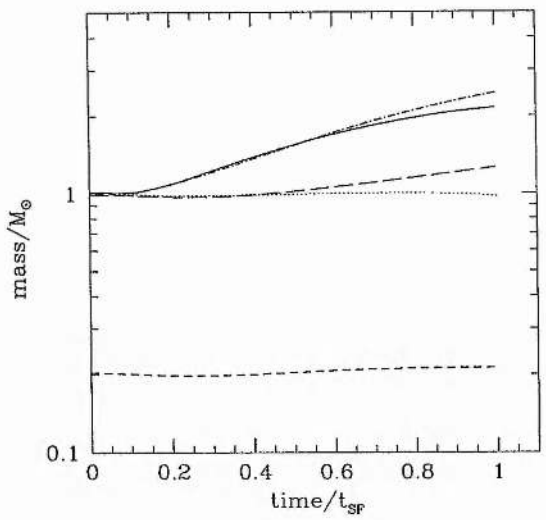

Figure 6.2:
The lines show the evolution of the mean Jeans mass for each of the simulations presented in this paper. The lines are as follows: solid line, simulation 1; dotted line, simulation 2; short-dashed line, simulation 3; long-dashed line, simulation 4; and simulation 5 is the dot/long-dashed line, which has an $\epsilon = 0.5$. The mean Jeans mass is calculated using a density derived from the spherical volume that contains half the cloud's mass. This is centred of the cloud's centre of mass. This density is then used in equation 4.1, along with the half mass radius, to evaluate the mean Jeans mass. See section 6.3 for more details.

Simulation	N_{part}	ϵ	$m_{J,o}$ $M_\odot$	M_{total} $M_\odot$	M_{res} ($M_\odot$) $M_\odot$	$\mathcal{M}_{turb}$ $M_\odot$	$m_{J,turb}$	α
1	204,800	1	1	32.6	0.0163	5.3	0.19	−4
2	400,000	1	1	32.6	0.0082	5.3	0.19	−4
3	400,000	1	0.2	6.3	0.0016	5.3	0.04	−4
4	400,000	1	1	32.6	0.0082	5.3	0.19	−6
5	400,000	0.5	1	32.6	0.0082	7.4	0.13	−4

Table 6.1: Initial conditions for the simulations. N_{part} is the number of particles used in the simulation. ϵ is the ratio of gravitational to kinetic energy and can thus be thought of as a kinetic Jeans number. The total mass in the cloud is given in the column labelled M_{total}. This, combined with the number of particles gives us the minimum mass for which we can accurately resolve gravitational forces, $M_{res} \sim 100 M_{total}/N_{part}$. The initial effective Mach number of the turbulence, $\mathcal{M}$, is calculated from the rms velocity of the field. The value of $m_{J,turb}$is the mass at which turbulent fragmentation would expect to set in, assuming that $m_{turb} = \bar{m}_J/\mathcal{M}$. The parameter α controls the power spectrum from the turbulence $P(k) \propto k^\alpha$. See section 6.2 for more details about the parameters in this table.

et al. 2004) The clouds in this study exhibit the characteristic features of turbulent clouds. Figure 6.1 shows column density images of the simulations. The left-hand panels in the figure contain images of the cloud as it appears after ~ 0.6 t_{ff} (where $t_{ff} = 1.4 \times 10^5$yr for

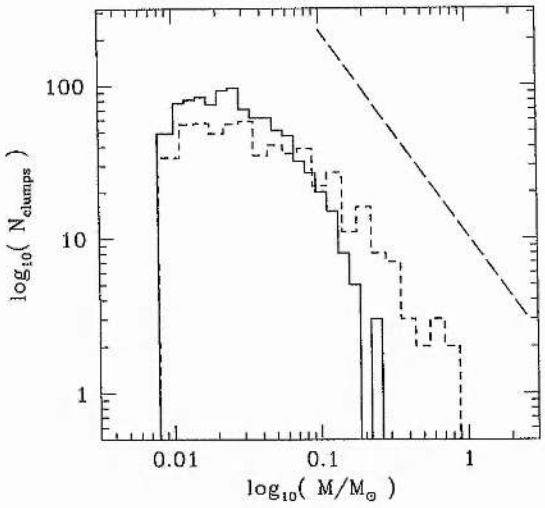

Figure 6.3:
Two clump mass spectra from simulation 2 are plotted, taken at different points in the evolution. The solid line corresponds to $0.6t_{ff}$ and the dotted line shows the clump mass spectrum at the onset of star formation. These correspond to the left and middle columns in figure 6.1. The dashed line gives the typical Salpeter slope of -2.35 (or as plotted, -1.35 in log-log space).

simulations 1 and 2, and 2.8×10^4yr for simulation 3). At this point in the simulations, the density enhancements produced by the turbulence are at their most pronounced.

Star formation does not occur during this initial turbulent phase. In fact this is true for all the simulations presented in this thesis. This does not however mean that the turbulence is not playing an important role in the cloud's evolution since both the energy balance and the gas structure are dramatically altered during this phase. The onset of star formation generally occurs at a time > 1 t_{ff}, although in simulation 1 it takes rather longer, for reasons discussed below. The state of the gas just before the onset of star formation is shown in the middle column in figure 6.1. We see that the gas has much less filamentary structure by this point and that the dense regions (where the star formation eventually occurs) are distinctly separated. These regions are close to the centre of the cloud. When star formation does occur, the protostars are confined to the dense regions. Rather than forming in isolation, they are found in small groups.

In this type of study, it is always difficult to decide at which point the simulation should be terminated. In this paper we have decided to allow the simulations to proceed until 10% of the gas has been either turned into, or accreted onto, sink particles (the 'protostars'). By this point, all the simulations have formed roughly 11 stars. It is likely that if the simulations were left to continue following the evolution of the clouds, more stars would form. As was stressed in our opening remarks however, the evolution of the stars and the cluster environment is not the purpose of this paper. This has been studied in much greater depth in the simulation of Bate et al. (2003b). Our aim here is to find the point at which the fragmentation sets in. We thus need only a few stars to form in the simulation to evaluate the energy processes involved in their formation.

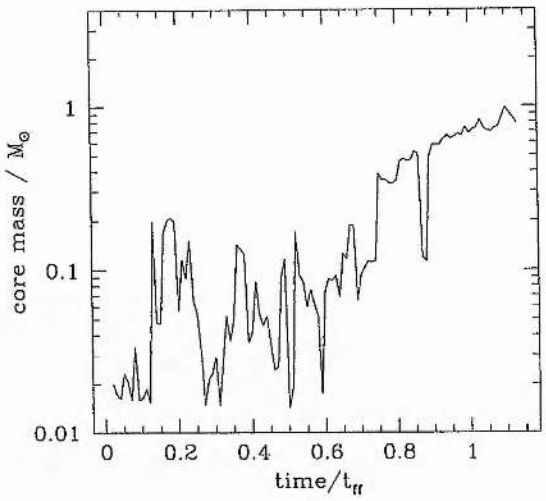

Figure 6.4: Shown in this figure is the clump history for the first particle to be turned into a 'sink' (protostar) particle. We trace back in time, before the particle is turned into a protostar, and find the mass of the clump in which the particle is embedded. Thus we can see the mass evolution of the clump as it moves towards star formation.

An important physical parameter in this paper is the mean Jeans mass. As is shown in table 6.1, simulations 1 and 2 starts with a Jeans mass of $1M_{\odot}$ and simulation 3 has a Jeans mass of $0.2M_{\odot}$. However, these global values can change as the simulation proceeds. Since we have a free boundary the mean density of the cloud can change. The random velocity field that is imposed in simulation 1 happens to have a significant amount of general expansion, causing the cloud to expand substantially more than the other runs. The decrease in density results in an increase in the mean Jeans mass in the cloud.

Figure 6.2 shows the evolution of the mean Jeans mass as function of time. To evaluate the mean Jeans mass in a cloud, we use the following method. First we work out the centre of mass of the cloud, and sort all particles in terms of their radius from this point. We then work through the particles radially, summing up the enclosed mass, until we have half the gas fraction for the cloud. The radius of the the last particle to be added to the mass count is then used as the half mass radius. This radius, along with half the cloud's mass, is used to define a mean density for the cloud, $\bar{\rho} = (3M_{1/2})/(4\pi r_{1/2}^3)$. We then get the mean Jeans mass by substituting this value for the mean density into equation 4.1 for the Jeans mass. This gives a value for the Jeans mass in the region where all the star formation occurs. We see from the figure that simulations 2 and 3 have a fairly constant mean Jeans mass but in simulation 1 it rises from $1M_{\odot}$ to about $2.5M_{\odot}$ by the time the star formation sets in. The expansion in this simulation delays the onset of star formation until $\sim 2.2t_{ff}$.

Figure 6.3 contains the clump mass spectrum at two instances in simulation 2. These are the clumps found by our structure finding algorithm (see section 3.2). The solid line spectrum is from 0.6 t_{ff}, which is the point in the evolution depicted in the left hand column of figure 6.1. The dashed line shows the clump mass spectrum just before the point of star formation. By comparing the two plots it is immediately clear that there

is considerable evolution in the mass of the clumps. At 0.6 t_{ff} there are no clumps over $0.4M_{\odot}$ whereas at $\sim$1 t_{ff} a considerable number of clumps have masses in the range 0.1 to $1M_{\odot}$. This implies that density features merge to form more massive structures.

We can see this merging process more explicitly in figure 6.4. We have selected the first SPH particle to be turned into a 'sink particle', or 'protostar', and have traced the clumps that this particle belonged to, up to the point where it becomes a protostar. Figure 6.4 shows how the mass of these clumps evolve. Clearly the clumps start small and then become larger as we move towards star formation. This suggests that the merging of clumps is in some way linked to the star formation process in the cloud. As we will see in later sections of this chapter, this merging process is a result of star formation. When the star formation begins, the particle that is about to become a protostar particle has found itself at the centre of a clump of nearly $1M_{\odot}$. This size of clump is among the largest in the simulation, as we see from the clump mass spectrum (dashed line) in figure 6.3.

The clump mass spectrum at the onset of star formation is well fitted by the Salpeter slope (Salpeter, 1955), which is shown by the dashed line, and also shows a turnover at about $0.1M_{\odot}$ to a shallower power law. As was mentioned in our opening discussion, it has been suggested the IMF comes directly from the clump mass spectrum, with each clump condensing into one star. We point out here that simulation 2 only forms 11 stars when we terminate the evolution. This is clearly at least two orders of magnitude less than the number of objects that exist in the clump mass spectrum, even if one only considers the clumps that roughly follow the Salpeter slope. This cannot simply be due to our choice of when to terminate the simulation. If the clumps were to have a Jeans mass and be bound then all the structure shown in the mass spectrum would collapse on less than the free-fall time of the cloud. This is simply because the free-fall time of an object is inversely proportional to the Jeans mass. Thus if all this structure was bound, a considerable fraction would have turned into stars by the point at which we stop the simulation.

Even when run for a much longer time, simulations of this type do not appear to produce as many stars as we have clumps in figure 6.3. We refer here to the simulation of Bate et al. (2003b), which does not form any more stars than the number of Jeans masses that are initially contained in the cloud. Furthermore, roughly half of these stars/brown dwarfs form in turbulent circumstellar discs, and are thus not part of the normal fragmentation process.

So clearly the turbulence is capable of creating a spectrum of objects that closely resembles the observed IMF in its shape but not all this turbulent structure is bound. We also see that there is a merging process at work, with small clumps joining together to create larger structures. At some point in the coagulation process, the clumps become bound allowing stars to form. In this chapter we wish to examine how this transition to bound structure occurs and whether the turbulence has a role in controlling the star formation.

6.4 The evolution towards star formation

6.4.1 Core energy evolution

In this section, we examine how star formation is initiated in a turbulent environment. We examine the boundness of the clumps and their evolution towards gravitational collapse in the simulations. To follow the evolution of the clumps as they become bound objects, we harness the Lagrangian nature of SPH. The particle representation of the fluid allows us to trace the origin of all the material that ends up in the protostars. In this section, we therefore analyse the energy states of the clumps which contain SPH particles that eventually become protostar particles. By finding all such clumps at discrete time intervals up to the point of star formation, we can build a picture of how the clumps evolve.

Figure 6.5 contains the energy details of all the clumps as a function of their mass. The points represent all those clumps, before star formation occurs, that contain particles that will eventually become protostars. There are three quantities plotted in figure 6.5 as a function of the clump mass. Firstly, we show the virial ratio, defined as the ratio of supporting energies (kinetic and thermal) to the absolute value of the gravitational energy. To be gravitationally bound, and therefore eventually liable to collapse, requires a virial ratio of less than 1. From figure 6.5 we see that low-mass clumps are far from being gravitationally bound whereas the more massive clumps are increasingly closer to becoming gravitationally bound. We note again that as the clumps are evolving in time from low-mass to higher-masses, the evolution in time is also from highly unbound structures towards the point where gravity is dominant over the supporting energies. Of particular interest is that the clumps attain a virial ratio of ≤ 1 only at the point where they have masses in excess of the mean Jeans mass of the cloud, $\bar{m}_J$. Thus, even though the turbulence has significantly affected the structure of the cloud on all scales, the mass at which clumps become gravitationally bound appears to be unchanged.

The second column in figure 6.5 plots the number of thermal Jeans masses contained in each clump as a function of the clump's mass. This is calculated from the ratio of the absolute value of the clump's gravitational energy to its thermal energy, raised to the power 3/2 (see equation 4.6). We see from the second column of figure 6.5 that the low-mass clumps contain but a small fraction of a Jeans mass. This fraction increases as the clumps evolve to higher masses to the point that the clumps contain multiple *thermal* Jeans masses by the time they are gravitationally bound. This occurs as the clumps contain significant kinetic support up to and including the point where gravitational collapse sets it. This is very important as a collapsing clump containing multiple Jeans masses is susceptible to fragmentation and can thus lead to the formation of binary and multiple systems. We will return to this point later in the paper.

The right-hand column of figure 6.5 plots the evolution of the ratio of kinetic to the absolute value of the gravitational energies as a function of clump mass. We see a similar evolution here where low-mass clumps contain too much kinetic energy to be bound and only attain a configuration where gravity is dominant over the kinetic energy once they have masses closer to the mean Jeans mass of the cloud.

Comparing the three figures in the top row (for simulation 1), we see that although

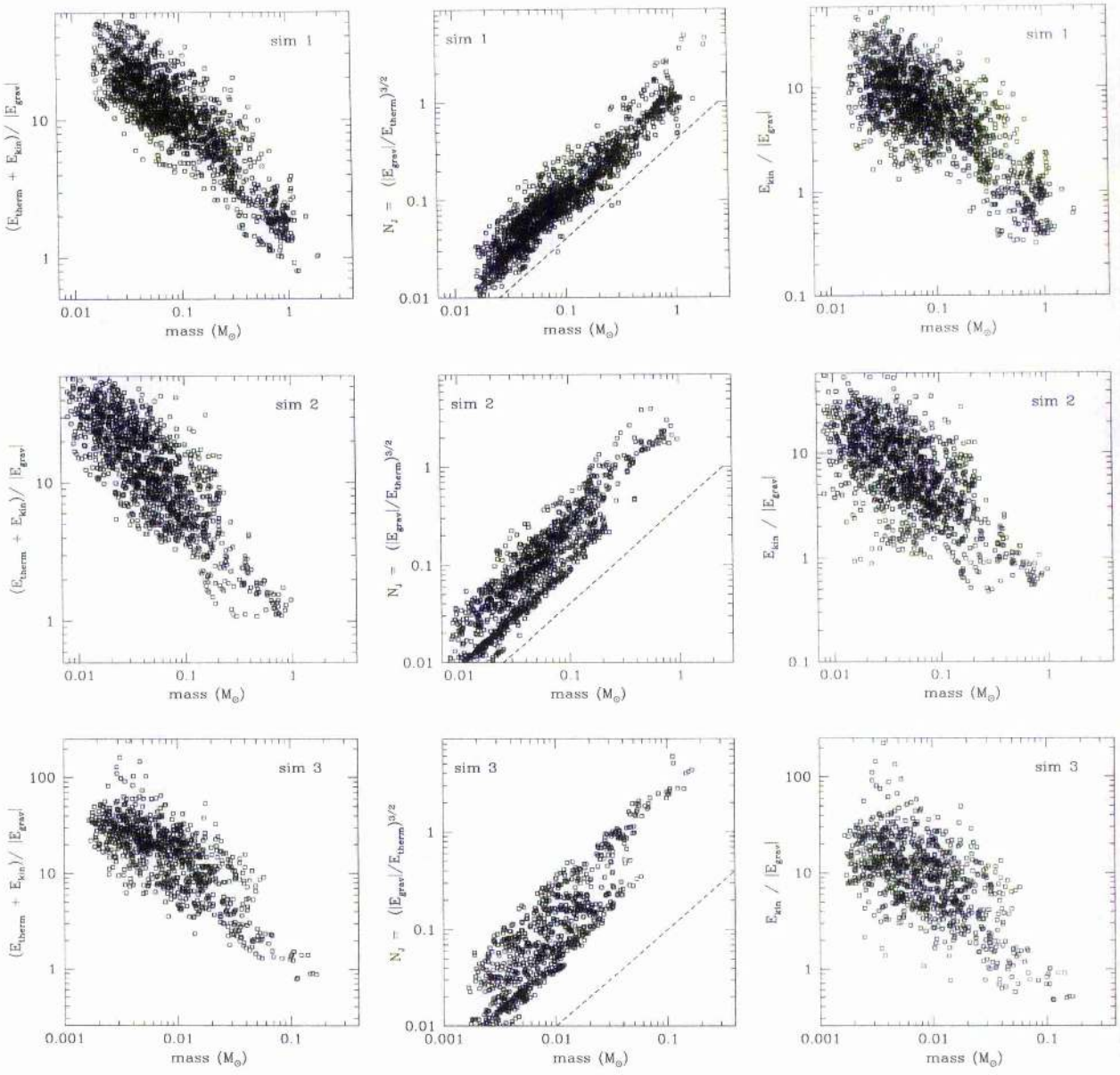

Figure 6.5: The graphs show various energy properties of the clumps as a function of clump mass for the 3 simulations with $\epsilon = 1$. Shown is the data for all clumps that contained a future sink particle (i.e. protostar) up until the point where the first protostar forms. Mass evolution is equivalent to time evolution. We note that the clumps appear to evolve in mass with a constant density. The dashed lines in the central column show the slope one would expect if the clumps are evolving in mass at a constant density (see the text in section 6.4.1 for explanation of this). This slope is = 1.

the clumps are gravitationally bound only once they have masses ≥ 1 $M_\odot$, their thermal and kinetic energies are independently more than the absolute value of the gravitational energies well before this point. This is similarly true for simulations 2 and 3. Thus the clumps are supported by a combination of thermal and kinetic energies as they approach collapse, with neither supporting energy being particularly dominant over the other. It is also the case that the lower mass clumps in all the simulations have both thermal and kinetic energies that are well in excess of their gravitational energy. The low mass clumps are thus rendered unbound by each of both their kinetic and thermal energies. We will discuss the relationship between the thermal and kinetic energies further in the next section (section 6.4.2).

The picture that forms from the analysis of the energy evolution of the clumps is one where the turbulence initially drives significant structure into the cloud but that this structure is not close to being gravitationally bound. Instead the clumps need to grow in mass until gravity can take on a dominant role in driving the evolution towards star formation.

The generation of structure by the turbulence does mean that the density of the clumps formed by the turbulence is greater than that of the initial, uniform, cloud. Thus, in the absence of any kinetic energies, the gas would be able to form stars from lower mass clumps than it can in the uniform cloud. We can see this clearly in figure 6.5 since at the point where the clumps attain a mass comparable to the mean Jeans mass in the unperturbed cloud, the clumps actually contain several Jeans masses. Also we note that, for example in simulation 2, the clumps gain a thermal Jeans mass at ~ 0.2 $M_\odot$. The mean Jeans mass in the cloud is ~ 1 $M_\odot$, indicating that the local increase in density (i.e., the 'clump') has decreased the required mass for gravity to overcome thermal energy support. The factor of 5 decrease in the Jeans mass associated with the post shock gas, is what is expected for a cloud with a turbulent Mach number of ~ 5 (see equation 4.8).

We see from figure 6.5 that the number of Jeans masses increases linearly with the mass of the clump. This can only occur if the Jeans mass is constant, which in an isothermal gas implies that the gas density is approximately constant. That the density in the clumps appears to be constant throughout the evolution should not be surprising as the cloud's ability to generate higher densities, due to self-gravity, can only occur once collapse sets in. Note that this means that the clumps in the simulations coagulate to form more massive structures while retaining their original density, set by the turbulent shock compression.

We also note that two of the plots in the middle column of figure 6.5, those for simulations 2 and 3, display some banding in the point distribution. This banding arises from different clumps being a slightly different densities. The plots mentioned show a strong band which would intersect $N_J = 1$ at a mass of $1M_\odot$ for simulation2 and 0.1 for simulation 3. These masses are just the mean Jeans mass in these clouds, thus the points in the bands denote clumps at the pre-shock density. Note however that these bands never continue to $N_J = 1$. Only the higher density clumps manage to continue to $N_J = 1$, and it is these high density clumps that become involved in the star formation.

An interesting point to note here is that the coagulation does not occur until quite late in the run up to star formation. This can been seen if we look back to figure 6.4. The

mass of the clump in which the future sink particle finds itself embedded varies wildly for the first 0.7 t_{ff} or so. Only after this time do we see that the mass starts to steadily increase. The clumps that appear towards the high mass end of the plots in figure 6.5 must therefore be formed quite late in the evolution. Since, as discussed above, the coagulation results in the clumps having multiple thermal Jeans masses at the point at which they are bound, the ability to fragment must only exist for a short period before star formation sets in. Pringle (1989) argues that fragmentation is more likely to occur if a body of gas gains multiple Jeans masses, and also structure, just prior to the final collapse. The bound clumps in our simulation thus provide a good environment for fragmentation.

6.4.2 Bringing together gas and forming the cores

In the previous section, we saw that the evolution towards star formation is the evolution from low-mass unbound clumps towards higher-mass clumps that become bound at or near the mean thermal Jeans mass in the cloud. To supplement this view, we now analyse the evolution of the energy of the gas that eventually comprises the first clump to undergo gravitational collapse. We select all the mass that is in this clump at the point where the first protostar forms and then evaluate its energetics at previous stages in the evolution. Note that this means that any intervening gas which does not comprise the final clump is not included.

The energies are calculated every $0.01t_{ff}$ from the beginning of the simulation to the point where star formation occurs. The kinetic energy is calculated with respect to the centre of mass of the particle distribution at each point in time. This process was performed for simulations 1 and 2, with the results shown in figure 6.6. To get a better idea of how the clump is accumulated, we plot the energy evolution of the inner 1/3 and 2/3 mass fractions of the material as well as the whole clump mass.

Since we are looking at a fixed mass of isothermal gas, the thermal energy content is set, as we can see from the long dashed lines in figure 6.6. The fixed mass quantity also means that the potential energy line provides a measure of the physical size of the mass distribution. We see that in both simulations there is a gradual increase in the absolute value of the potential energy. This means that the clump material is continuously contracting as it evolves towards star formation, suggesting that gravitational collapse is occurring on larger scales in which the clump is embedded.

The dotted lines in the plots in figure 6.6 follow the evolution of the kinetic energy of the clump material. Before the collapse sets in, the kinetic energy is generally dissipated in shocks, although it is possible for material to gain energy in collisions with higher momentum gas. The inner fractions of the material become subsonic long before the outer regions undergo free-fall. This idea has been discussed by Goodman et al. (1998) and was suggested to correspond to a break in the Larson line-width size relation.

We also note from figure 6.6 that the entire clump has rough equipartition between the kinetic and thermal energies before kinetic energy once again increases due to collapse. A consequence of this is that the clump material naturally has at least 2.8 thermal Jeans masses at the point at where is becomes bound. This follows straight from the energy condition,

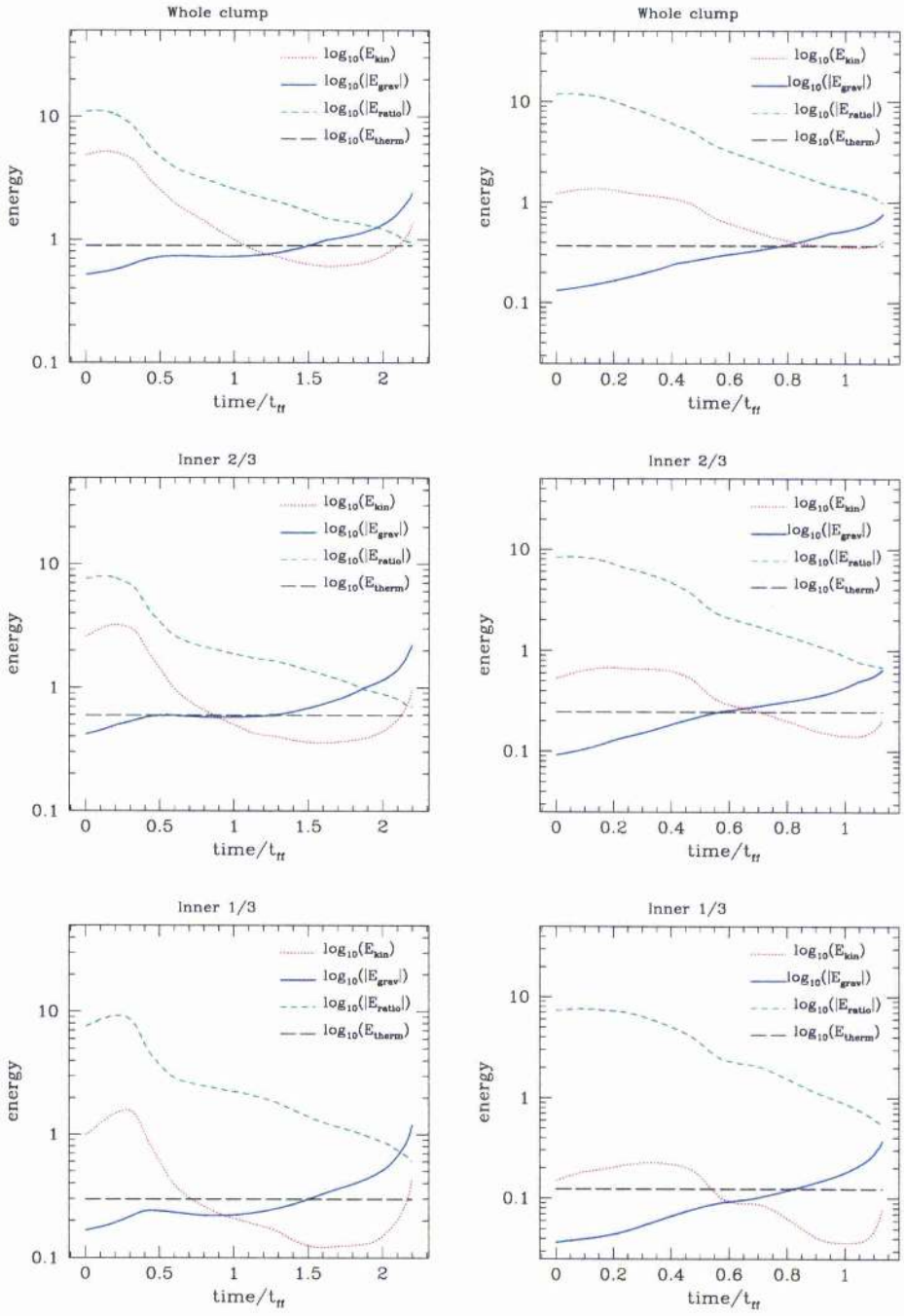

Figure 6.6: The plots show the energy evolution of the material that becomes the first clump to form a protostar for simulations 1 and 2. Note that the energies given here are in code units, but what is important is their relative values. The mass of these clumps are $2M_\odot$ and $0.8M_\odot$ for simulations 1 and 2 respectively. The energies are calculated with respect to the centre of mass of this material and the gravitational energy is therefore only that produced by the mass that makes up the clump. The plots in the left column show the data for the first clump to form in simulation 1 (see table 6.1) and the right column show the same data but for simulation 2. The short dashed line in the figure denotes $E_{ratio} = (E_{therm} + E_{kin})/|E_{grav}|$, the ratio of supporting to gravitational energy.

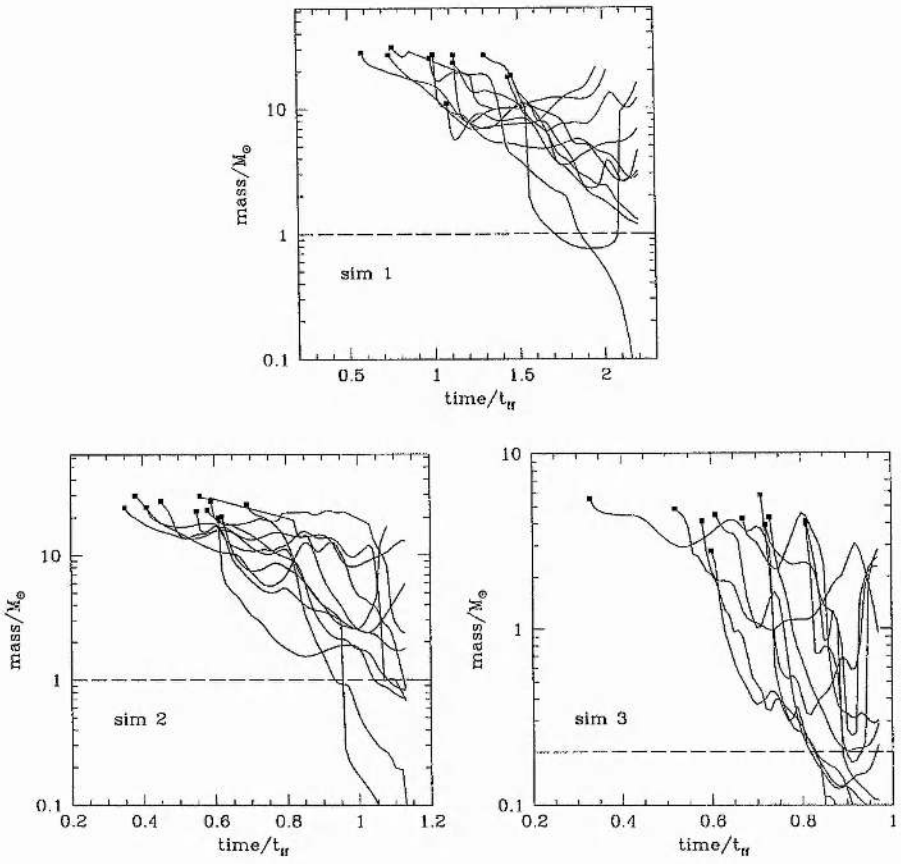

Figure 6.7: These plots show the minimum mass required to make a bound region, surrounding each future protostar particle as they make their way to becoming protostars. The point at which a future sink particle first finds itself at the centre of such a bound region is marked by a square. The solid lines then follow the evolution of these regions. The dashed lines denote the *initial* Jeans mass in the cloud for comparison.

$$|E_{grav}| = E_{kin} + E_{therm} = 2E_{therm} \tag{6.1}$$

since $E_{kin} = E_{therm}$. The number of Jeans masses is then given by,

$$N_J = \left(\frac{|E_{grav}|}{E_{therm}}\right)^{3/2} = 2^{1.5} = 2.8 \tag{6.2}$$

where we have made use of equation 4.6. The clumps are thus in a condition where they can fragment into 2 or more objects during the collapse process, although this obviously depends on geometry. A result of this energy balance is that the star forming clumps are naturally in a state to form binary and multiple systems (Pringle, 1989).

6.4.3 The role of the mean Jeans mass

Collapse always occurs in clumps that have a mass roughly equal to the mean Jeans mass in the region. We have also seen from the discussion that there is an evolution from small to large structures before clumps become bound. Is it possible that the mean Jeans mass, or even a region with more mass, is working on scales larger than the clump population, to bring them together?

In figure 6.7 we examine the energy state of the gas surrounding the particles that eventually become protostars for simulation 2. Every $t_{ff}/100$ we plot the minimum amount of mass needed around the future protostar particles in order to have a bound region. This is evaluated by working radially from each of the future protostars, adding the total energy contribution of one particle at a time. Note that the use of this method of evaluating the gravity assumes that the region is spherical. As a result it will generally make the regions appear more bound than they are. Thus our masses shown in figure 6.7 are lower limits to the required mass for forming a bound object.

At the very start of the simulation, the entire cloud is still not enough to form a bound object, since the cloud is initially slightly unbound ($|E_{grav}| = E_{kin}$, but there is also a thermal component, E_{therm}). As the kinetic energy is dissipated, the amount of mass required to form a bound region centred on the sink particle starts to decrease. As soon as a bound region is formed, it will start to collapse, and this will occur on roughly the free-fall time of the region, which is in turn dependent on the mean density, $\bar{\rho}$.

The clumps that are formed from the turbulence, while it is dissipating, are fairly small in comparison to the regions which are bound. For example, note from figure 6.3 that the most massive clumps present in simulation 2 at $0.6t_{ff}$ have a mass of $\sim 0.2M_{\odot}$; the smallest bound region at this point contains several solar masses. The structure produced by the turbulence is thus embedded in much more massive, bound, collapsing regions. For the most part, these relatively low mass clumps are formed and destroyed on their internal crossing time, their destruction arising from a combination of internal thermal and kinetic energies.

Once the turbulent motions become roughly sonic, and thus the collapse process is slowed by the removal of the kinetic energy dissipation in shocks, the mean Jeans mass is able to fragment out of the bound regions.[1] The mean Jeans mass still contains considerable sub-structure in the form of the clump population. As it collapses, it pushes these cores together, as we show in the cartoon in figure 6.8. Rather than being short lived transient objects, the cores can now start to exist as more coherent entities. The mean Jeans mass will collapse at roughly the sound speed, since the free fall time of a one Jeans mass sphere of gas is just the sound crossing time. The coagulation of the clumps inside the collapsing region will thus also occur at roughly the sound speed. As discussed in section 6.4.1, this will result in the clumps retaining their original density (roughly) as they coagulate to form more massive objects. The timescale for the coagulation to form a clump of mass $\sim \bar{m}_J$ is also the timescale on which the star formation occurs, simply the free-fall time t_{ff}. Thus at the point of star formation, the protostars find themselves

[1]Note that it is still not clear from this study why the mean Jeans mass should be able to control the fragmentation. We are merely showing in this chapter that it does.

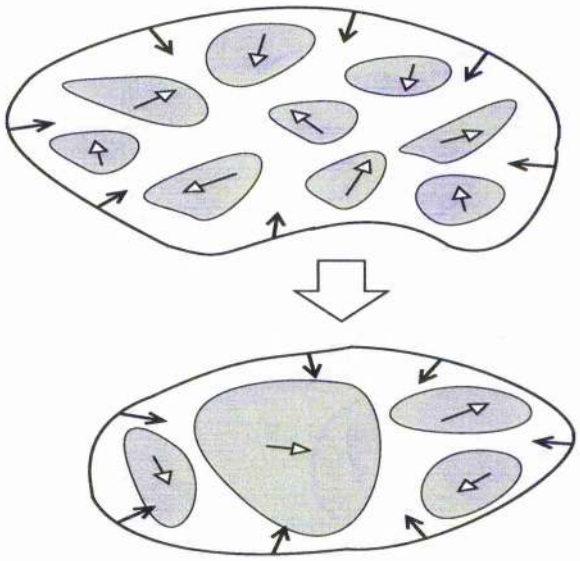

Figure 6.8:
A cartoon picture of the star formation process that occurs in these simulations. At some point in the simulation, a region of gas with mass equal to the mean Jeans mass in the cloud, $\bar{m}_J$, is able to fragment out from the surrounding gas. We denote this region in the two images above by the thick black line. This region contains sub-structure in the form of clumps, that have been produced by the shocks from the turbulent motions (top image, denoted by the shaded regions). These smaller scale clumps have random motions, and until this point in the simulation have been transitory objects. As the region collapses, the internal clump structure is pushed together, forming larger objects (shown in the bottom image). Since the collapsing region has 1 mean Jeans mass, the collapse will occur at roughly the sound speed. The result of this is that the coagulation occurs from clumps moving at roughly the sound speed, such that they manage to retain their approximate pre-coagulation density. The time-scale for all the clumps inside the region to coagulate is also the same timescale as the collapse of the region, namely the free-fall time, t_{ff}, associated with the mean density, $\bar{\rho}$. At the point of star formation, the newly formed protostars find themselves in a star forming clump with a mass equal to the mean Jeans mass in the cloud. The fact that the region has formed by bringing together many smaller objects of density $\rho_{turb} = \bar{\rho}\mathcal{M}$, coupled with the fact that the mean Jeans mass region is in rough equipartition of kinetic and thermal energies, means that the clump has several *effective* Jeans masses. The star forming clump is thus able to fragment, producing small clusters rather than single stars.

embedded in a clump which has a mass equal to $\bar{m}_J$. This explains the behaviour of the clumps in the left hand panels of figure 6.5.

We mentioned in the previous section that the gas is in rough equipartition of thermal and kinetic energies in the run up to star formation, and that the equipartition provides a source for fragmentation, since it results in the collapsing region having 2.8 effective Jeans masses. The 2.8 effective Jeans masses suggests that binary and multiple system formation should be common in these clouds. Note that rough equipartition between thermal and kinetic energies is the natural end point for supersonic energy dis-

sipation via shocks, assuming that driving mechanisms are either not important or not present.

6.5 Different cloud conditions

The simulations that we have looked at so far in this paper contain turbulent fields that are believed to be close to the conditions in star forming clumps, i.e. they have a power spectrum index of $\alpha = -4$ and the gravitational potential energy is balanced by the turbulence. These are also the conditions commonly used in studies of numerical star formation. In this section we relax these observational constraints and look at different initial conditions for our turbulent field.

Firstly we look at changing the turbulent power spectrum to one that contains more power on large scales than the previous simulations, with $\alpha = -6$. This corresponds to a cloud with a Larson type relation of $\sigma \propto L^{0.95}$ (Myers & Gammie, 1999). This type of turbulent field has more power on large scales and thus produces larger scale shocks. The clumps produced from this type of turbulence will have the chance to rid themselves of their kinetic energy and become bound. If the idea of turbulence creating small bound structure from turbulent flows is to work, it should at least be present when we use a power spectrum of this type. This cloud is referred to as simulation 4, and its details can be found in table 6.1.

We also look at changing the magnitude of an $\alpha = -4$ turbulent field. Increasing the effective turbulent Mach number from 5.3 to 7.4 means that the cloud should produce smaller objects with respect to the mean Jeans mass than simulations 1 to 3. The cloud is given an $\epsilon = 0.5$ such that the kinetic energy is two times the gravitational energy in magnitude. The cloud is hence globally unbound (see Clark & Bonnell 2004 for a discussion of such clouds).

6.5.1 Changing the turbulent power spectrum

The top row in figure 6.9 contains the column density images for simulation 4, with $\alpha = -6$. Immediately we can see that the turbulence has a very different form from the previous simulations. The velocity field has more power on large scales, producing strong filaments that are less flocculent than those arising from the $\alpha = -4$ power spectrum. Since the turbulence has more power on large scales than the $\alpha = -4$ simulations, the structure seen in figure 6.9 is longer lived than before.

At the onset of star formation in the cloud, the gas has essentially formed into one long filament, in which a number of dense knots are visible. Part of this filament collapses to form a small cluster of 6 stars. Some of this filamentary structure is preserved and one can see that a number of stars condense out of the strip of gas that feeds the small cluster. By the point at which it is terminated, the simulation forms 10 stars in total.

Looking at the evolution of the clumps that contain future sink particles (shown in the top row of figure 6.10), we see the same trends that were discussed in section 6.4.1 and

shown in figure 6.5 for the previous simulations. We now notice however that the clumps are becoming bound at much smaller masses than in the original simulations, at about 0.3 - 0.4 $M_{\odot}$. We also see that the clumps have a Jeans mass when the clump mass reaches $\sim 0.1M_{\odot}$ (figure 6.10, middle column, top row), again slightly less than in the previous simulations, but still roughly consistent with the prediction of expression 4.8.

There is much less kinetic energy on small scales in this simulation, a consequence of the power spectrum of the initial turbulent field. As a result, clumps with $E_{kin} < |E_{grav}|$ now span a considerable range in the plot, roughly 2 orders of magnitude, compared to the previous simulations where the kinetic energy was only dissipated in the larger clumps. This aids in the formation of bound structure. Also, with less energy present on the small scales, the larger scale flows will be more coherent, giving direct fragmentation more time to occur in the shocked regions. Note that complete dissipation of the internal kinetic energy of a clump is never really possible, since once the gas motions become sonic they are no longer involved in shocks. Thus there is always a sizable kinetic component in the energy balance of the clumps. This residual kinetic energy is the reason why the bound clumps form at 0.3 - $0.4M_{\odot}$, rather than the $0.2M_{\odot}$ size that we would expect from expression 4.8.

It would therefore appear that it is possible to reduce the size of bound objects that condense out from a turbulent environment. The problem is that the form of the turbulence is not at all similar to what is observed in star forming regions. In fact the turbulence here has more in common with pure colliding flows than the turbulence model that has been used in trying to explain the IMF. The nature of the star formation in this cloud is clearly more closely associated with the shock structure. Stars form directly from the filaments as opposed to the previous simulations where larger, rounded, regions characterise the sites of star formation.

6.5.2 Higher Mach number

The images from simulation 5 are given in the bottom row of figure 6.9 and the energy ratios of the clumps can be found in the bottom panels of figure 6.10. This simulation is similar to that described by Clark & Bonnell (2004) in that they are both initially unbound by their internal kinetic energy.

The stronger shocks in this simulation produce a more distinct structuring in the early phases of this simulation, for about the first $0.5t_{ff}$. However there is still no star formation induced in the shock generated clumps. In fact star formation actually takes quite a considerable time to set in, with the first star forming at $1.7t_{ff}$. The simulation also only manages to form 5 stars, less than half the number formed by each of the first four simulations. As was described in Clark & Bonnell (2004), unbound clouds such as these have a large initial expansion. Since they fail to produce any stars directly from the turbulent flows, star formation is delayed while the cloud expands and alters the free-fall time of the gas. After expanding, the central regions, provided they are still bound, gradually start to collapse. The amount of fragmentation depends on the number of Jeans masses contained by the bound region, how aspherical the region has become, and how much substructure it has maintained.

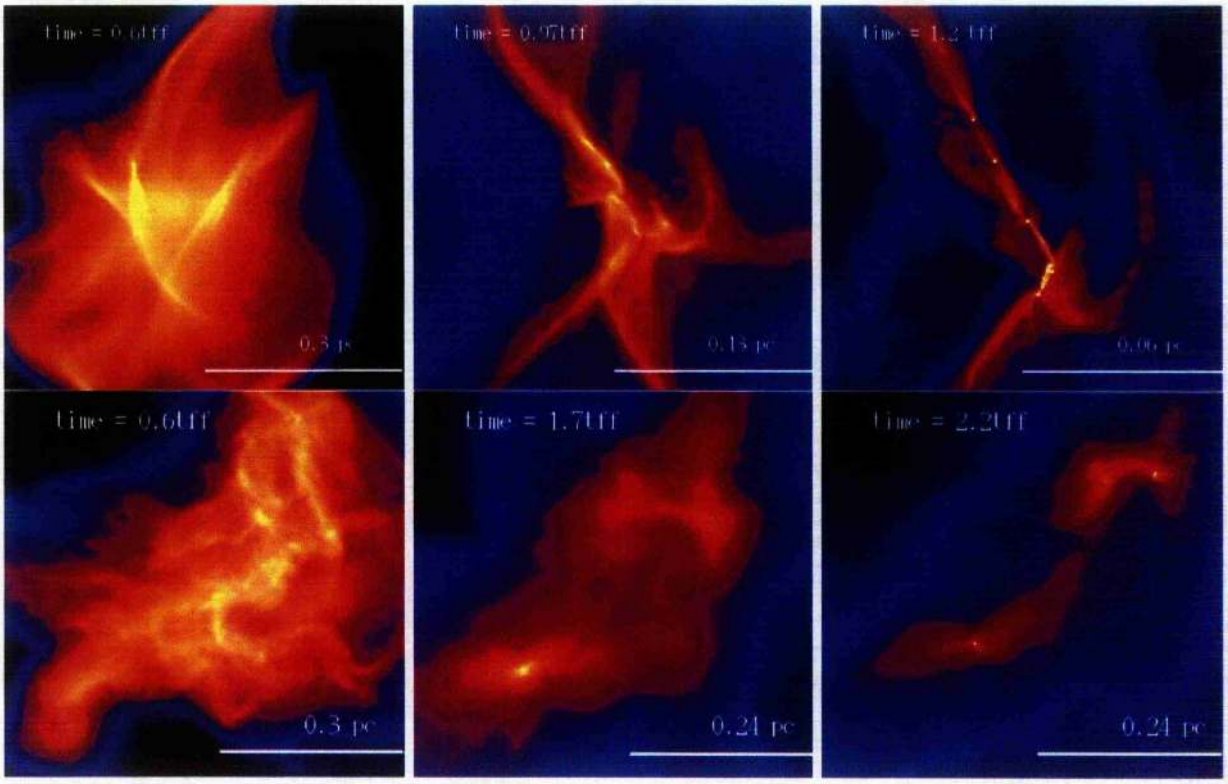

Figure 6.9: The column density images for the simulations presented in section 6.5. The top row contains images from simulation 4, in which the turbulent power spectrum is altered. The bottom row contains images from simulation 5 which has a turbulent field with a higher Mach number.

Looking at the energy ratios in figure 6.10 we see that the clumps involved in the star formation process follow the same trends as the clumps in simulations 1 to 3. Thus the presence of a higher Mach number turbulent field does not produce any difference in the energy properties of the clumps. Again, the density structure produced by the turbulent flows is not controlling the star formation. In fact if we look closely at the middle panel, which shows the number of Jeans masses contained by a clump as function of its mass, we note that the effective Jeans mass for the clumps in these simulations is $1M_{\odot}$. The expansion phase of the cloud has allowed the small clumps produced by the turbulence to be eradicated by the time the star formation sets in. This is why the column density images in figure 6.9 for this simulation look so smooth at the point of star formation. The structure that is left over by the time the star formation occurs is simply the result of the mean Jeans mass, as it fragments out of the inner regions.

6.6 Discussion

The main implication of the results presented in this chapter is that the density structure produced by the supersonic turbulent motions is not connected to the star formation process. The clumps are simply structure. This may be partly why the study of Delgado-

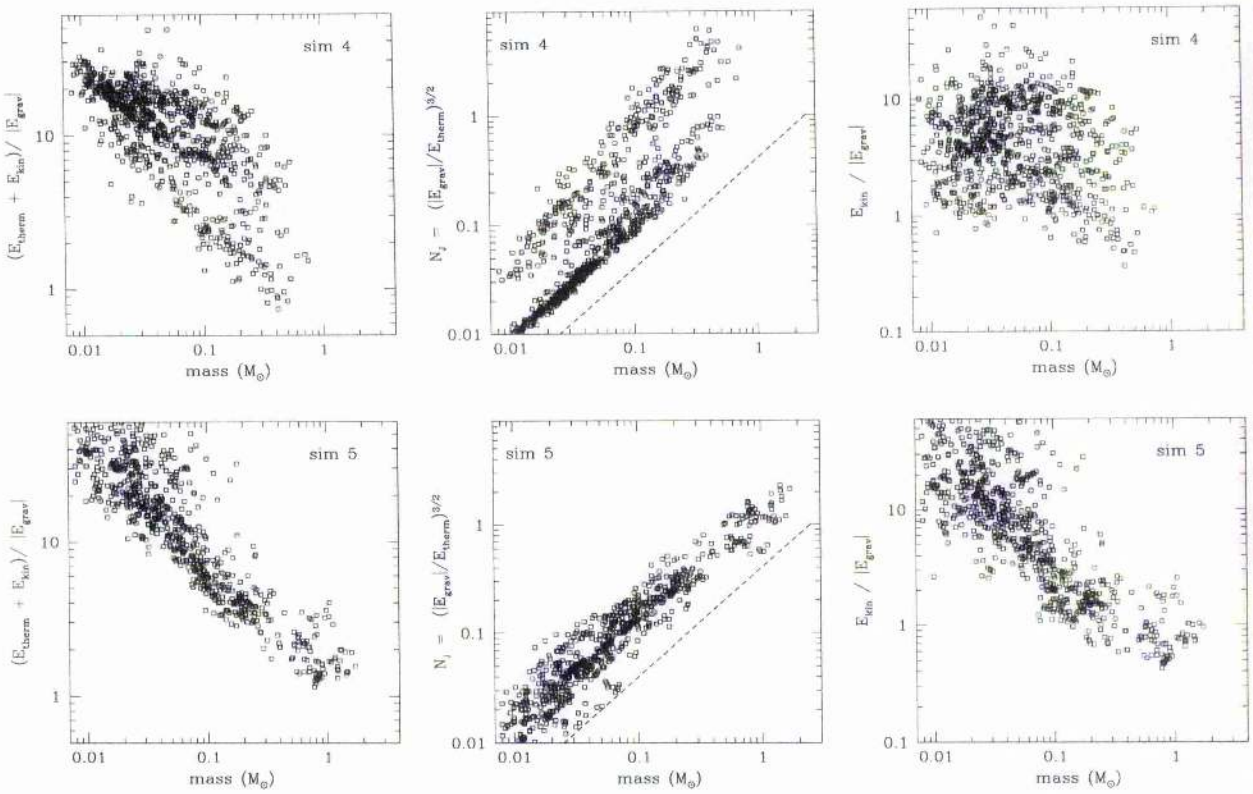

Figure 6.10: This figure shows the same information as was laid out in figure 6.5 but for simulations 4 and 5. The top row contains the plots for simulation 4 and the bottom row contains the plots for simulation 5.

Donate et al. (2004) found that the power spectrum of the initial turbulent field had little influence over the final mass spectrum of the protostars.

Apart from the tendency of our clumps to be naturally in a state suitable for fragmentation, there is some observational evidence to back the coagulation picture that we present here. Morata, Girart, & Estalella (2005) studied the CS core in the L673 region and found that there exists a relationship between the mass and energy of the clump population. Similar to our results in section 6.4.1, they find that the clumps of mass $\sim 0.2M_{\odot}$ are below the required mass for virial equilibrium. Furthermore, the more massive the clumps are, the closer they are to being virialised. Morata et al. (2005) also studied the chemistry of this region and have concluded that the clump of mass $\sim 1.2M_{\odot}$ that is bound is more chemically evolved than its lower mass, unbound, counterparts. They thus suggest that these results show a necessary evolution from low to high mass clumps before star formation occurs. Obviously this chemical analysis needs to be applied to more regions before this coagulation/mass evolution process can be established as a key phase in star formation.

It is still unclear as to whether the turbulence in star forming regions is driven or decays freely on the crossing time. Much attention has focused recently on the idea that star formation occurs rapidly (Hartmann, 2000), with evidence to suggest that the process has a duration similar to the crossing time (Elmegreen, 2000a). If this is true for

all scales, as the evidence presented by Elmegreen would suggest, then driving mechanisms are not required to support the gas in the period before star formation sets in, since the energy dissipation and the star formation occur on the same timescale. For this scenario, either driving mechanisms do not exist or have too little time to take effect such that their influence is only marginal.

If however the only timescale that is important for the star formation rate is the crossing time at the scale of the GMC, then driving mechanisms may play an important role, since the star formation at the small scales will occur on a much shorter timescale. One might at least expect that the flows at the large scales would drive mechanical energy down to the small scales, where the star formation can occur. The clumps in such an environment might well be expected to form and evolve differently from those in our study where the driving mechanisms are omitted.

The nature of star formation in a driven turbulent environment has been comprehensively studied by Klessen (2001). The study looked at clump formation, clump mass spectra and the clustered nature of star formation in clouds where the kinetic energy was driven at a variety of wavelengths. The study revealed that the main difference between small and large scale driving is that the former results in much more isolated star formation, with less clustering than is produced in clouds where turbulence is driven on large scales. Interestingly, his analysis of the clump structure and energies reveals that the first clumps to become bound are generally among the largest structures formed by the turbulence, similar to our study.

6.7 Conclusions

From our study we find that turbulent motions are not directly responsible for bound clumps, and hence star formation, in simulations such as those published by Bate et al. (2003b) and Delgado-Donate et al. (2004). There is no one-to-one mapping between clumps and stars, and thus we can conclude that turbulence is not the source of the IMF in such simulations. Instead the role of turbulence is to determine where star formation can occur, via the local dissipation of kinetic energy, and to produce small scale structure in the gas. The clumps formed from the shocks in a Larson type, $\sigma \propto L^{1/2}$, velocity field are generally unbound, both thermally and kinetically. Small mass clumps, such as those with a mass comparable to a brown dwarf, are typically over supported by their thermal energy by an order of magnitude. This is also true of the kinetic energy support. Thus the formation of sub-stellar mass objects by the formation and collapse of an individual clump of similar mass does not occur in these simulations.

The physical parameter that controls the collapse is the mean thermal Jeans mass in the region of the star formation. Once large regions become bound after shock dissipation, the mean Jeans mass fragments out from its surroundings and starts to collapse. Within the collapsing region is substructure, in the form of the clumps generated by the turbulence. As a region with a mean Jeans mass collapses, it prevents the lower mass clumpy structure, which is unbound, from re-expanding, pushing it together. A merging process is therefore at work, whereby small unbound clumps coalesce into a larger bound clump, which eventually becomes the size of the mean Jeans mass.

The collapse of a mean Jeans mass clump occurs while the region is in rough equipartition of kinetic and thermal energy. As a result, the region contains 2.8 effective thermal Jeans masses, encouraging the formation of multiple objects. The star formation in our simulations thus generally occurs in small groups. This picture of star formation is akin to that observed for embedded clusters (Mundy, Looney, & Welch 2000; Duchêne et al. 2004).

CHAPTER 7

Unbound clouds and the star formation efficiency

7.1 The star forming environment

The formation of stars in giant molecular clouds appears to be a very inefficient process. Global estimates of the star formation efficiency, based on the mass in molecular clouds and the Galactic star formation rate (Scalo, 1986; Evans, 1999), are of order a few percent while small-scale estimates for stellar clusters approach 50% (Lada, 1992; Lada & Lada, 2003). The dispersion in estimates can, to some extent, be decreased under the assumption that molecular clouds are long-lived entities that exist for many dynamical times, although this necessitates a supporting mechanism to balance gravity (McKee et al., 1993).

As star formation from molecular gas involves the gravitational contraction through many orders in magnitude in size, it is commonly assumed that the largest scale objects associated with star formation, molecular clouds, are themselves bound. In this case, the problem is how does a large bound region ($10^4 - 10^6$ $M_\odot$) only permit a small fraction of its mass to undergo gravitational collapse. Various mechanisms, such as magnetic fields and feedback from young stars, have been invoked over the years in order to support molecular clouds and explain the low efficiency of star formation (Shu et al., 1987; Franco et al., 1994). In this chapter, we explore an alternative scenario whereby molecular clouds are not bound on the large scale, circumventing the need for any additional supporting mechanisms.

In a recent paper, Elmegreen (2000a) has collected observational evidence implying that GMCs are short-lived objects, with dispersal times comparable to their crossing times ($t_{dyn} \sim 3 \times 10^7$years). The formation of stars then has to occur in a short burst ($\sim t_{dyn}$), as has been suggested from recent observations (Hartmann et al., 2001; Hartmann, 2002), rather than as an ongoing process. This implies that molecular cloud formation is dynamical, and self-gravity need not play a dominant role. Such a scenario has recently been advanced by Pringle et al. (2001) where the passage of a spiral arm triggers the agglomeration of unbound molecular gas and the ensuing shock dissipates sufficient kinetic energy to allow self-gravity to (locally) form stars. The observed molecular clouds could then be transient structures with lifetimes comparable to their dynamical times (Elmegreen, 2000a; Pringle et al., 2001; Larson, 2003). In this picture it would seem likely that these regions are globally unbound and highly dynamic, with only a small fraction achieving gravitational instability before the cloud dissipates. This is possible if the internal bulk

motions of the cloud are stronger than the self-gravity of the region. The supersonic nature of the motions produces shocks which dissipate kinetic energy, eventually leading to regions becoming gravitationally unstable. The efficiency of the star formation would then be governed by the strength of the internal kinetic energy at the point of the cloud's formation, along with how much support can be removed in shocks. The internal energy of the cloud in this picture would be a combination of the random motions in the pre-cloud material and the residual energy left over from the formation shock. This would naturally lead to different clouds having different star formation efficiencies and potentially explain the variance in the observed estimates.

Observational estimates of the mass, and therefore the energies, of the molecular gas is inherently difficult and uncertain. Heyer et al. (2001) have investigated the dynamic stability of molecular regions in the outer Galaxy. Results suggest that the molecular material is unbound until the mass of the region approaches $10^5 M_{\odot}$. It is however noted in the paper that obtaining a value for the hydrogen mass via measurements of CO flux involves the assumption that the gas is virialised. If the region in question is then unbound, the subsequently derived value for the mass of molecular hydrogen is an over-estimate of the region's true mass. As a result, regions will appear more bound than they actually are. This places serious doubt on the generally accepted idea of globally bound GMCs.

The ability of turbulence to characterize the interstellar medium (ISM) along with its role in star formation in GMCs has been extensively studied by a number of authors. For a complete review we point the reader to the article by Mac Low & Klessen (2004). It is now well established that large scale turbulent motions can produce the filamentary structure that is commonly observed in star forming regions (Vazquez-Semadeni et al., 1997; Ostriker et al., 1999; Ballesteros-Paredes et al., 1999a; Padoan & Nordlund, 1999) and that even MHD turbulence decays on a dynamical timescale (Mac Low et al., 1998; Stone et al., 1998) such that a driving mechanism is required if the clouds are to exist for many dynamical times. These studies highlight that transient objects can form from large scale flows in the ISM, supporting the work of Elmegreen (2000a) that star forming regions are short lived in nature. Recent work on subregions within GMCs has also shown that driven turbulence, and more importantly the scale of the driving, can affect the local efficiency of the star formation (Klessen et al., 2000; Klessen, 2001). The periodic boundary conditions in this last study make it difficult to find estimates of the global star formation efficiency of transient molecular regions, since the mean mass density cannot decrease. Any newly formed stars can thus continue to accrete until all the gas in the computational volume has been used up. Global calculations have tended to study clouds that are only marginally unbound and hence do not provide information on transient GMCs (Bate et al., 2003a; Bonnell et al., 2003)

It is the picture of GMC formation presented by Pringle et al. (2001) that we use as the motivation for this chapter. They suggest that molecular clouds are formed via the accumulation of small parcels of material. In this manner, we interpret the internal motions of the cloud as a result of the original random motions of the constituent parcels of gas. The internal motions therefore need not be turbulent in the strict definition and so we use the notion of 'turbulence' loosely here. The formation mechanism for molecular regions proposed here is distinctly different from that studied by Ballesteros-Paredes et al. (1999b). Since we are concerned with a transient object and one which is not part of some large scale flow, we do not require boundary conditions in our model. Futhermore, since

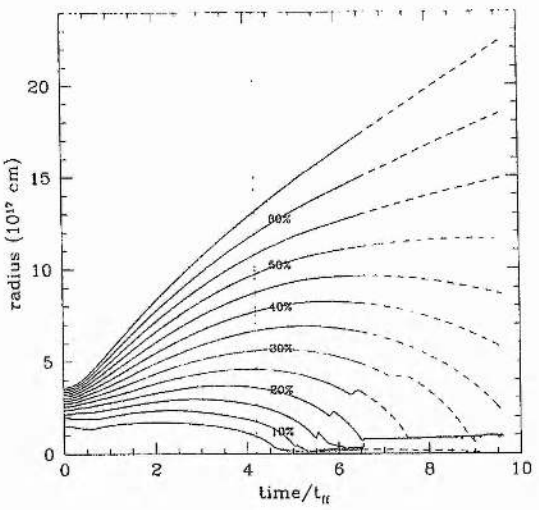

Figure 7.1: The evolution of Lagrangian radii enclosing a fixed fraction of the total mass. The solid lines are from the original simulation and the dashed lines are from the period where the smallest binaries is merged. The vertical dotted line denotes the time in the simulation at which the first protostar is formed.

the cloud in study is transient, we do not include any feedback effects into the internal motions as is consistent with the ideas presented by Elmegreen (2000a).

We present here a numerical simulation in which the turbulent gas is both initially unbound and free to expand, showing that this does result in star formation but with a relatively low efficiency. In section 2 we describe the details of the simulation technique with a discussion of the evolution and efficiency of the star formation given in section 3. We summarise and discuss the implications of this result in section 4.

7.2 The simulation

The simulation starts from a uniform sphere of mass $31.6M_{\odot}$ at 10K with a radius of 0.13pc. The material is modelled as an ideal gas of molecular hydrogen and the equation of state is isothermal. With these properties, the Jeans mass of the cloud is $1M_{\odot}$ and the Jeans number, $J_o = (M/M_{Jeans})^{3/2} = |E_{grav}|/E_{thermal} = 10$. These conditions give an initial density of 2.2×10^{-19}g cm^{-3} and hence the free-fall time, t_{ff}, is 1.4×10^5 years. The gas is given turbulent support modelled by a Gaussian random field with a power spectrum $P(k) \propto k^{-4}$, where k is the wavenumber of the velocity perturbations and corresponds to a Larson type law of $\sigma \propto L^{-0.5}$ (Larson, 1981; Ostriker et al., 2001). The turbulent kinetic energy of this study is characterised by the parameter $\epsilon = |E_{grav}|/E_{kinetic}$ and it is the unbound case of $\epsilon = 0.75$ which is presented here, resulting in a turbulent Mach number (as calculated from the kinetic energy) of ~ 5.5 ($c_s \approx 0.2$kms^{-1}).

In this calculation we used a sink radius of 48AU with the sinks being formed at a density of 1×10^{-14}g cm^{-3}. To minimise computational expense, we smooth the gravitational forces between stars at a distance of 48AU. We use 204800 SPH particles to model

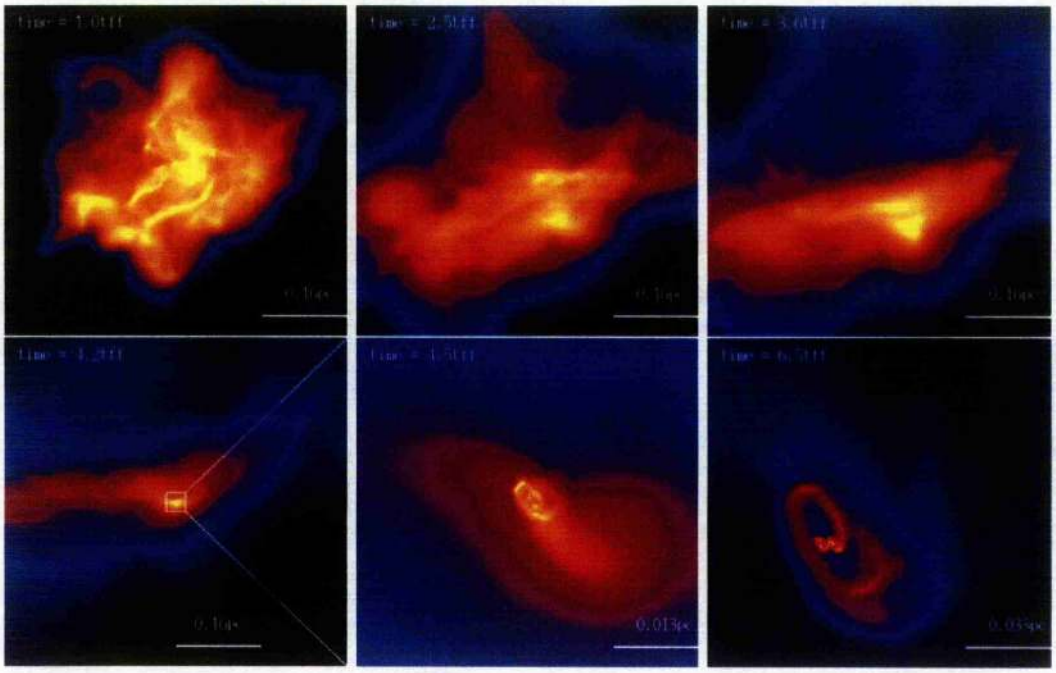

Figure 7.2: The panels show logarithmic column density snapshots from the simulation, following the evolution of the molecular cloud. The maximum densities in the first four panels are 0.21, 0.17, 0.13 & 3.8 g cm^{-2} respectively and the last two panels have a maximum density 100g cm^{-2}, taken to arbitrarily represent the protostars. Minimum column densities are 0.001g cm^{-2} for the first four panels and 0.01g cm^{-2} for the last two. The turbulent velocities injected into the cloud at the beginning of the simulation quickly erases the uniform density and imposes a characterising filamentary structure. The kinetic energy is larger than the potential causing the cloud to expand, with the outer layers escaping the self-gravity of the system. Left behind by the escaping mass is a small dense region. The gas at the centre of the dense region, it is able to rid itself of kinetic energy via shocks with the shrouding material. Eventually gravity manages to dominate and produce a dense core ($t \sim 4t_{ff}$) which fragments to form a 3 body hierarchical system with one protostar being ejected (visible at the top right of the last panel in the figure).

the gas and are hence able to resolve self-gravitating objects as small as 0.015M$_\odot$ (Bate & Burkert, 1997).

At the end of the simulation 4 protostars were formed containing roughly 17% of the mass of the original cloud. The formation of a tight binary with a separation of 134AU, considerably reduced the time step of the integration making it computationally expensive to run the simulation for longer than $6.5t_{ff}$. Unfortunately, this prevented satisfactory examination of the outer regions in the cloud, which evolve on much longer time-scales than the material near the stellar system. Replacing the binary with a point mass, we were able to run the simulation much further, allowing a better examination of the evolution of the outer regions. The results of this part of the simulation are represented by the dashed radii curves in figure 7.1. It must be noted here that for a radius of less than 3×10^{17}cm (or $\sim$ 0.1 pc) from the protostars the results for the accretion are not as accurate as the original simulation due to the large accretion radius of the point mass, but this does not

affect the results outside this region. All calculations of kinetic energies and radii in this chapter are obtained from the centre of mass of material that will *eventually* end up in the stars, rather than the centre of mass of the entire cloud. The Lagrangian particle nature of SPH makes this possible. This gives a picture of the star formation process as seen by the material that is actually involved and allows for a better estimate of the star formation efficiency.

7.3 Evolution

7.3.1 General Properties

The evolution of this cloud can be split roughly into three phases: turbulent compression, general expansion of the gas, and a final gravitational collapse for a subset of the material. Column density snapshots from the simulation can be seen in figure 7.2, showing the effect of the turbulent motions and how the gas eventually evolves to form a small stellar system.

The simulation starts with a uniform sphere of gas with a turbulent velocity field. The large random motions quickly dominate with shocks producing the filamentary structure typical of turbulent regions. Densities at the centre of these filaments reach ~ 25 times the initial density of the cloud. Despite this increase in density, they are not self-gravitating structures. In fact they are highly transitory, existing for only a few tenths of a free-fall time. The turbulent motions lead to essentially one dimensional compression which does not produce a decrease in the local Jeans mass (Doroshkevich, 1980; Lubow & Pringle, 1993; Clarke, 1999) and hence the gas is generally unbound. A 1-D compression does not increase the ratio $|E_{grav}|/E_{therm}$ of a parcel of gas. Thus, it cannot alter the boundness of a clump unless it decreases its thermal energy content. Significantly, these transitory structures provide the seeds for the fragmentation that occurs during the later collapse phase.

Figure 7.1 shows the Lagrangian radii[1] that contain fixed fractions of the cloud's mass, and how these change with time. The global expansion is readily apparent from the figure, as is the extent of the expansion by the onset of star formation. The initial turbulence decreases during the first free-fall time. During this phase, the turbulent motions result in a general expansion of the cloud. After the random motions have been damped out in the shocks, expansion is the main component of the velocities. During this phase, most of the detailed filamentary structure is erased, with only one large elongated body of gas remaining.

Around $t = 2t_{ff}$, the expansion for a small fraction of the material, up to roughly 5%, stops and this gas starts to fall back in. As the Lagrangian radii show, this is an inside out process. The inner 5% starts contracting before the outer layers and in-fall occurs progressively later as we move away from the centre. It does differ however from the classic inside-out process described by Shu (1977), since the system is not collapsing from a static starting point, but rather from the re-contraction of an initially expanding medium. The inner 5% corresponds roughly to a thermal Jeans mass and is able to collapse

[1] A radius that moves in time.

once the kinetic energy has been dissipated. Gravitational contraction forms a small dense core which becomes the natal site for a stellar system. The highly aspherical form of the core allows fragmentation to occur, preventing the formation of a single star. The gas splits into four protostars, arranging themselves in two tight binaries. This system then decays with one star being ejected and the remaining 3 left in a hierarchical triple system. At the end of the initial simulation, the protostars contain roughly 17% of the original mass of the system, and a further 5% is incorporated into the various circumbinary and circumstellar discs. The inner binary is composed of protostars of mass 0.95 and $1.79M_{\odot}$. The mass of the third protostar that makes up the bound triple system is $2.13M_{\odot}$ and the escaper is the lightest member at $0.37M_{\odot}$.

7.3.2 Star formation efficiency

The most significant feature of this simulation is that a large fraction of the gas is expelled from the cloud, resulting in a naturally low star formation efficiency. Escaping gas arises due to excess and undamped energy in the cloud. The mass that is bound therefore represents an upper limit to the possible final system mass. In principle, the most reliable method of determining the star forming efficiency of the cloud is to let the simulation run until all gas has either escaped or been accreted. Obviously this is impractical with current computational methods, so we must look to other methods to obtain our results. Unfortunately, simply calculating the energy of each SPH particle at the end of simulation does not unambiguously yield a value for the efficiency. The long-range nature of gravity is such that unbound material contributes to the potential energy of the entire cloud. Consequently, material that appears to be bound might actually become unbound once the escaping regions have blown away. Fortunately, the fraction of unbound material, and thus escaping mass, yields an accurate upper limit to the amount of material available for star formation.

The evolution of the unbound fraction is followed in figure 7.3. We see a sharp fall in this fraction during the first free-fall time. This is simply a result of the decaying turbulent energy field, as kinetic energy is dissipated in shocks. After $t = t_{ff}$, the unbound fraction remains roughly constant for the remainder of the simulation. At the point of star formation, at least 40% of the cloud is unbound, thereby placing an upper limit on the star formation efficiency at 60%.

The Lagrangian radii in figure 7.1 give another estimate for the star formation efficiency. The dashed lines, obtained from the period in the simulation where the close binary is merged into a single protostar, reveal that the radius containing 50% of the mass appears to have reached a constant value. This indicates that the 50% fraction is the boundary between in-falling and expanding matter. This suggests a slightly lower value for the efficiency than we obtained by looking at the energy. In fact the Lagrangian radii containing 60% of the cloud shows no sign of re-contracting.

Although turbulence does not directly induce fragmentation in the cloud for the reasons given in the previous section, it does play an important role in determining the mass that gets converted into stars. The fraction of mass with an increasing $|E_{grav}|$ represents the material that is actively involved in compression. From figure 7.3 we see

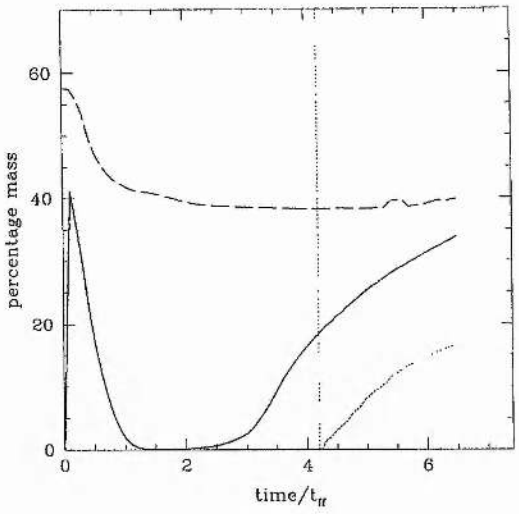

Figure 7.3: Shown here is the evolution of various important features of the cloud. The long dashed line shows the fraction of material that is unbound to the system, and the short dashed line is the amount of material that has been accreted by the protostars. The solid line represents the amount of material which has an increasing $|E_{grav}|$ and is thereby involved in compression. Again, the vertical dotted line represents the onset of protostar formation.

that this fraction undergoes a sharp initial rise and a gentler fall during the first free-fall time. Again this is just a consequence of the turbulent compression and creation of transient filamentary structure. During this phase, just over 40% of the mass is involved in these shocks and as a result loses kinetic energy. Having lost this energy, the gas is able to contribute to star formation. At the end of the simulation all the mass contained in the protostars and the circumbinary disc had originally been involved in shocks during the turbulent phase. The turbulent compression in this simulation is therefore linked to the fraction of the mass which is involved in the star formation process.

It must be noted here that in reality the tenuous outer layers of the cloud, are unlikely to be able to find their way onto the stellar system. Clouds like the one presented here, or cores as they are known at this scale, do not exist in isolation but commonly in crowded regions (Motte et al., 1998; Testi & Sargent, 1998). In such an environment, tidal forces can have an important effect on the dynamics of gas, stripping away loosely bound material. As well as contending with tidal effects the low density regions outside dense cores are associated with high velocity flows (Larson, 1981; Padoan et al., 2001), providing a hostile environment for quiescent, tenuous gas.

7.4 Implications for the star forming process

The results presented here follow the evolution of a molecular cloud containing a supersonic turbulent velocity field which has greater energy than that of the cloud's self-gravity. Despite the globally unbound nature of the cloud, the freely decaying turbulence (from

shocks) results in dynamically quiescent regions where gravity is able to drive collapse and subsequent star formation. Since not all of the cloud is involved in the shocks, less than half the mass is able to undergo star formation, with the remaining material escaping the self-gravity of the system. Four protostars are produced by the gravitational fragmentation, three of which are in a triple system which is formed by the ejection of the fourth body.

The fact that bound structure formed from a dynamically unbound cloud, has important implications for the star formation process. This illustrates that GMCs need not be globally bound in order to produce their observed stellar populations, although more detailed calculations at the correct scale are needed to confirm this. Internal turbulent motions are able to dissipate enough kinetic energy in supersonic shocks to leave coherent regions where gravitational forces can dominate. The rest of the cloud can then escape, allowing GMCs to dissolve of their own accord instead of requiring some unbinding mechanism. The end result is a GMC that is naturally inefficient at forming stars. This supports a large scale picture of star formation in which GMCs are formed dynamically from the accumulation of molecular gas (Pringle et al., 2001; Elmegreen, 2000a). Self-gravity need play no role in the formation and evolution of GMCs up to the point of star formation.

Star formation from globally unbound giant molecular clouds is able to provide a simple and interesting alternative to the efficiency problem that is normally attributed to a combination of magnetic fields and feedback processes. All gas which is able to dissipate enough kinetic energy to become bound will be involved in the star forming process. The ruling factor on the efficiency is therefore the amount of gas that is involved in shocks, which is in turn linked to the strength and power spectrum of the turbulent field (Klessen et al., 2000). More simulations will be needed to investigate how the efficiency is linked to both the initial Jeans number and the Mach number of the turbulence.

CHAPTER 8

Unbound GMCs: the origin of OB associations

8.1 Introduction

OB associations are historically identified simply as extended groups of OB stars, having diameters of tens of parsecs (Ambartsumian, 1955). Furthermore they are rather more diffuse than open clusters, with the mass density of OB type stars at ~ 0.1 $M_{\odot}$ pc^{-3} (Blaauw, 1964; Ambartsumian, 1955; Garmany, 1994; Lada & Lada, 2003). It was found that these associations contain substructures which are referred to as 'OB subgoups' (Blaauw, 1964). These subgroups are unbound from one another as was deduced from their expansion about the centre of the region (Blaauw, 1952). Some regions or 'subgroups' are shown to be associated with molecular gas. In general these regions are not coeval but can exhibit a spread of ages amongst the subgroup populations as large as 10 Myr (Blaauw, 1964). The fact that OB associations are very young, with some of the subgroups possessing ages of the order of a millions years, suggests that the unbound nature of the subgroups from one another is primordial.

The relationship between OB associations and other types of clusters found in the galactic disc, such as open clusters and embedded clusters, is still rather unclear. The OB associations do however have a classic theory regarding their formation. Elmegreen & Lada (1977) proposed that OB associations form via triggering. The ionising wind from a young massive star drives a shock wave through the surrounding molecular gas of the parent cloud. Eventually this shock front becomes gravitationally unstable and forms a new generation of stars. When the massive stars in the new generation switch on, the process repeats. In this manner, the star formation is self propagating, with one generations of OB stars triggering the formation of the next. Since the shocked layer in which the new group of OB stars forms is moving away from the older OB stars, at a few kms^{-1}, the new group is unbound from its parent group. The region then naturally has the dynamics of the observed OB groups. Motivation came from observations of stars forming at the boundaries of molecular clouds and HII regions, such as NGC7538, M17 and M8 (Habing, Israel, & de Jong 1972; Lada et al. 1976).

The issue is complicated however when one considers the detailed stellar population of OB associations (Garmany, 1994; Brown, 2001). In the self propagating model, OB type stars form in the shocked layers where conditions are naturally more suited to forming high mass stars, due to the effective sound speed of the gas Elmegreen & Lada (1977).

Low mass stars form spontaneously in the rest of the cloud. Thus the model assumes a two step formation process whereby low mass stars and high mass stars are formed by different mechanisms and in physically separated locations. The IMF of the OB associations however do not exhibit this feature and generally possess the standard field star IMF, at least within the Salpeter range (e.g. Sco OB2, de Geus 1992; Preibisch & Zinnecker 1999). Since up to nearly 90% of star formation is thought to occur in embedded clusters, with a field star IMF and primordial mass segregation[1] (for a discussion see Lada & Lada 2003), it may be that the formation of OB associations has more in common with standard clustered star formation.

Bonnell, Bate, & Vine (2003) and Bonnell, Vine, & Bate (2004) have modelled cluster formation in a turbulently supported cloud. They modelled a $1000M_{\odot}$ molecular cloud that was initially supported against collapse by a turbulent velocity field. It was found that the dissipation of the large scale supersonic flows produced a number of distinct subclusters. Each subcluster contains at the core a massive star. The subclusters were mass segregated and each had a protostellar population consistent with that of the observed field star IMF. Both the mass segregation and the IMF are the result of competitive accretion. Since the cloud was initially bound, even more so after the dissipation of the turbulent energy, all the subclusters are themselves bound to one another. They quickly merge within roughly 0.5 Myr (roughly twice the free-fall time for the original cloud). If this merging process were to occur on large scales, such as a whole GMC, one would never be able to form OB associations. The massive stars at the centres of the subclusters would find themselves in one large cluster.

Our proposal in this chapter is that OB associations are just a series of clusters that form in *unbound* GMCs. The expanding cloud produces a series of clusters that are unbound from one another due to the fact that the flows that form them are also unbound from one another. The clusters, which become OB subgroups, then simply expand away from their mutual centre of mass along with the gas from the cloud, rather than merge into a single cluster. Thus only one star formation mechanism is at play here: clustered formation. The OB association therefore will have the universally observed IMF.

8.2 Details of the GMC Simulation

Our simulation starts with a uniform density sphere of molecular hydrogen of radius 20pc with a mass of 1×10^5 $M_{\odot}$. The gas is isothermal and has a temperature of 10K. These numbers (mass, size and temperature) are typical of those reported for GMCs in the solar neighbourhood (Blitz, 1991). We model the gas with 500,000 SPH particles and are thus able to accurately follow the formation of self-gravitating regions down to a mass of $20M_{\odot}$ (Bate & Burkert, 1997; Whitworth, 1998). The free fall time associated with this cloud, the time taken for the unsupported gas to collapse under gravity to a central point, is roughly 4.7 Myr. The cloud has an initial Jeans mass of $30.4M_{\odot}$. We do not include any feedback processes, such as stellar winds and jets or the effects of massive stars such as ionisation fronts and supernovae.

[1]Mass segregation in clusters is where the progressively more massive stars are found towards the centre.

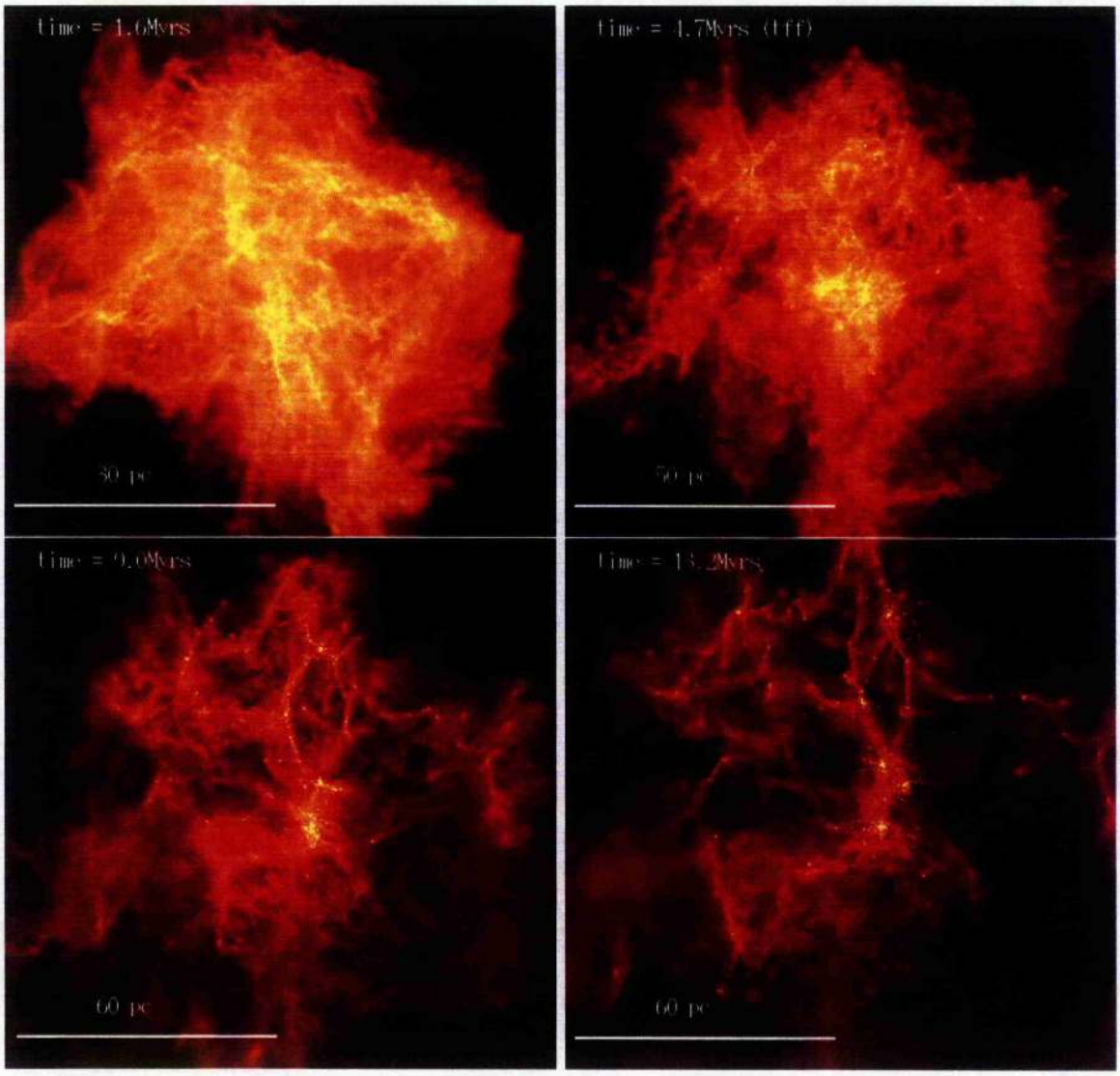

Figure 8.1: The panels show column density images from the simulations. The first panel shows the state of the gas after the crossing time ($t_{cr} \sim 1/3t_{ff}$), and the following panel shows the gas at the free fall time. The remaining two images show how the cloud evolves to form a system of clusters. The maximum column density plotted is 0.12, 1.21, 2.90 and 4.86 g cm^{-2} respectively and the minimum column density is 10^{-3} g cm^{-2} in all the images.

To model the turbulence, we support the cloud with a Gaussian random velocity field with a power spectrum of $P(k) \propto k^{-4}$ which is consistent with a velocity field with a Larson-type relation of $\sigma \propto L^{0.5}$ where σ is the velocity dispersion and L is the length scale of the region (Myers & Gammie, 1999). At the beginning of the calculation the ratio of gravitational to kinetic energy is 0.5 ($E_{kin} = 2E_{grav}$). We stress that the turbulent kinetic energy is able to decay freely in this simulation since we include no driving mechanism. The timescale for the energy decay is the crossing time (Mac Low et al., 1998; Stone et al., 1998) which for the initial velocity field is $t_{cr} = 4.2$ Myr, slightly less than the free fall time.

We set the sink particles to form at a density of 1000 times the initial density, with a subsequent accretion radius of 0.17pc. When a particle finds itself at the centre of a dense, bound and collapsing region it is turned into a sink particle and its 50 to 100 neighbours are accreted onto it. With the resolution used for this simulation the sink particles start with a mass of at least $15M_{\odot}$ before further accretion. Therefore we cannot think of these point mass objects as 'protostars', as was the case in Bate, Bonnell, & Bromm (2003a), but instead assume that they represent 'proto-clusters'. To prevent the 'sink particles' behaving as point masses in gravitational interactions, we smooth the sink-sink gravitational forces to a distance of $r_{min} = 0.2$ pc.

In the analysis that follows, we discuss the properties of star formation centres, or 'SFCs'. These can either consist of a single protocluster (or sink particle) or a coherent group of protoclusters. To identify SFCs where more than one sink particle is involved, we make use of the mass segregation that occurs naturally when the protoclusters interact in self gravitating groups (see for example Bonnell et al. 2004). First we sort all the protoclusters by mass. We then take the most massive protocluster and tag it and its fellow protocluster neighbours within 0.5pc to be members of 'SFC 1'. We then go down the mass sorted list of protoclusters until we arrive at the next most massive protocluster that has not been associated with SFC 1. It becomes tagged as being a member of 'SFC 2'. All the protoclusters within 0.5pc of this protocluster are now tagged as being members of SFC 2, unless they are already members of SFC 1. This process continues down the list of protoclusters until all have been assigned membership to a SFC. There is thus a resolution of 0.5pc which distinguishes one SFC from another. We find that the choice of 0.5 pc used in attributing memberships does not significantly affect the SFC population, since the protoclusters formed in the simulation are either well separated (and thus in isolation) or exist in dense groups. The radius of the SFC is given by the radius of the furthest protocluster from the centre of mass. If there is only one protocluster then the radius is simply the accretion radius, which is 0.17pc.

One problem with trying to model turbulence in a numerical simulation of this type is that it is not always possible to resolve the velocity structure at all scales. Turbulence is assumed to be hierarchical, following a Larson-type relation of $\sigma \propto L^{\alpha}$ (Larson, 1981). In SPH, while a particle can have a kinetic energy based on its velocity, it can have no internal velocity structure. As a result, the kinetic energy below a certain mass scale (actually the mass of an SPH particle and its neighbours) is not included in the calculation. We therefore stress that our simulation is lacking the kinetic energy that should be present at scales of less than $\sim 20M_{\odot}$. The details of how individual stars form are thus not available from this simulation, and we must restrict ourselves to the large scale properties of star formation and the formation of clusters.

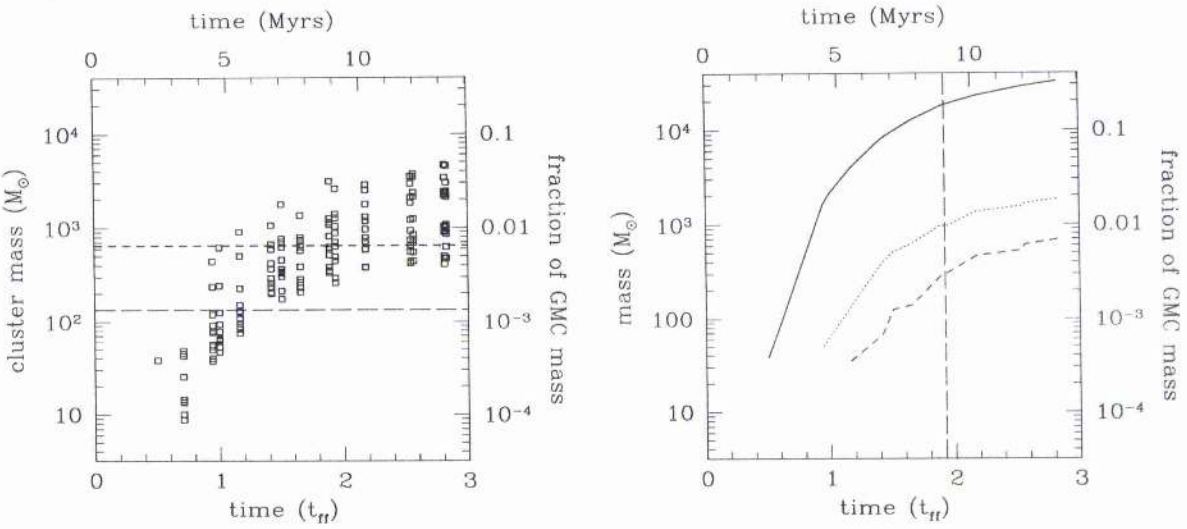

Figure 8.2: Shown in the left hand panel are the masses of the 16 most massive SFCs and how they evolve in time. The horizontal long-dashed line gives the mass at which a SFC can form a star of $> 10M_\odot$ and the short dashed line shows the mass needed by a SFC to form a star of $> 25M_\odot$. This assumes the IMF given in section 8.4 along with a star formation efficiency of 50% in the SFCs (see section 8.4 for a more detailed discussion). The solid line in the right hand panel shows the mass contained in the SFCs (gas particles + protocluster/sink particles). The dotted line in the plot shows the mass in stars greater than $10M_\odot$ and the short-dashed line shows the mass in stars greater than $25M_\odot$. The vertical long-dashed line denotes the point at which we estimate a supernova event to occur (note that t_{ff}= 4.7Myr).

8.3 General Evolution

Figure 8.1 shows column density images from different points during the simulation and allows us to see clearly the evolution of the gas and regions of star formation. We see from the figure that the structure of the cloud changes remarkably quickly. It starts as a churning network of gaseous filaments and within 10Myr (when the simulation was terminated) evolves into an ensemble of distinct clusters, by which time the gas has lost much of its early character. The fact that an unbound GMC can form stars and star clusters reinforces the predictions made in Clark & Bonnell (2004).

The point at which the first bound objects condense out of the unbound flows occurs at roughly 2.4 Myr. This is roughly half the crossing time for the region (although some authors use $t_{cr} = R/V$ instead of $t_{cr} = 2R/V$ as is used here). This time is consistent with the kinetic energy dissipation rate (Mac Low et al., 1998; Stone et al., 1998) and the formation of a turbulently dominated density structure (Padoan et al., 2001).

Rather than simply discuss the individual protoclusters that form (the sink particles) it makes sense here to discuss the bound groups of these protoclusters as well, which we will simple refer to here as 'star formation centres' or SFCs. The formation of the SFCs actually occurs very rapidly. The mass of the 16 most massive of these centres is

shown as a function of time in figure 8.2. Within 5Myr (or $\sim$ 2.5 Myr after the onset of star formation) the 15 most massive SFCs all have masses greater than about 100 $M_{\odot}$, and are beginning to get to a size where there is good possibility of them forming massive stars (this will be discussed in section 8.4).

A desirable feature of an initially unbound GMC is that cloud dispersal and star formation are occurring simultaneously. This removes the necessity for feedback mechanisms to disperse the cloud, or at the very least makes their task much easier. The timescale for star formation is thus comparable to the timescale for the cloud's dispersal. The dynamics of an unbound cloud is therefore naturally in keeping with the recent observations that star formation and cloud dispersal occur in a few crossing times. There is also the added bonus that star formation efficiencies will be kept low, since most of the gas around a protocluster clump will be unbound to it and moving away. This prevents the material getting involved in the accretion once a SFC starts to form.

Figure 8.3 shows the density distribution of the gas at three points in the simulation. The vertical dot-dashed line marks the original density of the cloud. Just before the first protocluster forms at 2.4 Myr we see that the most common density is roughly 7×10^{-22} gcm^{-3} (the solid line curve), an order of magnitude higher than at the start of the simulation. Note however that very little material at this point is as dense as 7×10^{-21} gcm^{-3}, showing that the turbulence does not allow much material to get up to typical star forming densities (Falgarone, Phillips, & Walker, 1991; Padoan, 1995; Zinnecker, 2002).

After 7 Myr the peak in the distribution falls back to roughly the starting density, however there is much more spread in the distribution. This spread is controlled by two mechanisms. The high density tail increases as the SFCs grow by accretion and the subsequent rise in the potential energy. This causes yet more material to fall into the star forming regions. The low density tail increases since the cloud is freely expanding. By 13 Myr, only $\sim 3t_{cr}$, we see that the majority of the gas has fallen to very low densities. By this point it is unlikely that observations of such a cloud would reveal much in the way of molecular gas and would instead only be visible as HI. The cloud can now be assumed to be 'dispersed'. Even if the GMC fails to be a site of massive star formation, the dispersal would still occur on a timescale consistent with Elmegreen's (2000) observations.

Note also from figure 8.1 that the cloud contains cavities and dense regions of star formation. These are created in the simulation purely by the turbulence. This type of structure in star forming clouds is often attributed to the effects of high mass stellar feedback, such as winds and supernovae, and is thought to be the trigger for star formation in the region (e.g. Elmegreen & Lada 1977). Instead, we realise that turbulence can mimic these effects. Furthermore the cavities in the simulation would be easily ionised by any high mass stars that form in the SFCs (Dale et al., 2004). We would then have a series of SFCs separated by a region of HII gas, just as is found in the classic picture of triggered star formation.

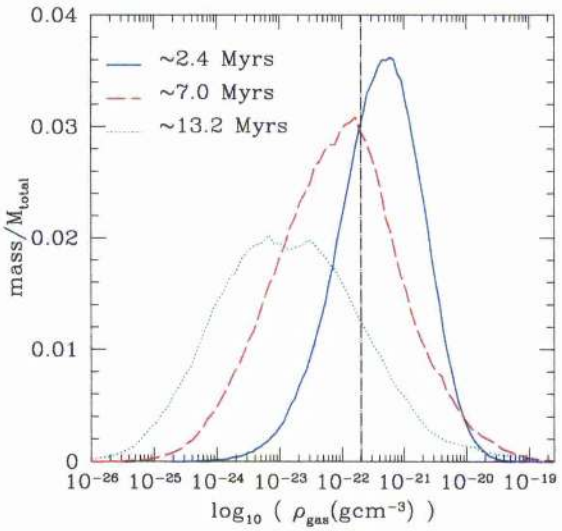

Figure 8.3: The plot shows the density distribution of the gas at three points in the simulation. The solid line follows the gas density just before the formation of the first protocluster, at 2.4 Myr (or $\sim \frac{1}{2}$ t_{cr}). The dashed and dotted lines show the density distribution of the gas at a time of $\sim$ 7 Myr and $\sim$ 13.2 Myr respectively. The vertical dot dashed line shows the density of the gas at the beginning of the simulation. Note that the simulation only involves a gas of pure molecular hydrogen.

8.4 The Formation of Stars and Expected Efficiency

In this section we use some simple assumptions about the star formation that occurs in the SFCs to determine the numbers of high mass stars and the star formation efficiency that one might expect from the simulation. It is still beyond the capabilities of current computational resources to model the details of how individual stars form in a body of gas as large as a GMC. In the simulation presented here we cannot model any gas dynamics below the $20M_{\odot}$ scale. We can however give the reader a feel for the star formation that is present by using the results of previous simulations, along with some assumptions about the star formation efficiency and the form of the IMF.

It has been shown from numerical simulations that star formation occurs on roughly the local crossing time for the turbulence when the region is dynamically bound (Bate et al., 2003a; Klessen, 2001). On the small scales such as those represented by our protoclusters, $\sim$ 0.1pc, the crossing time is of the order 10^5 years. We can therefore assume that all of our protoclusters form stars and that the star formation in our protoclusters takes place quickly, rapidly enough to be regarded here as instantaneous compared to the evolution of the whole GMC.

The simulation presented also has no method of incorporating feedback into the GMC model. As is shown in figure 8.2 in the right hand plot, the mass accreted into the SFCs gradually increases as the simulation progresses. At the point where the simulation is terminated, 30% of the GMC has been accreted by the protoclusters. It is unlikely that this value is representative of how much mass would actually be involved in the

star formation by this time, since feedback mechanisms such as ionisation, winds and supernovae would seriously alter the amount of gas that would be available for accretion into the SFCs. What is needed is an estimate of when one would expect the star formation process to be halted by feedback mechanisms. This requires some knowledge of the star formation taking place within the SFCs.

We have already pointed out that the protoclusters in the simulation group into large SFCs. From now on in the paper we will use the details of these regions, rather than the individual protoclusters, to assess the nature of the star formation in the GMC. Table 8.1 gives the details of the SFCs after 9 Myr. The masses quoted for the SFCs in table 8.1 includes all particles (SPH and protoclusters) that fall within the radius of the region. The gas particle component is however quite small, generally less than 20%.

Although the star formation efficiency of GMCs is thought to be in the range of 1 to 10%, at the cluster level it is thought to be about 20 to 50% depending on the region (for a discussion we point the reader to Lada & Lada 2003 and Kroupa 2001). In this paper we assume that the star formation efficiency in our SFCs is 50%, but will include a discussion about the case in which 100% of the mass is turned into stars. The assumed efficiency here is high but this is deliberate since it actually assumes as little as possible about the effect that the feedback mechanisms from the young stars are having on the accretion processes in the SFC. We will also assume that the IMF of the stellar population in the SFCs follows a two step power law form, $dN \propto m^{-\alpha}dm$, with $\alpha = 1.5$ for $0.08 < m/M_{\odot} \leq 0.5$ and $\alpha = 2.35$ (Salpeter, 1955) for $0.5 < m/M_{\odot} \leq 100$. This IMF, in conjunction with our assumption that 50% of the mass of the SFCs is turned into stars, allows us to estimate the stellar population produced by the simulation.

As already mentioned in the previous section, figure 8.2 shows in the left hand plot how the mass of the 15 largest SFCs evolves with time. The horizontal lines mark the point at which high mass stars can form. From our IMF model, 15% of the mass should be contained in stars with masses greater that $10M_{\odot}$. Thus a $10M_{\odot}$ star will be present provided that there is $10/0.15 = 67M_{\odot}$ in the stellar population. Applying our assumed star formation efficiency of 50%, the SFCs must therefore have a mass of $134M_{\odot}$ if they are to harbour a $10M_{\odot}$ star. The horizontal long-dashed line in the figure denotes the point at which the SFCs achieve this mass. Doing the same for $25M_{\odot}$ stars, which should comprise 7.7% of the stellar mass in our chosen IMF, we find that the SFCs need to contain $25/(0.077 \times 0.5) = 650M_{\odot}$ if they are to contain a $25M_{\odot}$ star. This is represented by the horizontal short-dashed line in the figure.

From our simple assumptions about the small scale efficiency and the form of the IMF, we can estimate at what point in the simulation the star formation process will be disrupted by feedback mechanisms. From figure 8.2, we can estimate that the formation of $10M_{\odot}$ stars would occur at about $0.8t_{\rm ff}$(or at $\sim$ 4 Myr). A star of mass $25M_{\odot}$ would form after $\sim 1.1t_{\rm ff}$(or $\sim$ 5 Myr). Since the mass of the SFCs is increasing fairly rapidly at this point, stars with even higher masses would be expected to be present shortly after this, within 0.5 Myr or so. It would thus appear that the GMC is able to get enough mass into the SFCs for them to be able to form a full stellar population within about 1 Myr. This is consistent with the observations of the small age spread in the stellar population of the Orion cluster (Hillenbrand et al., 2001b).

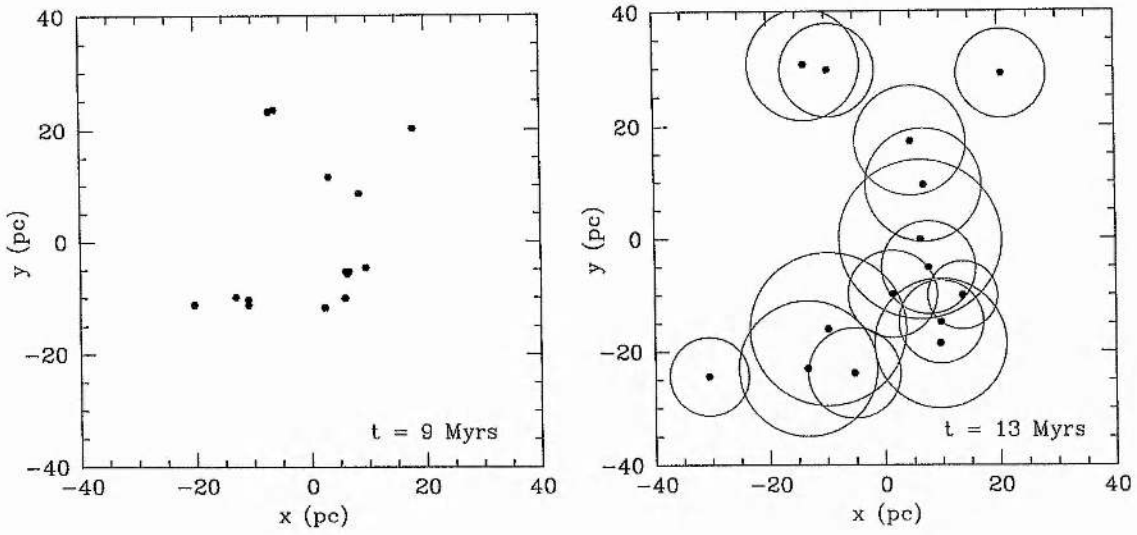

Figure 8.4: Plotted are the positions of the SFCs large enough, by t = 9 Myr, to contain stars of mass greater than $10M_{\odot}$. The plot on the left shows the positions of the SFCs at t = 9Myr and the plot on the right shows how the SFCs will be positioned after 13Myr, assuming that a SN event expels the GMC gas and the SFCs continue on their original path. The circles show the size of the SFCs after the 4 Myr period, assuming they expand with their internal velocity dispersion. See section 8.5 for a discussion.

Very rapidly after the first stars form we see that $10M_{\odot}$ objects will be present. This means that shortly after their formation, SFCs are going to contain ionising sources. Such stars are commonly suggested to be responsible for controlling the star formation efficiency by expelling the gas from the cluster in which they form (such as our SFCs), thus preventing the protostellar population from accreting or preventing new stars from forming. However Dale et al. (2004) have noted that the ionisation from these stars does not appear to significantly affect the accretion rate in the clusters. The clumpy/fractal nature of the gas at the centre of the cluster where the OB type stars are situated acts to shield vast regions of the cluster from ionisation. Rather than pushing through the dense material, the ionising photons just find the path with the least resistance out of the cluster. This is low density gas which would not normally be associated with protostellar accretion in the first place. Similarly, the gas structure may also prevent the winds from OB stars expelling gas from the cluster. It has been suggested that winds are able to escape via the fractal holes, without imparting much momentum to the dense regions (Henning, 1989).

It is therefore not clear if ionisation or winds are able to expel gas from a cluster, thereby halting the star formation process. One mechanism that certainly will produce the desired effect is a supernova explosion. In fact it has been estimated that these events will not only remove the gas from a cluster, but also be able to disperse the natal GMC. Thus a high mass star's death will definitely mark the end of the star formation period in our cloud. Stars with masses greater than $25M_{\odot}$ have very short main-sequence lifetimes, of about 3-5 Myr, and we see from the figure that they form at $\sim$ 5 Myr after GMC formation. If we assume that a supernova event will occur at $\sim$ 4 Myr after the formation of the very high mass stars, then we estimate the first supernova event to occur at about

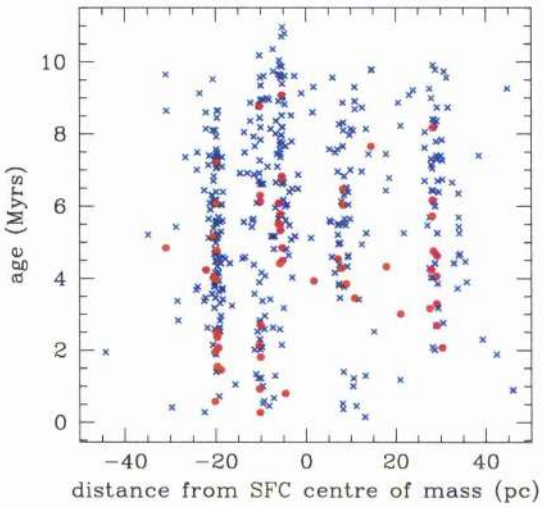

Figure 8.5: The figure shows the age of the protoclusters (note, not the SFCs but the individual 'sink particles') as a function of distance. The ages are shown at a time of 13 Myr after the cloud formation. The distance shown is the y component from the centre of mass of all the protoclusters. The crosses denote the age based on when the protoclusters form and the hexagons points denotes the age based on when an individual protocluster can harbour a star of greater than 10 $M_{\odot}$. See section 8.5 for more details. It is clear from the distribution of points here that there is no discernible age spread with position in the region. The star forming centres are essentially the same age.

9 Myr or when the OB stars are $\sim$ 4 Myr old.

Assuming the supernova event will halt the star formation, we can now get an estimate of the star formation efficiency in the GMC. The vertical dashed line in figure 8.2 denotes the point at which we might see the first SN event. At this time, $\sim$ 0.1 to 0.2 of the GMC's mass is contained in the SFCs. However we have assumed up until now that the efficiency in the SFCs is not 100% but 50%, therefore our estimate of the star formation efficiency in the GMC is roughly 5 to 10%. This is easily comparable to the expected efficiencies in GMCs for Elmegreen's (2000) rapid cloud formation/dispersal model.

The above analysis relied on a lot of assumptions about the nature of the star formation in the SFCs. In particular, it is guilty of invoking a star formation efficiency in the SFCs in order to determine the star formation efficiency of the cloud: one could argue that this is not entirely self-consistent. Here we redo the above analysis but without the SFC efficiency assumption. If all the mass in the SFCs is used in forming a stellar population, then the mass required by a SFC before a $25M_{\odot}$ star forms is $25/0.077 = 325M_{\odot}$. The first SFC to achieve this mass does so at about 4 Myr, only 1 Myr less than our previous estimate. Thus we can predict the supernova to occur at $\sim$ 8 Myr. At this point in the simulation there is about 7 - 8% of the cloud incorporated in the SFCs. Thus the expected star formation efficiency is still less than 10%, suggesting that our analysis is not heavily dependent on the assumptions.

SFC No.	M_{SFC} ($M_\odot$)	ΔV (km s^{-1})	R pc	t_{cr} Myr
1	3095	3.97	0.84	0.41
2	1248	3.09	0.56	0.36
3	1141	3.22	0.47	0.29
4	1073	3.14	0.47	0.29
5	820	2.58	0.53	0.40
6	622	3.88	0.18	0.09
7	589	2.14	0.55	0.50
8	513	2.24	0.44	0.38
9	379	1.93	0.44	0.45
10	349	2.69	0.21	0.15
11	334	2.91	0.17	0.11
12	288	2.24	0.25	0.21
13	244	2.39	0.18	0.15
14	242	1.50	0.46	0.60
15	187	2.18	0.17	0.15
16	186	2.17	0.17	0.15

Table 8.1: The table gives the properties of all the star formation centres (SFCs) that would be expected to contain massive stars by t = 9 Myr (see section 8.4 for a discussion of this). ΔV is the internal SFC velocity dispersion and assumes the region is in virial equilibrium such that $\Delta V = (GM_{SFC}/R)^{1/2}$. The crossing time is then calculated from $t_{cr} = 2R/\Delta V$. Note that M_{SFC} is the total (gas + stars) mass enclosed within R.

8.5 Dynamical Evolution of the Clusters and their relation to OB associations

As already discussed, the simulation produces a series of star formation centres (SFCs). Of these regions, 16 of them (see table 8.1) are massive enough to contain a star of greater than 10 $M_\odot$ by the time at which we estimate a SN explosion will destroy the GMC. From figure 8.1 we see that these SFCs are expanding as a group away from one another (in fact this is true of the GMC structure in general). Furthermore, the distance between SFCs is roughly 10pc after about 13Myr. Thus the group of clusters have the appearance of an OB association, with the individual SFCs being OB subgroups that are expanding about some common point. In this section we examine the properties of the SFCs and compare them to the observations of OB associations.

In figure 8.4, the left hand panel shows the positions of the SFCs that are large enough to contain stars greater than $10M_\odot$ at t = 9Myr, assuming a star formation efficiency of 50% and the IMF presented in section 8.4. Their positions are plotted at the time we estimate the SN event to start expelling gas from the cloud. We now assume that the SN event removes the gas from the GMC quickly enough such that the motions of objects have no time to adjust to the change in potential. We assume that this is true both at the scale of the SFC motions and at the smaller scale of the stellar motions inside the

SFCs. The right hand panel shows the positions of the SFCs after a further 4 Myr, i.e. at t = 13 Myr, assuming that they continue on the path they had before the gas expulsion. The circles denote the size of the SFCs at t = 13 Myr, which have been evaluated from $r = r_{SN} + \Delta V \times 4$ Myr, where ΔV is the region's internal velocity dispersion and r_{SN} is the radius of the SFCs at the point when the SN event occurs (i.e. at $\sim$ 9 Myr). This assumes that the star forming regions will disperse at roughly their internal velocity dispersion once the gas has been expelled.

Figure 8.4 clearly shows that the SFCs are expanding away from one another. By determining the average radius of the SFCs from their common centre of mass, both at t = 9 Myr and at t = 13 Myr, we can get an estimate of their expansion velocity from their dynamical centre. At t = 9 Myr the average distance of the SFCs from their centre of mass is 18.4pc, while after 13 Myr it is 25pc. This corresponds to an expansion velocity (that is a 3-dimensional velocity) for the SFCs of $1.5 \mathrm{kms}^{-1}$. We compare this, for example, to the observed expansion of the OB subgroups in Per OB, which is roughly $2 \mathrm{kms}^{-1}$ (Fredrick, 1956; Blaauw, 1964). We also see that if the SFCs themselves are able to expand after the gas expulsion, they become an extended distribution of stars after only 13 Mys, as is shown by the circles in the figure.

The stellar mass density is another important feature of OB associations. Generally, OB associations have a density of OB stars of roughly $0.1 M_{\odot}$ pc^{-3} (see the introduction for references). In this simulation at t = 9 Myr, the density of OB type stars is $0.16 M_{\odot}$ pc^{-3}, and the mass density of stars $\geq 25 M_{\odot}$ is $0.1 M_{\odot}$ pc^{-3}. This is calculated by taking the total mass in the SFCs of stars of greater than the required mass type and dividing by the volume of the region containing all the SFCs with these types of stars. After the system has had time to evolve for 4 Myr, the densities are 0.06 and $0.04 M_{\odot}$ pc^{-3} for the OB type stars and those with masses $\geq 25 M_{\odot}$ respectively. Note these figures are based on the SFCs having a star formation efficiency of 50% and containing the IMF of stellar objects that was presented in section 8.4.

We can compare this to the density of high mass stars in the SFCs at the point of the SN explosion. If we take the largest SFC , with mass $1763 M_{\odot}$ and radius of 0.7pc, and assume again that 50% of this is contained in stars. Then the total mass in stars of mass greater than $10 M_{\odot}$ is $1763 \times 0.15/2 = 132 M_{\odot}$. The density of massive stars is then $132/0.7^3 = 384\ M_{\odot} \mathrm{pc}^{-3}$.

The turbulent flows are thus able to create a series of star forming regions that have roughly the same properties as those found in OB associations. Since the regions (the SFCs) are formed within large flows, the stars that form will have roughly the same motion as the gas stream that formed them, potentially explaining why Blaauw (1991) finds that the gas surrounding OB subgroups is generally moving with the group.

Observations of some OB associations also indicate distinct age spreads between their subgroups. This generally takes the form of an age progression from one side of the association to the next. The ages are generally derived from where the very high mass stars turn off the main sequence, which is a much more reliable method than using pre-main-sequence (PMS) tracks of low mass objects. Also the high mass end is normally the only part of the mass spectrum that is well established in OB associations. This age spread has been the motivation behind the triggered sequential star formation model developed

by Elmegreen & Lada (1977), which is in turn motivated by the observations of Blaauw (1964). However, we note here that the Orion OB association exhibits no discernible age progression in the subgroups (Brown et al., 1999).

Does our simulation show a convincing age spread between the subgroups/SFCs? In figure 8.5 we plot the age of the protoclusters (the sink particles that group together to form the SFCs) and their position from their common centre of mass. All the points are plotted at t = 13 Myr, with the positions being the y-direction in the simulation, since the SFCs are more spaced out in this direction. The ages are determined in two ways. The crosses denote the ages determined by when the protocluster first forms. The filled hexagons are determined by the time when the protoclusters reach a mass of $134M_{\odot}$, the point at which a $10M_{\odot}$ star can form. Note that in the previous sections we determined when $10M_{\odot}$ stars could form based on the mass contained in an SFC , rather than its constituent protoclusters and gas. We are forced to use the individual protoclusters here since the SFCs are not coherent objects throughout the entire evolution of the simulation.

We see clearly from figure 8.5 that while a large range of ages exist at any particular distance from the centre of mass, no trend is present in the ages with distance. Thus our simulation predicts that the OB association would be essentially coeval. However this is just a symptom of our idealised initial conditions. The initial uniform density sphere, with multiple Jeans masses, allows the entire cloud to proceed directly to star formation, via the dissipation of kinetic energy. Since the turbulence is the same throughout the cloud, star formation occurs simultaneously in quite separate locations. If on the other hand our GMC needs to be accumulated in a large scale shock, as suggested by Pringle et al. (2001), then there would naturally be an age spread as the layer in which the GMC forms starts to grow. The most important point in this picture is that the whole region would not be at the same density, but instead would have to evolve to star forming densities as the GMC accumulates.

8.6 Conclusions

The simulation presented in this chapter highlights that GMCs need not be regarded as objects in virial equilibrium, or even bound, for them to be sites of star formation. Globally unbound GMCs can form stellar clusters very quickly, on roughly their crossing time. Furthermore, the unbound state of the cloud ensures that whole region is also dispersing while it is forming stars. They are thus naturally transient features. This evolutionary picture of a cloud forming, producing a stellar population, and then dispersing has been shown by Elmegreen (2000) to be apparent in a number of independent observations.

Using some simple assumptions about the form of the star formation in the star formation centres (SFCs) of our simulation, we have provided an estimate of the star formation efficiency in the GMC. At the point one would expect the first supernova events, we find that the star formation efficiency is about 5 - 10%. This assumes that the SFC environment in the simulation yields an efficiency of $\sim$ 50%. Removing this assumption about the SFCs, and letting the SN event be the only control over the efficiency, we find that the cloud has a global star formation efficiency of $\sim$ 7-8% (for our assumed IMF).

We argue that unbound GMCs may provide a simple mechanism for forming OB associations, a concept that was touched upon by Ambartsumian (1955, 1958). OB stars form at the centre of a population of SFCs. These SFCs, which condense out of the unbound flows in the GMC are naturally expanding away from one another, as the positive energy disperses the cloud's gas. Not only does the mechanism explain the OB association dynamics but it also explains the observed substructure, generally referred to as OB subgroups. Since the OB association is just a series of independently formed clusters, one would also expect the association to have the field star IMF.

CHAPTER 9

Conclusions and further work

9.1 Conclusions

In the course of this PhD, we have examined the nature of star formation in environments where the gas initially contains random supersonic motions, which we refer to loosely in this thesis as 'turbulence'. The aim of this PhD was to establish the effect of the turbulent motions on the manner in which stars are able to form. We set out to answer two questions. Firstly, can the turbulence locally trigger star formation, such that stars form in regions where colliding flows meet? Secondly, can star formation occur in clouds that are globally unbound? The first question is important, since the turbulent motions that are observed to exist in star forming regions have been claimed to be responsible for not only the triggering of gravitational collapse (e.g. Elmegreen 1993), but the form of the IMF (Padoan & Nordlund, 2002) and even the star formation efficiency (e.g. Mac Low & Klessen 2004). While simulations have been conducted in which the gas contains turbulent motions, it has never been established whether the star formation is really controlled by the turbulence in the manner that has been suggested (see Mac Low & Klessen 2004 for a full discussion). The second question also has important implications. By relaxing the assumption that star forming regions are globally bound, the regions can naturally achieve a low star formation efficiency and also be a short lived entity, as the recent observations suggest (Elmegreen, 2000a).

To get answers to these questions, we used an SPH code to model the gas of the star forming region and the inclusion of 'sink' particles allowed us to follow the formation and evolution of dense bound regions, such as where protostars or small clusters would be formed. These simulations were similar to those conducted by Bate et al. (2003a), Delgado-Donate et al. (2004), Bonnell et al. (2003), Bonnell et al. (2004) and Bate & Bonnell (2005). We could thus use these previous studies as a comparison.

The first 4 chapters in this thesis provide: an introduction and overview of star formation; a discussion of the SPH method used in this thesis; a brief description of how we generate our turbulent velocity fields and examine the density structure in the gas; and an overview of the main ideas in gravitational collapse and how this may be induced via shock compression of the gas. These chapters provide the background to the work that is presented in chapters 5, 6, 7 and 8, where we present the results of the investigation.

In chapters 5 and 6 we examined the nature of the star formation in small clouds of mass ~ 30 $M_{\odot}$ and mean initial Jeans mass of $1M_{\odot}$. These clouds therefore have roughly 30 Jeans masses initially. Chapter 5 focuses on the differences in the star formation that arise when the magnitude of the kinetic energy in the turbulent velocity field, which is supporting the cloud against gravity, is changed. In this chapter, both the evolution of the clump properties and the resulting protostellar population are examined. In chapter 6, the emphasis is on examining the energy state of the clump population as the clouds progress towards star formation. In chapter 6 we focus mainly on the clouds where the energy in the turbulence is equal to that of the cloud's gravitational energy.

These two chapters provide a number of useful results. The dynamical state of the cloud has an effect on the properties of the cluster that it forms. Clouds with low levels of turbulence, generally form more stars, and produce more tightly bound systems, than those with higher levels of turbulence. Despite the differences in the properties of the clusters from clouds with different levels of turbulence, competitive accretion is always the dominant process that determines the masses of the stars. The turbulence also does not appear to 'trigger' the star formation, since the clouds with the higher levels of turbulence take longer to form stars than their less energetic counterparts.

The clump mass spectrum generated by the turbulence is, at the point of star formation, broadly similar in shape to the stellar mass spectrum. The vast majority of these clumps however are unbound, since the magnitude of both the thermal and kinetic energies, taken individually, is larger than the magnitude of the clump's gravitational energy. We therefore conclude that the observations of Motte et al. (1998), which show the clump mass spectrum for ρ Ophiuchus to be similar in shape to the stellar IMF, does not prove the existence of a one-to-one mapping between stars and clumps. In fact, our results tend to suggest that the clump mass spectrum is not related to the star formation, or the final mass spectrum of the stellar population.

The turbulence does appear to be able to decrease the Jeans mass in some of clumps but these clumps never become bound since their internal kinetic energy is still too great. The amount by which the Jeans mass is decreased is indeed consistent with the new density in the shocked regions. Note however that the amount by which the Jeans mass is decreased locally in the clump, is inversely proportional to the Mach number of the flows which created the clump. For our fairly dense clouds, with reasonably high Mach numbers of 5 or so, the formation of thermally bound substellar mass objects never occurs.

Only the clumps which are roughly equal in mass to the mean Jeans mass in the cloud, are able to overcome both their internal thermal and kinetic energy. These are the clumps in which star formation occurs. In the run up to star formation, the gas which eventually constitutes the final star forming clump gains rough equipartition of its thermal and kinetic energies. At this point no further dissipation of kinetic energy can occur since the velocities in the gas are roughly sonic. This results in the final bound clump having roughly 2.8 effective Jeans masses, and thus allows the clump to fragment. Rather than forming only single stars/sub-stellar objects, these star forming clumps are thus naturally the sites of binary and multiple system formation.

We can conclude from chapters 5 and 6 that the turbulence that is present in simulations of small clouds with conditions similar to ours, such as such as those of Bate et al.

(2003a); Bate & Bonnell (2005); Delgado-Donate et al. (2004), is not directly responsible for the star formation. The turbulence in these simulations does not trigger star formation or control the masses of the protostars which form. The shock dissipation of the kinetic energy allows the mean Jean mass in the cloud to control the star formation. The turbulence thus acts to provides some density structure out of which fragmentation may occur.

In chapter 7 we go on to further examine the unbound clouds, which had been briefly studied in chapters 5 and 6. This time we focused on the fact that unbound clouds, even fairly small ones such those we had just studied, are able to form stars. The condition that star forming regions must be globally bound can therefore be relaxed, and we argue that this can also apply to GMCs. While this may seem contrary to our analysis in chapters 5 and 6, where we argued that a clump must be bound before it can form a star, note that our clouds here have many more Jeans masses that the clumps that were discussed. When a cloud has many Jeans masses, and is unbound by its internal motions or 'turbulence', some of the cloud can become bound during the kinetic energy dissipation that takes place during the shocks. This bound region is generally at the centre of the cloud, with the outer regions getting blown away by the turbulence.

The fact that some, but not all, of the cloud is able to become bound means that the resulting star formation efficiency of the cloud is less than 100%. This is simply because the material available for accretion onto the newly formed protostellar system is only that material that has become bound to the system during the shock energy dissipation. We find that the mean Jeans mass in the bound region controls the star formation, and the number of Jeans masses contained in the bound region is comparable to the number of protostars that are formed. The star formation efficiency in GMCs and smaller dark clouds, may therefore be connected to the initial binding energy of the cloud, or region, in which star formation occurs.

In chapter 8, we take this investigation into unbound clouds a stage further, and model an unbound GMC. We don't have the resolution in this simulation to follow the small scale evolution of the cloud, so instead concentrate on the large scale morphology of the GMC and make assumptions about the details of the star formation at the smaller scales. We make three initial assumptions. First we assume a star formation efficiency in our cluster regions of 50%. Second we assume that the stars which form, have a range of masses that are described by our prescribed stellar mass function. This mass function is a two step power law, $dN \propto m^{-\alpha} dm$, with $\alpha = 1.5$ for $0.08 < m/M_{\odot} \leq 0.5$ and $\alpha = 2.35$ (Salpeter, 1955) for $0.5 < m/M_{\odot} \leq 100$. The third assumption is that when a high mass star ends its life, the star formation in our clusters is halted. Only the action of a supernova event ceases the star formation.

Using these assumptions, we find that the star formation efficiency of the GMC as whole is roughly 5-10%. Even when we relax the first assumption that the star formation efficiency in the clusters is 50 %, and instead allow all the mass in the cluster to be part of the stellar population, we find that the global star formation efficiency for the GMC is still roughly 7-10%. We also point out in this chapter, that star formation, and cloud dispersal, all occur within a few crossing times, consistent with the findings of Elmegreen (2000a). Thus unbound GMCs provide a naturally fast and inefficient mechanism for producing stars.

We end chapter 8 by showing that the morphology and dynamics of the system of clusters that are formed in this GMC have similar properties to OB associations. The supersonic flows which are present in the cloud form regions of bound gas (via kinetic energy dissipation) that are naturally unbound from one another. Due to the unbound nature of the cloud as whole, these regions are also expanding from the cloud's centre. When clusters form in these bound regions, it creates a population of clusters that are naturally expanding away from one another, and are unbound as an ensemble. The clusters in GMC are radially expanding away from their common centre of mass at $\sim$ 2 km/s, comparable to the observed expansion of OB subgroups. Furthermore, theses clusters are also massive enough to contain OB type stars.

9.2 Related future work

The work which was performed as part of this PhD is still far removed from providing a complete, or comprehensive, picture of star formation. One main criticism that can be made of the work in chapters 5 and 6 is that the density structure and velocity structure are not self-consistent. We start with a uniform density cloud and superimpose onto the particle distribution a velocity field which corresponds to that of supposed 'turbulent' velocity fields. In real clouds however, the velocity structure and the density structure of the gas are related, presumably since the supersonic flows are responsible for the observed density features. In our simulations, the gas velocities and densities are only self consistent once the velocities have had a chance to structure the gas, which occurs roughly after half a crossing time or so. By this point, much of the kinetic energy in our cloud has been dissipated. Also the velocities present at each size scale, a detail which is initially controlled by the power spectrum of the velocity field, decay at different rates. The smaller scale flows decay quicker than those on larger scales. This changes the power spectrum of the turbulence. Thus at the onset of star formation, the velocity structure in our clouds is no longer similar to the initial conditions. To test whether the results of chapters 5 and 6 are valid for the conditions in star forming regions, simulations should be conducted in which the velocity and the density structure are related from the start.

The unbound clouds also provide a potentially interesting field for study. One thing we did not establish are the required parameters for star formation in such objects, i.e., for what values of J_o and ϵ would one expect stars to be able to form. An answer to this question might be useful for explaining why the clumps in the Rosette cloud are forming stars, while those in the 'Maddalena' cloud (G216-2.5) are not (as yet) (Williams et al., 1994). Another question is how the star formation efficiency of these unbound clouds/clumps, that are found to be capable of forming stars, might be connected to the values of J_o and ϵ. One could thus make estimates for the expected star formation efficiency in GMCs, which can be easily compared to observations.

Bibliography

Abt H. A., 1983, ARA&A, 21, 343

Ambartsumian V. A., 1955, The Observatory, 75, 72

—, 1958, Reviews of Modern Physics, 30, 944

Ballesteros-Paredes J., 2004, Ap&SS, 289, 243

Ballesteros-Paredes J., Hartmann L., Vázquez-Semadeni E., 1999a, ApJ, 527, 285

Ballesteros-Paredes J., Vázquez-Semadeni E., Scalo J., 1999b, ApJ, 515, 286

Bate M., 1995, Ph.D. Thesis

Bate M. R., 2000, MNRAS, 314, 33

Bate M. R., Bonnell I. A., 1997, MNRAS, 285, 33

—, 2005, MNRAS, 356, 1201

Bate M. R., Bonnell I. A., Bromm V., 2003a, MNRAS, 339, 577

—, 2003b, MNRAS, 339, 577

Bate M. R., Bonnell I. A., Price N. M., 1995, MNRAS, 277, 362

Bate M. R., Burkert A., 1997, MNRAS, 288, 1060

Bazell D., Desert F. X., 1988, ApJ, 333, 353

Benz W., 1984, A&A, 139, 378

—, 1990, in Numerical Modelling of Nonlinear Stellar Pulsations Problems and Prospects, pp. 269–+

Benz W., Cameron A. G. W., Press W. H., Bowers R. L., 1990, ApJ, 348, 647

Benz W., Hills J. G., 1987, ApJ, 323, 614

Benz W., Slattery W. L., Cameron A. G. W., 1986, in Lunar and Planetary Institute Conference Abstracts, pp. 40–41

Bertschinger E., 1986, ApJ, 304, 154

Bhattal A. S., Francis N., Watkins S. J., Whitworth A. P., 1998, MNRAS, 297, 435

Blaauw A., 1952, Bull. Astr. Neth., 11, 405

—, 1964, ARA&A, 2, 213

—, 1991, in NATO ASIC Proc. 342: The Physics of Star Formation and Early Stellar Evolution., p. 125

Blitz L., 1991, in NATO ASIC Proc. 342: The Physics of Star Formation and Early Stellar Evolution, pp. 3–+

Blitz L., Magnani L., Mundy L., 1984, ApJL, 282, L9

Blitz L., Stark A. A., 1986, ApJL, 300, L89

Blitz L., Thaddeus P., 1980, ApJ, 241, 676

Blitz L., Williams J. P., 1997, ApJL, 488, L145+

—, 1999, in NATO ASIC Proc. 540: The Origin of Stars and Planetary Systems, pp. 3–+

Bonnell I., Bastien P., 1992, ApJ, 401, 654

Bonnell I., Martel H., Bastien P., Arcoragi J., Benz W., 1991, ApJ, 377, 553

Bonnell I. A., Bate M. R., Clarke C. J., Pringle J. E., 1997, MNRAS, 285, 201

—, 2001a, MNRAS, 323, 785

Bonnell I. A., Bate M. R., Vine S. G., 2003, MNRAS, 343, 413

Bonnell I. A., Clarke C. J., Bate M. R., Pringle J. E., 2001b, MNRAS, 324, 573

Bonnell I. A., Vine S. G., Bate M. R., 2004, ArXiv Astrophysics e-prints

Boss A. P., 1993, Bulletin of the American Astronomical Society, 25, 1439

—, 1996, ApJ, 468, 231

Boss A. P., Bodenheimer P., 1979, ApJ, 234, 289

Boss A. R., 1986, ApJS, 62, 519

Brown A. G. A., 2001, in Revista Mexicana de Astronomia y Astrofisica Conference Series., p. 89

Brown A. G. A., Blaauw A., Hoogerwerf R., de Bruijne J. H. J., de Zeeuw P. T., 1999, in NATO ASIC Proc. 540: The Origin of Stars and Planetary Systems., p. 411

Carpenter J. M., 2000, AJ, 120, 3139

Carpenter J. M., Snell R. L., Schloerb F. P., 1996, in IAU Symp. 170: CO: Twenty-Five Years of Millimeter-Wave Spectroscopy, pp. 148–+

Cernicharo J., 1991, in NATO ASIC Proc. 342: The Physics of Star Formation and Early Stellar Evolution, pp. 287–+

Chapman S., Pongracic H., Disney M., Nelson A., Turner J., Whitworth A., 1992, Nature, 359, 207

Clark P. C., Bonnell I. A., 2004, MNRAS, 347, L36

Clarke C. J., 1999, MNRAS, 307, 328

Cowie L. L., 1980, ApJ, 236, 868

Crutcher R. M., 1999, ApJ, 520, 706

Dale J., Bonnell I. A., Bate M. R., Clarke C. J., Pringle J. E., 2004, in prep

Dame T. M., Elmegreen B. G., Cohen R. S., Thaddeus P., 1986, ApJ, 305, 892

de Geus E. J., 1992, A&A, 262, 258

Delgado-Donate E. J., Clarke C. J., Bate M. R., 2004, MNRAS, 347, 759

Doroshkevich A. G., 1980, Astronomicheskii Zhurnal, 57, 259

Dubinski J., Narayan R., Phillips T. G., 1995, ApJ, 448, 226

Duchêne G., Bouvier J., Bontemps S., André P., Motte F., 2004, A&A, 427, 651

Duchêne G., Bouvier J., Simon T., 1999, A&A, 343, 831

Duquennoy A., Mayor M., 1991, A&A, 248, 485

Elmegreen B. G., 1982a, ApJ, 253, 655

—, 1982b, ApJ, 253, 634

—, 1991, in NATO ASIC Proc. 342: The Physics of Star Formation and Early Stellar Evolution, pp. 35–+

—, 1993, ApJL, 419, L29+

—, 1997, ApJ, 486, 944

—, 1999, ApJ, 515, 323

—, 2000a, ApJ, 530, 277

· ·, 2000b, MNRAS, 311, L5

Elmegreen B. G., Elmegreen D. M., 1978, ApJ, 220, 1051

Elmegreen B. G., Lada C. J., 1977, ApJ, 214, 725

Evans N. J., 1999, ARA&A, 37, 311

Evrard A. E., 1998, in Untangling Coma Berenices: A New Vision of an Old Cluster, pp. 136–+

Falgarone E., Phillips T. G., Walker C. K., 1991, ApJ, 378, 186

Fehlberg E., 1968, NASA T.R., 287

Field G. B., Saslaw W. C., 1965, ApJ, 142, 568

Franco J., Shore S. N., Tenorio-Tagle G., 1994, ApJ, 436, 795

Franco J., Tenorio-Tagle G., Bodenheimer P., Rozyczka M., Mirabel I. F., 1988, ApJ, 333, 826

Fredrick L. W., 1956, AJ, 61, 437

Garmany C. D., 1994, PASP, 106, 25

Genzel R., 1991, in NATO ASIC Proc. 342: The Physics of Star Formation and Early Stellar Evolution, pp. 155–+

Ghez A. M., Neugebauer G., Matthews K., 1993, AJ, 106, 2005

Gittins D. M., Clarke C. J., Bate M. R., 2003, MNRAS, 340, 841

Goodman A. A., Barranco J. A., Wilner D. J., Heyer M. H., 1998, ApJ, 504, 223

Goodwin S. P., Whitworth A. P., Ward-Thompson D., 2004, A&A, 414, 633

Greaves J. S., Holland W. S., Pound M. W., 2003, MNRAS, 346, 441

Habing H. J., Israel F. P., de Jong T., 1972, A&A, 17, 329

Haisch K. E., Lada E. A., Lada C. J., 2001, ApJL, 553, L153

Hartmann L., 1998, Accretion processes in star formation. Cambridge University Press, 1998.

—, 2000, in 33d ESALAB Symp., Star Formation from the Small to the Large Scale, pp. 107–+

—, 2002, ApJ, 578, 914

Hartmann L., Ballesteros-Paredes J., Bergin E. A., 2001, ApJ, 562, 852

Heintz W. D., 1969, JRASC, 63, 275

Henning T., 1989, Astronomische Nachrichten, 310, 363

Henriksen R. N., 1986, ApJ, 310, 189

—, 1991, ApJ, 377, 500

Herbst W., Assousa G. E., 1977, ApJ, 217, 473

Heyer M. H., Brunt C., Snell R. L., Howe J. E., Schloerb F. P., Carpenter J. M., 1998, ApJS, 115, 241

Heyer M. H., Brunt C. M., 2004, ApJL, 615, L45

Heyer M. H., Carpenter J. M., Snell R. L., 2001, ApJ, 551, 852

Heyer M. H., Terebey S., 1998, ApJ, 502, 265

Hillenbrand L. A., Carpenter J. M., 2000, ApJ, 540, 236

Hillenbrand L. A., Carpenter J. M., Feigelson E. D., 2001a, in ASP Conf. Ser. 243: From Darkness to Light: Origin and Evolution of Young Stellar Clusters, pp. 439–+

—, 2001b, in ASP Conf. Ser. 243: From Darkness to Light: Origin and Evolution of Young Stellar Clusters., p. 439

Inutsuka S., Miyama S. M., 1992, ApJ, 388, 392

Jeans J. H., 1902, Phil. Trans. Roy. Soc., 199, 1

Jura M., 1975, ApJ, 197, 575

Kimura T., Tosa M., 1993, ApJ, 406, 512

Klessen R. S., 2001, ApJ, 556, 837

Klessen R. S., Burkert A., 2000, ApJS, 128, 287

Klessen R. S., Burkert A., Bate M. R., 1998, ApJL, 501, L205+

Klessen R. S., Heitsch F., Mac Low M., 2000, ApJ, 535, 887

Kolmogorov A. N., 1941, Dokl. Akad., Nauk. SSR, 26, 115

Kroupa P., 1995a, MNRAS, 277, 1491

—, 1995b, MNRAS, 277, 1507

—, 2001, MNRAS, 322, 231

Kroupa P., Aarseth S., Hurley J., 2001, MNRAS, 321, 699

Kroupa P., Petr M. G., McCaughrean M. J., 1999, New Astronomy, 4, 495

Kwan J., 1979, ApJ, 229, 567

Kwan J., Valdes F., 1983, ApJ, 271, 604

Lada C. J., Alves J., Lada E. A., 1996, AJ, 111, 1964

Lada C. J., Dickinson D. F., Gottlieb C. A., Wright E. L., 1976, ApJ, 207, 113

Lada C. J., Lada E. A., 2003, ARA&A, 41, 57

Lada E. A., 1992, ApJL, 393, L25

Lada E. A., Evans N. J., Depoy D. L., Gatley I., 1991, ApJ, 371, 171

Larson R. B., 1978, MNRAS, 184, 69

—, 1981, MNRAS, 194, 809

—, 1992, MNRAS, 256, 641

—, 1995, MNRAS, 272, 213

—, 2003, Reports of Progress in Physics, 66, 1651

Leisawitz D., Bash F. N., Thaddeus P., 1989, ApJS, 70, 731

Low C., Lynden-Bell D., 1976, MNRAS, 176, 367

Lubow S. H., Pringle J. E., 1993, MNRAS, 263, 701

Luhman K. L., Rieke G. H., Young E. T., Cotera A. S., Chen H., Rieke M. J., Schneider G., Thompson R. I., 2000, ApJ, 540, 1016

Mac Low M., Klessen R. S., 2004, Reviews of Modern Physics, 76, 125

Mac Low M., Klessen R. S., Burkert A., Smith M. D., 1998, Physical Review Letters, 80, 2754

Maddalena R. J., Thaddeus P., 1985, ApJ, 294, 231

McKee C. F., Zweibel E. G., Goodman A. A., Heiles C., 1993, in Protostars and Planets III, pp. 327–+

Miller G. E., Scalo J. M., 1979, ApJS, 41, 513

Mizuno A., Hayakawa T., Tachihara K., Onishi T., Yonekura Y., Yamaguchi N., Kato S., Hara A., Mizuno N., Kawamura A., Abe R., Saito H., Yamaguchi R., Ogawa H., Fukui Y., 1999, PASJ, 51, 859

Monaghan J. J., 1992, ARA&A, 30, 543

—, 1994, ApJ, 420, 692

Morata O., Girart J. M., Estalella R., 2005, in press

Morris J. P., 1994, in Monash University, Applied Mathematics Reports and Preprints, p. 94

Motte F., Andre P., Neri R., 1998, A&A, 336, 150

Mouschovias T. C., Shu F. H., Woodward P. R., 1974, A&A, 33, 73

Muench A. A., Lada E. A., Lada C. J., Alves J., 2002, ApJ, 573, 366

Mundy L. G., Looney L. W., Welch W. J., 2000, Protostars and Planets IV, 355

Myers P. C., 1983, ApJ, 270, 105

Myers P. C., Benson P. J., 1983, ApJ, 266, 309

Myers P. C., Gammie C. F., 1999, ApJL, 522, L141

Myers P. C., Goodman A. A., 1988, ApJL, 326, L27

Nishi R., 1992, Progress of Theoretical Physics, 87, 347

Oort J. H., 1954, Bull. Astr. Neth., 12, 177

Opik E. J., 1953, Irish Astronomical Journal, 2, 219

Ostriker E. C., Gammie C. F., Stone J. M., 1999, ApJ, 513, 259

Ostriker E. C., Stone J. M., Gammie C. F., 2001, ApJ, 546, 980

Padoan P., 1995, MNRAS, 277, 377

Padoan P., Juvela M., Goodman A. A., Nordlund Å., 2001, ApJ, 553, 227

Padoan P., Nordlund Å., 1999, ApJ, 526, 279

—, 2002, ApJ, 576, 870

Padoan P., Nordlund A., Jones B. J. T., 1997, MNRAS, 288, 145

Parker E. N., 1966, ApJ, 145, 811

Phelps R. L., Lada E. A., 1997, ApJ, 477, 176

Preibisch T., Zinnecker H., 1999, AJ, 117, 2381

Pringle J. E., 1989, MNRAS, 239, 361

Pringle J. E., Allen R. J., Lubow S. H., 2001, MNRAS, 327, 663

Rees M. J., 1976, MNRAS, 176, 483

Salpeter E. E., 1955, ApJ, 121, 161

Sanders D. B., Scoville N. Z., Solomon P. M., 1985, ApJ, 289, 373

Scalo J., 1990, in ASSL Vol. 162: Physical Processes in Fragmentation and Star Formation, pp. 151–176

Scalo J. M., 1986, Fundamentals of Cosmic Physics, 11, 1

Scoville N. Z., Hersh K., 1979, ApJ, 229, 578

Scoville N. Z., Solomon P. M., Sanders D. B., 1979, in IAU Symp. 84: The Large-Scale Characteristics of the Galaxy, pp. 277–282

Shu F. H., 1974, A&A, 33, 55

—, 1977, ApJ, 214, 488

Shu F. H., Adams F. C., Lizano S., 1987, ARA&A, 25, 23

Siess L., 2001, in ASP Conf. Ser. 243: From Darkness to Light: Origin and Evolution of Young Stellar Clusters, pp. 581–+

Simon M., Close L. M., Beck T. L., 1999, AJ, 117, 1375

Simon M., Ghez A. M., Leinert C., Cassar L., Chen W. P., Howell R. R., Jameson R. F., Matthews K., Neugebauer G., Richichi A., 1995, ApJ, 443, 625

Solomon P. M., Sanders D. B., Scoville N. Z., 1979, ApJL, 232, L89

Stone J. M., Ostriker E. C., Gammie C. F., 1998, ApJL, 508, L99

Testi L., Sargent A. I., 1998, ApJL, 508, L91

Tout C. A., Livio M., Bonnell I. A., 1999, MNRAS, 310, 360

Tsuribe T., Inutsuka S., 1999, ApJ, 526, 307

Vázquez-Semadeni E., Kim J., Shadmehri M., Ballesteros-Paredes J., 2005, ApJ, 618, 344

Vázquez-Semadeni E., Passot T., Pouquet A., 1995, in Revista Mexicana de Astronomia y Astrofisica Conference Series, pp. 61–+

Vazquez-Semadeni E., Ballesteros-Paredes J., Rodriguez L. F., 1997, ApJ, 474, 292

Vishniac E. T., 1983, ApJ, 274, 152

Whitworth A. P., 1998, MNRAS, 296, 442

Whitworth A. P., Bhattal A. S., Chapman S. J., Disney M. J., Turner J. A., 1994, A&A, 290, 421

Whitworth A. P., Bhattal A. S., Francis N., Watkins S. J., 1996, MNRAS, 283, 1061

Williams J. P., de Geus E. J., Blitz L., 1994, ApJ, 428, 693

Yoshida T., Habe A., 1992, Progress of Theoretical Physics, 88, 251

Zinnecker H., 1982, New York Academy Sciences Annals, 395, 226

—, 2002, Ap&SS, 281, 147

Zuckerman B., Evans N. J., 1974, NASA STI/Recon Technical Report N, 75, 10885

Zuckerman B., Palmer P., 1974, ARA&A, 12, 279